**POLITECNICO DI MILANO**

**Scuola di Ingegneria Industriale e dell'Informazione**

**Corso di Laurea Magistrale in Ingegneria Biomedica**

# Integration of muscle forces and gravity loads in a finite element model of the lumbar spine

**Supervisor:** *Prof. Ing.* **Tomaso Maria Tobia VILLA**

**Co-supervisor:** *Ing.* **Luigi LA BARBERA**

**Master Graduation Thesis by:**

**Elisabetta DAL POZZO, Id. number: 854934**

**Michele CARBONI, Id. number: 842171**

**Accademic Year 2016-2017**

*To all those who supported us*

# Contents

# List of Figures

# List of Tables

# ABSTRACT

The spine is a complex structure whose biomechanics is not yet fully understood. The goal of the computational and experimental models is to reproduce its functionality for better understanding the loads and the stresses that act along the spine. In this aim, the present thesis is based on the integration of muscle fascicles and weights's action for the reproduction of upright standing in a realistic condition. Generally, a 500 N follower load is the common loading condition for simulating standing [11]. It acts like a cable between vertebrae inducing a pure compression force along the spinal curvature. Unfortunately, this simplification of the load is subjected to criticism [49]. For this reason, the thesis was developed for evaluating if the lumbar finite element musculo-skeletal model could reproduce the available in-vivo data in a better way with respect to follower load. The implementation of muscles in the model, required an adequate fascicles positioning preceded by a detailed analysis of the state of the art. Moreover, the fascicles were associated with a force value. For the selection of these values, literature's models were analysed and percentages of muscular activation were chosen. Subsequently a campaign of simulations was conducted varying muscular forces' activation. The muscles forces induced an extensory action that counterbalanced the flexory action of the weight of the tissues and organs surrounding and overlying the lumbar spine. These weight forces have been applied in specific points in the space: the centres of mass. Finally, the results obtained from simulations were critically anal-

ysed. It was found that the choice of muscular forces is strongly related to the in-vivo data used for comparison and to the specific model used. A model with a poor lordosis will need a greater muscular activation for obtaining a lordosis in agreement with literature. Future developments will concern the simulation of other loading conditions like flexion or extension, the use of a more lordotic lumbar model or the implementation of a model comprehensive of the thoracic part.

# SOMMARIO

La colonna vertebrale è una struttura complessa la cui biomeccanica non è ancora del tutto nota. Lo scopo dei modelli computazionali e sperimentali è di riprodurne la funzionalità col fine di comprendere meglio carichi e sforzi agenti lungo la colonna. Con questo obiettivo, la tesi presente si propone di integrare i fasci muscolari e l'azione delle forze peso per riprodurre lo standing in condizioni più realtistiche possibili. Generalmente un follower load di 500 N viene usato per la simulazione dello standing [11]. Esso agisce come un cavo tra le vertebre, creando una pura forza di compressione lungo la curvatura spinale. Sfortunatamente questa semplificazione del carico è soggetta a critiche [49]. Per questa ragione la tesi è stata sviluppata col fine di valutare se il modello muscoloscheletrico lombare agli elementi finiti possa riprodurre i dati in-vivo in maniera più conforme rispetto al follower load. L'implementazione dei muscoli nel modello richiede un'adeguato posizionamento dei fasci, preceduto da un'analisi dettagliata dello stato dell'arte. Inoltre, a ogni fascio muscolare sono stati associati dei valori di forza. Per la scelta di questi valori, i modelli presenti in letteratura sono stati analizzati e successivamente sono state selezionate le percenuali di attivazioni muscolari da utilizzare. Sono poi state eseguite delle campagne di simulazioni al variare delle attivazioni delle forze. Queste ultime inducono un'estensione della colonna che serve a controbilanciare l'azione flessoria data dal peso dei tessuti e organi che circondano e sovrastano la colonna lombare. Queste forze peso sono poi state applicate in particolari

punti dello spazio: i centri di massa. Infine i risultati ottenuti dalle simulazioni sono stati oggetto di un'analisi critica. Da quest'ultima è risultato che la scelta delle forze muscolari è fortemente legata ai dati in-vivo utilizzati per il confronto e allo specifico modello utilizzato. Sviluppi futuri potrebbero riguardare simulazioni con altre condizioni di carico quali flessione ed estensione, l'uso di un modello lombare più lordotico o l'implementazione di un modello comprendente la colonna toracica.

# Chapter 1

# INTRODUCTION

The vertebral column is constantly subjected to loads in all directions and of all magnitudes. There are more than thirty muscles together with tendons and ligaments which respond to spinal loads providing spinal balance, stability, and mobility [50]. The complexity of the structure is such that today the real loads acting along the spine are still unknown [51]. Umpteen computational models of the spine have been developed for the study of the spine biomechanics and many others experimental works have been conducted with the aim of understanding and better reproducing its function [29] [52] [31] [53] [17][9] [14]. A correct estimation of the loads can increase the knowledge about spinal mechanics and this can contribute with improvements in biomedical devices, in biomechanical research, in management of spinal disorders, in understanding of back disorders and back pain. With this purpose, this work is based on the development of a complete musculo-skeletal lumbar model which could reproduce satisfactorily the biomechanics of the spine. The realization of this target needs not only an adequate choice of the muscular components, but also the adding of realistic loading and boundary conditions. Further purpose of the thesis is to evaluate if the model implemented for a particular condition, in this case the standing condition, would provide advantages with respect to the

widespread modelization of the literature. As already said, the kinematics, the results and, in general, the performance of the model are definitely influenced by the loading conditions applied. Some studies [11] [14] have been conducted for the evaluation of different loading modes: concentrated force and moment, use of muscular forces, but more frequently simulations are performed using a follower load, that is a tube-slider-cable mechanism in which the compression forces are transmitted along the vertebral centres. Follower load is considered as equivalent of the action of the weight forces of the spine, of the surrounding tissues and organs combined with the muscular action[54]. Overall these actions induce an axial compression of the column along its curvature. This simplification of the load is however subjected to criticism by authors like Wong. From his computations [49], Wong established that muscle forces play a non-negligible role for the stresses distribution in the vertebrae and suggested the necessity of modelling muscular complexity for fractures assessment, for the planning of surgical procedures or for the design of spinal devices. Generally the implementation of muscular components are believed to be difficult due to the presence of a great number of fascicles [11]. Moreover the choice of muscular forces is not an easy issue: the direct in-vivo measurements through EMG, very often, is not possible and the alternative is the use of an optimization algorithm but, in literature there is still no common method of choice. In this work, therefore, a careful analysis of the studies that implemented muscle components was first made, and then, the latter were integrated into the finite element model. First, the number of muscle fascicles involved in the studies was analyzed. As in most of the works [17] [12] [53] the choice was to implement a simplified number of fascicles. There are studies that implemented up to 180 beams [16] but complexity is not always indicative of greater reliabilty of the model. Subsequently, it was necessary to decide muscle allocation. At this stage of the thesis, the article

by Chuang et al. [18] was useful for processing. They, by means of a finite element model, simulate a quantity of muscles in line with expectations and also provide the spatial coordinates of those muscles. Unfortunately, they do not provide their location with respect to the spine. So the need was to re-adapt these coordinates to our model and find their distance from the spine. For this reason, it was decided to consider Stokes et al. [16]. Stokes, unlike Chuang, does not use a number of simplified fascicles but allows to determine their position with respect to vertebral centers. Therefore, thanks to the comparison between the muscle components of the two studies, it was possible to re-adapt the Chuang's coordinates to Stokes' spine and, subsequently, by further comparison between our spine and Stokes' one, it was possible to determine the muscle's position in the model. Subsequently, external loads similar to those in vivo had been created. The idea was to determine the weight force of each component involved and to apply it in appropriate points: the centers of mass. The model includes lumbar and sacral vertebrae, therefore, all the lumbar and overlying components contribute to a weight that is counterbalanced by muscles. For a better understanding, the following part has been subdivided. For the first part, or the lumbar one, with reference to the study by Pearsall et al. [19], the body has been separated into so many slices as the vertebrae and each has been assigned to a mass center and to a force weight. The second part includes anything above the lumbar spine: the chest, the head, the neck, the arms, and the compression of the thoracic muscles. It was decided to calculate a single equivalent weight force and moment by applying them to the center of L1. For this calculation, it is necessary to know the position of the entire spine subjected to gravitational load action. The choice was to consider the deformed spine of El-Rich et al. [21] since they, not only simulate standing, but, as stated by the authors themselves, the prescribed deformed posture is generally in agreement with sagittal profiles recorded

from different subjects rather than represent the profile of a single subject. Last but not least, muscular forces have been implemented in the model. First, the percentages of muscle activation in articles simulating standing were evaluated. Following an analysis of this data, appropriate activation values were chosen to be implemented in the model. In particular, Kiefer et al.[20] show activation rates that are consistent with the general trend of literature: greater activation on L4 and L5 levels and greater force values of lumbar multifidus than other muscles. Simulation campaigns were then conducted by varying the total force associated with the activation percentages. The last phase of this thesis is the critical analysis of the results obtained in terms of intradiscal pressure, lordosis, intervertebral rotations, angles between endplates and lumbosacral angle. These data were compared with in vivo, in vitro and numerical data in the literature. A further comparison was conducted with follower load's simulations in order to evaluate what was said earlier.

## 1.1 Structure of thesis

The thesis is structured as follows: The first chapter of the thesis deals with the state of the art. An initial anatomical and functional description of the spine opens the chapter and then passes to an exhibition of the various types of models and simulation in the literature. Next chapter deals with the materials and methods used. It describes the basic finite elements model (without muscles) and then presents the description of the work done in this thesis from the implementation of muscles, muscular forces and external loads. The third chapter outlines the results. The first results that are presented relate to simulations of the base model and are useful for understanding the possibilities and limits of this. The results of simulations with the musculo-skeletal model are then reported. Intradiscal

pressure, lordosis, intervertebral rotations, angles between endplates and lumbosacral angles are analyzed. Finally, in the last chapter, we evaluate the results obtained by analyzing them against the target and evaluating any future prospects. The appendices A and B, respectevely for chapters materials and methods and results, contain additional images and tables useful for implementing the exposed model.

# Chapter 2

# STATE OF THE ART

## 2.1 Anatomical and fucntional principles of the spine

### 2.1.1 Overview of the spine

In vertebrate animals, the spine is a flexible structure that extends from the skull to the pelvis. Its importance lays in several functions: it protects the spinal cord, transmits body weight, and in general provides stiffness for the body, acting a primary role in movements. The spine is generally composed of thirty-three irregular bony structures called vertebrae. These are mainly composed of bone and hyaline cartilage, in proportions that vary along the spine length. As shown in figure 2.1 the vertebrae are divided into cervical (C1-C7), thoracic (T1-T12), lumbar (L1-L5), sacral (S1-S5) and coccygeal (Co1-Co3/Co5). The sacral (S1-S5) and the coccygeal vertebrae are positioned in the lowest part of the spine and are generally fused together and unable to move independently.

For each level, the vertebrae have different shapes and dimensions according to their function, position and loading: this allows optimal weight distribution and increases the overall efficiency of the spine.
The cervical vertebrae are the smallest ones and they have the role of sup-

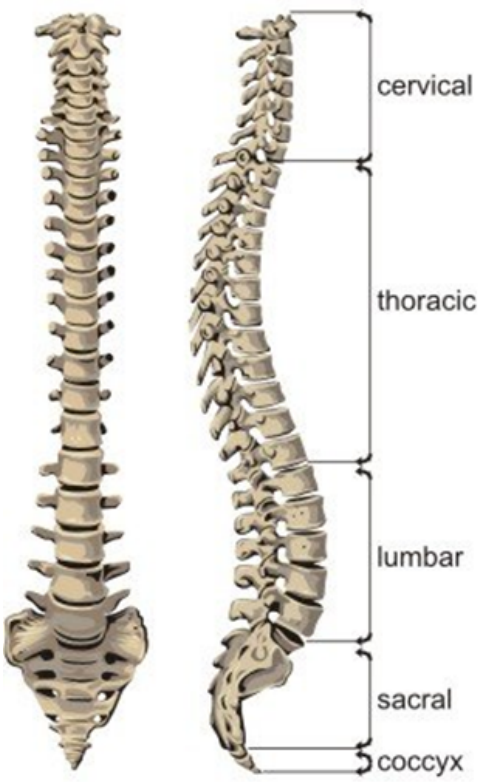


*Figure 2.1: Sagittal view of the spine [1]*

porting the skull and protecting the brainstem and the spinal cord. Their structure allows great motion to neck and head.

The thoracic vertebrae are linked to ribs that articulate with the transverse process. Their dimensions increase from T1 to T12. They are larger than the cervical vertebrae and their spinous process is longer. The presence of the ribcage limits the movement of these vertebrae but makes them more stable and increases the thoracic spine's resistance.

The lumbar vertebrae carry more weight than the others. They are the largest and more robust spinal bones and can guarantee a wide range of motion in all directions: they allow flexion and extension in the sagittal plane, lateral bending in the frontal plane and axial rotation in the transverse plane.

The sacral spine is located behind the pelvis, between the two hip bones, and connects the spine to the pelvis. Finally, the coccyx or tailbone is composed of three, four or five vertebrae (depending on subjects) that are fused together.

As in this thesis is focused on the lumbar section of the spine, a brief description of this is provided. The lumbar vertebrae are five and their dimensions increase downwards, but the anatomy remains quite similar: as the other vertebrae, they are composed of a vertebral body, a vertebral arch, and posterior bony processes (fig. 2.2). The vertebral body is massive, and its transverse diameter is larger than the distance between the front and the back; the anterior part is thicker than the posterior one and both the upper and lower endplates (that are in contact with the intervertebral discs) are concave. It is made of cancellous bone, that is a porous tissue, surrounded by a layer of cortical bone, more compact and harder than the previous one. The intervertebral discs are placed between two adjacent vertebrae. Their function is to absorb the shocks as they are a fibrocartilaginous joint: the external part, called annulus fibrosus, is made of relatively stiff radial lamellae made of collagen fibers that can sustain compressive forces and tensile forces in all directions. The internal part, instead, is called nucleus polposus and it assures a distribution of pressure along the whole disc. Also the nucleus can withstands compression forces thanks to its gel-like matter filled with proteoglycans, collagen, and a large amount of water.

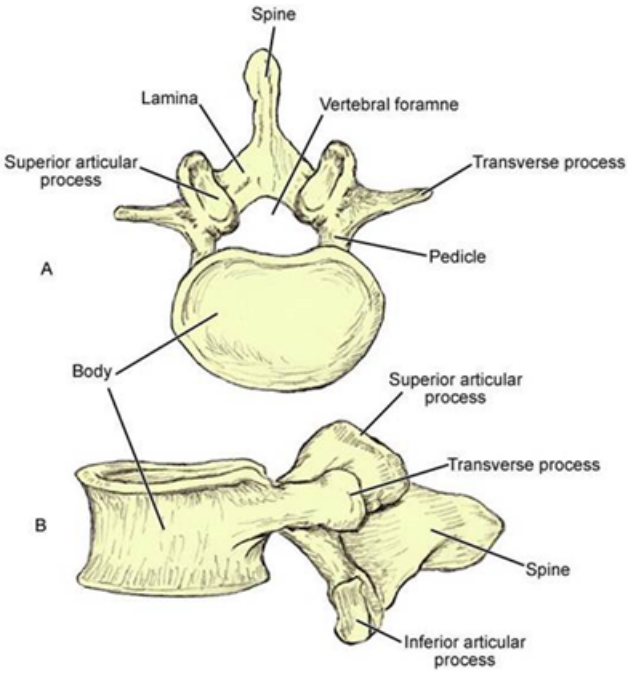


*Figure 2.2: Sagittal and transverse view of a lumbar vertebra [2]*

The vertebral arch, positioned posteriorly with respect to the vertebral body, is composed of two pedicles, two laminae and seven bony processes: one spinous process, four articular processes and two transverse processes that are linked together by facet joints and ligaments. This part of the vertebrae is characterized by a complex geometry aimed at providing several functions, so here is presented more precise description of it:

- Pedicles: the two pedicles, one for each side, are short and thick stubs of hard bone; they act like a bridge between the anterior and posterior part of the vertebra;

- Laminae: the two laminae are strong and large, they extend posteromedially from the pedicles and form a roof for the spinal canal, providing support and protection for the spinal cord. The ligament flava attaches to the upper surface of the lamina. This ligament connects adjacent laminae through all the spine;

- Spinous process: the spinous process is the most posterior part of the vertebral arch and it is perpendicular to the laminae. It is broad, thick and it extends horizontally. The spinous processes of two vertebrae join together through the ligaments, and they are important for muscles attachment;

- Transverse process: the transverse processes are located laterally, between the pedicles and the lamina. Several muscles and ligaments attach directy on them;

- Vertebral foramen: between the vertebral body and the vertebral arch there is located the vertebral foramen, an opening crossed by the spinal cord. It is triangular and larger than the thoracic one but smaller than the cervical one. It provides support and protection for the spinal nerves and the blood vessels that pass through it;

- Facet joints: facet joints are synovial joints between the inferior articular process and the superior articular process of the lower vertebra. They are surrounded by a capsule of connective tissue which covers the joint and produce the lubricant: the synovial fluid. The synovial fluid has the important role of making the joint frictionless as much as possible.

### 2.1.2 Curvature of the spine

Lordosis comes from the Greek word *lordōsis*, 'bent backward' and it is the normal inward curvature of the lumbar spine. For the evaluation of lordosis, the lumbar lordotic angle (LA) value is used (fig. 2.3). There are many controversies related to its evaluation, but in general it is the angle between the superior endplate of the first lumbar vertebra and the superior endplate of the first sacral vertebra [55]. It can be assessed form X-ray imaging, performed on the subject in standing position, when the spine tends to assume

its physiological optimal profile.


*Figure 2.3: Lumbar lordosis evaluated with the lordotic angle (LA) [3]*

Another variable of interest related to lumbar lordosis is the sacral angle (SA): this is calculated on the lumbosacral joint, located between the fifth lumbar vertebra and the first sacral segment. The sacral angle is the angle between the first sacral vertebra and the horizontal line, measured in the sagittal plane.
In healthy adults, this is about 30 degrees [56]. If the lumbar lordosis increases, the lumbosacral angle increases as well, and so do the stresses at the lumbosacral joint. Lower spine disorders may occur when lumbar lordosis is too accentuated, thus resulting in back pain.

### 2.1.3 Ligaments of the lumbar spine

Ligaments are strong fibrous bands that stabilize the spine and prevent it from excessive motion. The ligaments in the lumbar spine are the supraspinous, that terminates at L4 or L3, the intertransverse, the interspinous, the anterior and posterior longitudinal ligaments, the iliolumbar and the ligament flavum (fig. 2.4). Each ligament has a specific function: the anterior

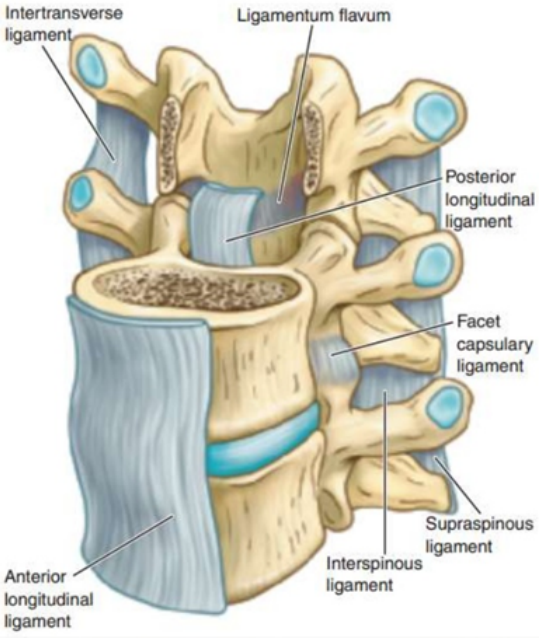


*Figure 2.4: Overview of the ligaments of lumbar vertabrae [4]*

longitudinal ligament limits extension, while the posterior longitudinal, the ligamentum flavum, the supraspinous and the interspinous ligaments limit forward flexion; the intertransverse ligament limits contralateral lateral flexion and the iliolumbar ligaments opposes to anterior sliding of L5 and S1 [4].

### 2.1.4 Muscles of the lumbar spine

In general, muscles are made of bundles of fibers grouped into fascicles; in skeletal muscles, these attach to bones through specific collagen fibers called tendons. Skeletal muscles are striated and innervated by the somatic nervous system under voluntary control. The nervous impulse originates from the brain and travels through the spinal cord towards the muscle. As a response to the stimulus, the muscle contracts or relaxes. A muscle is defined synergist if it helps the so-called agonist to carry out the movement associated, or neutralizer if it holds a bone allowing the action of the ago-

nist, or antagonist if it contracts when the other relaxes and vice versa.
An important role is assigned to spinal muscles: they are responsible for the movement of the spine and the stability of it. In absence of muscles, the osteoligamentous spine would not be able to bear compressive loads and, as shown from evidences, the spine would buckle under a critical load much lower than the loads expected in vivo [57]. Muscles are classified according to the associated movement and function they provide, such as extension, flexion and rotation. In general, anterior flexors, located anteriorly, enable lifting objects and arching of the lower back; lateral flexors, located laterally as rotators, help keeping the adequate posture, and, finally extensors, located posteriorly, allow standing and lifting. Lumbar muscles are spinal muscles that act on the lumbar portion of the spine; their architecture is complex, and they contribute to the stability of the spine together with the thoracic, cervical and abdominal muscles. These last are divided into three layers: the external oblique, the internal oblique and the transversus abdominal. Moreover, the rectus abdominis is located anteriorly, to complete the overall action of abdominal musculature. In figure 2.5 is shown a cross-sectional view of the trunk, where the multitude of muscles present in the trunk can be seen.

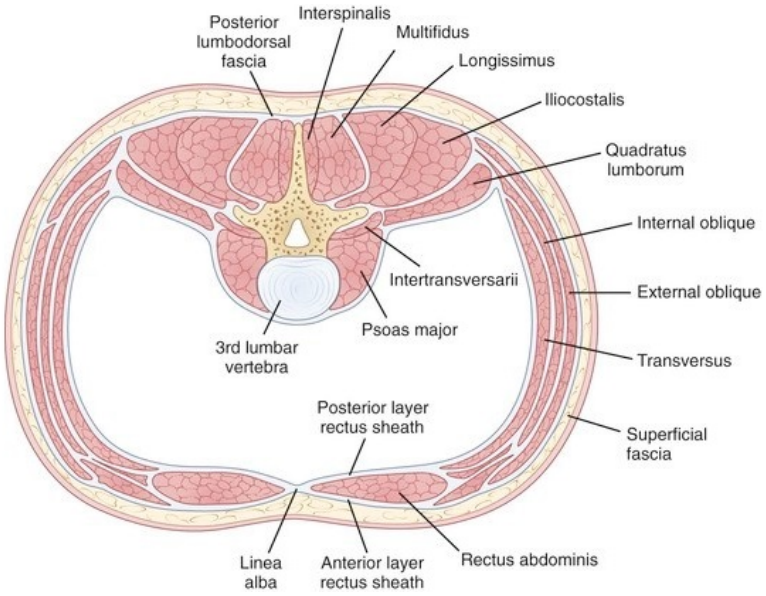


*Figure 2.5: Cross-sectional view of the thorax taken at the L3 level; here all muscles acting on the spine and their positioning can be observed [5]*

Now a focus on the anatomy and function of the main muscles involved in lumbar spine stability and motion is presented:

- Lumbar multifidus: it is a thin and long muscle that extends through the whole spine. It originates in the sacrum, in the iliac spine, in the mammillary processes of the lumbar vertebrae, in the transverse processes of the thoracic ones and in the articular processes of the cervical vertebrae [58]. It is the largest of the lumbar back muscles, composed of several fascicles (fig. 2.6). The shortest ones originate in the caudal end of the dorsal surface of the vertebral lamina and insert in the mammillary process of the two vertebrae below with the exception for the fascicle on L5 that is anchored on the sacrum. The largest fascicles of multifidus are divided into five groups, one for each lumbar vertebra. Each fascicle starts from the spinous process of the considered vertebra and radiates towards the mammillary processes of the vertebrae below, the sacrum and the iliac crest. The function of the

multifidus can be explained by decomposing its line of action: a short horizontal and a long vertical vector can be defined. Therefore, it provides posterior sagittal rotation of each vertebra using the spinous process as a lever. It also has a role as a stabilizer of the spine during horizontal rotation of the trunk: it opposes to the flexion caused by the contraction of the abdominal muscles that produce rotation;

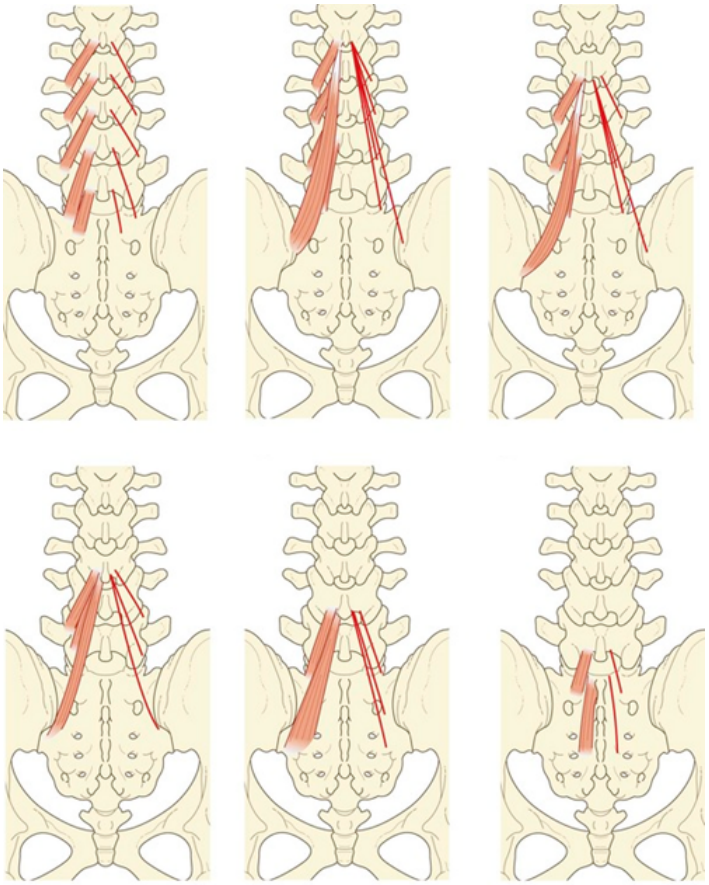

*Figure 2.6: The lumbar multifidus is composed of several fasciles, each acting on the vertebrae with different orientations; here some of them are highlighted, together with their lines of action [6]*

- Longissimus pars lumborum: five fascicles can be identified for this muscle, one for each vertebra. Their origin site extends from the accessory process to the medial end of the dorsal surface of the trans-

verse process. The insertion site is instead located on the sacrum. The fibers of L1, L2, L3, L4 converge to the lumbar intermuscular aponeurosis, a tendon that attaches to the ilium near the L5 fibers insertion area. The line of action of the fascicles can be divided into two vectors: a horizontal and a vertical component. The combined action is intended for providing extension and rotation: the horizontal vector of the longissimus produces a posterior translation along with a lateral flexion or a posterior sagittal rotation, given by the vertical vector, when a unilateral contraction or bilateral contraction occurs, respectively. It can be noticed that the posterior sagittal rotation given by this muscle is lesser than the one provided by the multifidus due to its shorter lever arms [59];

- Iliocostalis pars lumborum: it is composed of four fascicles that originate on the tip of the transverse process of the L1, L2, L3, and L4 and insert in the iliac crest. The fibers are arranged slightly more laterally than the longissimus ones. As this last muscle, iliocostalis provides posterior sagittal rotation or lateral flexion and posterior translation mainly for the lower vertebrae. These fascicles are also responsible for the axial rotation of the lumbar spine using the transverse process as a lever. As it produces axial rotation combined with posterior sagittal rotation, it helps multifidus opposing the flexion caused by the abdominal muscles [59];

- Psoas major: also reffered to simply as iliopsoas, it is a long and fusiform muscle that originates from the lesser trochanter of the femur and inserts in the anterolateral part of the spine, from T12 to L5 (fig. 2.7). It is anchored to the medial three-quarters of the anterior surface of the transverse process, to the intervertebral disc, and to the upper part of the vertebral bodies. Near the disc, instead, the

more medial fibers attach directly to the upper margin of the vertebral body. Its main function is to flex the thigh at the hip joint and the spine. It has eleven fascicles whose line of action was defined by Bogduk et al. [7], Yazdani-Ardakani et al. [60], Dumas et al. [61] and Stokes et al. [16] as the line from the vertebral attachment site towards a point, similar for all the lines. That point is anterior to the iliopubic eminence where the tendon passes over the ilium and curves toward the lesser trocanther [62]. Biomechanical analysis showed that it has a low influence on the flexion of the spine: the position of its fibers are close to the axes of rotation of the vertebrae, so that only small moments can be created even at the maximum contraction. Its main influence is the compression of the lower vertebrae. [62] [7]. In literature, the role of this muscle is generally controversial: some authors found that it acts as stabilizer of the lordosis during upright standing position [63] and other that it has no action during this activity [64]; some think that it is a lateral flexor of the spine [65], [64], others that acts as a controller during walking [66];

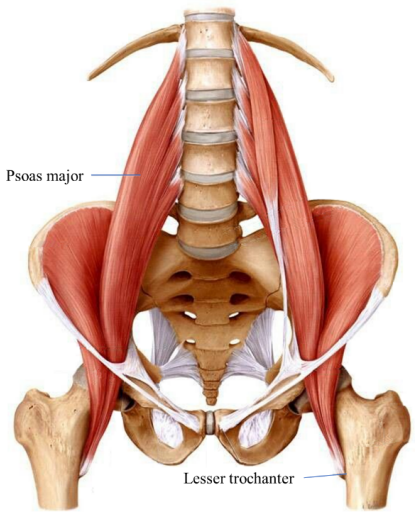


*Figure 2.7: The iliopsoas action involves both the lumbar spine and the femur [**?** ]*

- Quadratus lumborum: it is a wide rectangular muscle with a very complex structure that connects the lumbar transverse processes, the ilium and the 12th rib. It can be divided into four types of fascicles (fig. 2.8):

  - The iliocostal fibers that start in the ilium and finish in the 12th rib (fig. 2.8 C);
  - The lumbocostal fibers that connect the lumbar transverse processes and the 12th rib (fig. 2.8 B);
  - The last fascicle that connects the lumbar transverse process and the body of the 12th thoracic vertebra(fig. 2.8 A).

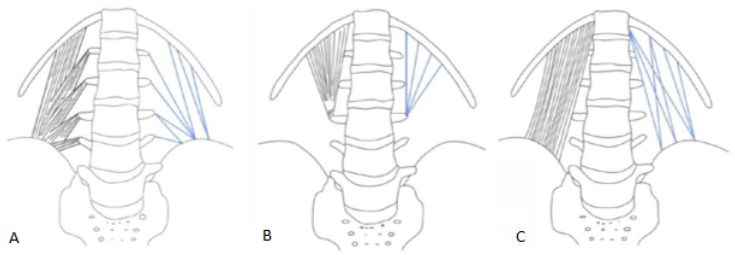


*Figure 2.8: Location of the different fascicles composing quadratus lumborum [7]*

The quadratus lumborum fascicles, with particular attachments can change considerably from subject to subject, as well as the they can considerably vary in size. The precise function of the quadratus lumborum is not yet well known due to its irregular and variable structure, but it is involved in many roles. The presence of a large amount of fibers on the 12th rib is thought to fix it during respiration, but the majority of the fibers, the largest ones, are the iliolumbar and iliocostal ones; the main function of this muscle is then associated with the role of these fibers that provide lateral flexion of the spine. They are also potential extensor of the spine but their associated moment is limited with respect to its lateral flexion capability and is less than

the extensor moment generated by the posterior back muscles;

- Interspinalis: these are short muscles that anchor to the spinous process of adjacent lumbar vertebrae. They produce posterior sagittal rotation of the spine, but the force they generate is small;

- Intertransversarii mediales and lateralis: as the interspinales they are very small muscles and they allow lateral flexion of the spine and posterior sagittal rotation.

As it can be seen from the figure 2.9, interspinalis and intertransversarii provide a low contribution in the spinal motion due to their limited length as their value lies not in the force they can exert, but in the muscle spindles they contain [7]. In fact it is suggested that their major function is to act as large proprioceptive transducers [7].

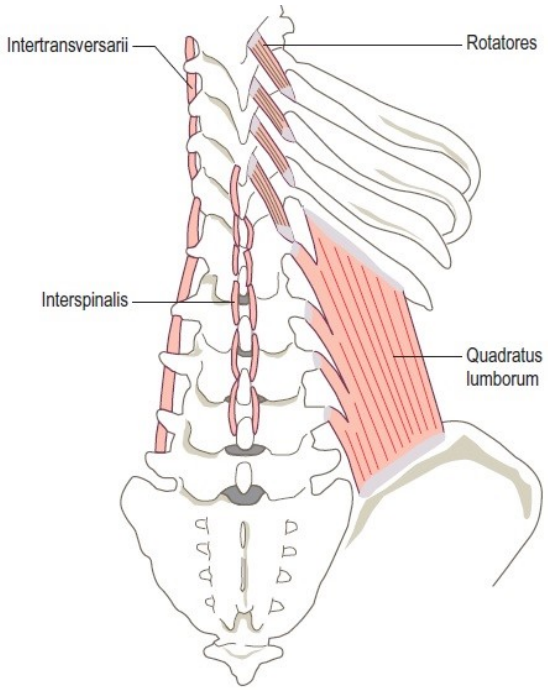


*Figure 2.9: Posterior view of the spine, highlighting the position of the quadratus lumborum, interspinalis and intertransversarii muscles [8]*

## 2.2 Modelling methods for the spine

Biomedical engineering makes wide use of models for experimentations. The reliability of a model is then of critical importance to guarantee that results can truly reflect in-vivo behaviours. A suitable model for the spine can be employed for several aims, ranging from the study of the spine biomechanics, to the analysis of both the effects of a pathology and the consequent surgery interventions. In the past both experimental and numerical models have been developed; the former often derives from human cadaver explants [31] [67] [68], while the latter is commonly a beam-rigid or finite element approach. In recent years this last has established as one of the most reliable method, due to its high repeatability and cost efficiency [13].

### 2.2.1 In-vitro testing

At first, a review on in-vitro testing, that represent the first attempts to study the spine biomechanics, has to be made, as many of the data obtained in such a way has been subsequently used for validation of numerical models.

A setup for experimental tests generally consists of two or more vertebral levels explanted from human cadaver, so that all bony elements, intervertebral discs and ligaments remain intact, while removing all the other soft tissue [69]. For the study of the lumbar spine in particular, a typical specimen extends form the first to the fifth lumbar vertebrae, possibly including also part of the sacrum. The lower part of the structure is mounted rigidly to the frame of the tester, while the upper endplate of L1 is fixed to a rigid plate (fig. 2.10). This last, when loaded, allows forces and moments to redistribute among the spinal levels, causing motion to the sample.

The test apparatus is typically equipped with transducers to register

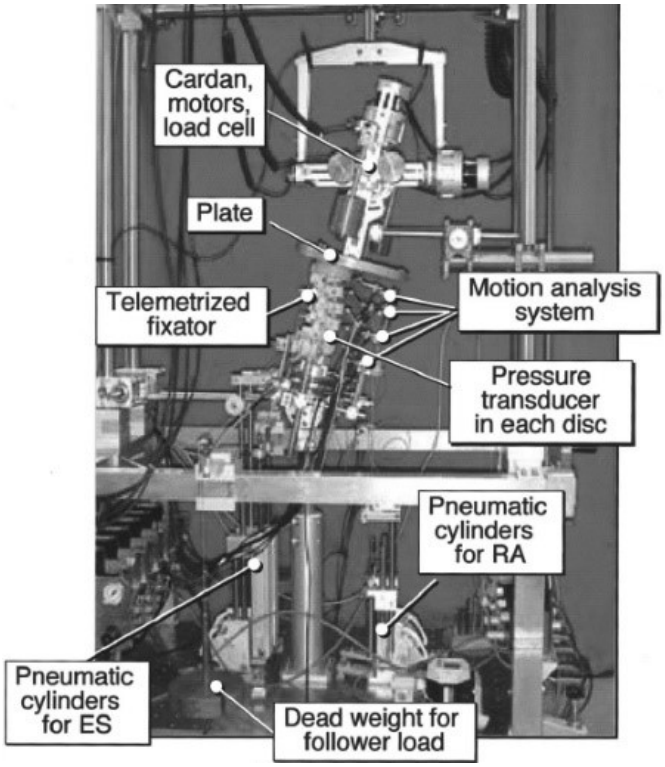


*Figure 2.10: In-vitro testing setup, as used in [9]*

some variables of interest for the problem. Kinematics is the main aspect to be investigated and so relative displacements between the vertebrae are monitored and the consequent range of motion (ROM) calculated. Moreover, effects on the intervertebral discs are of great importance and so IDP (intervertebral disc pressure) are obtained through a set of pressure transducers positioned inside the nucleus pulposus. With the appropriate loading and boundary conditions, through this setup it is possible to simulate different situations and to load the spine similarly to how it would happen in-vivo. A combination of forces and moments can reproduce the following movements (fig. 2.11):

- Flexion/extension: if the resultant moment is applied about the medio-lateral direction (in the sagittal plane);

- Lateral bending (left and right): if the resultant moment is applied about the antero-posterior direction (in the frontal plane);
- Axial rotation (left and right): if the resultant moment is applied about the vertical axis (in the transverse plane).

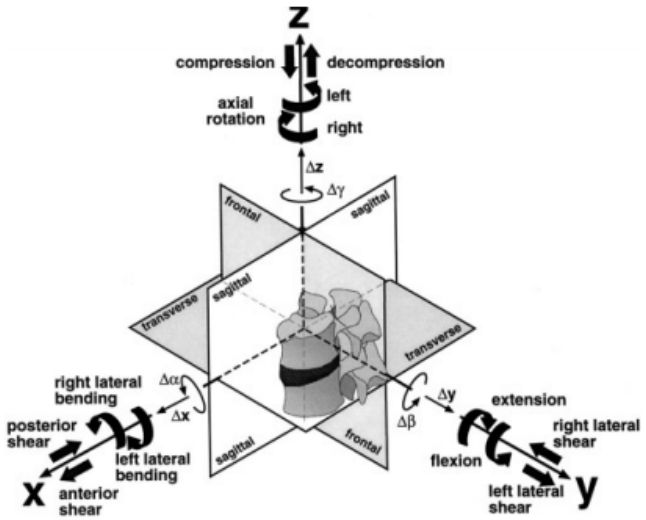


*Figure 2.11: Translations and roations in the 3-D space that can be reproduced on the spine [10]*

These situations can be achieved with the application of pure moments alone, or together with shear and compressive forces [14] and the magnitude of the chosen loads could be selected to cover up to the maximum range of motion obtainable without causing any injury to the involved structure [31]. Such loading conditions are aimed at simulating the real stresses the spine is subjected to in-vivo: in every moment in fact the human body is subjected to a certain load, mainly deriving from gravity, which means that, in absence of ad adequate structure, all anatomical segments would collapse to the ground. The main role of the spine is to provide sustain for the whole body, working in synergy with the trunk muscles, guaranteeing a correct posture and acting to obtain the desired motion

in the three-dimensional space. In addition to the aforementioned motions, also standing can be reproduced; the loading conditions for this situation are often provided by the application of a follower load. This is a purely compressive force that follows the curvature of the spine maintaining, for each vertebral joint, its direction parallel to the joining the centroids of two adjacent vertebrae. The result of applying such a load, is to compress the spine and to only slightly modify the lumbar lordosis [11]. The application of a follower load is experimentally achieved by transmitting a force via a cable passing through the vertebrae centres, appropriately defined.
All the cited testing methodologies are able to reproduce several conditions, but include an implicit simplification: the applied loads are intended to represent the overall action of both gravity and muscle forces at once. In reality the action of trunk musculature, that is of primary importance for spinal stability, is much more complex, due to the multitude of local fascicles and the several lines of action of them. On the other hand, recreating a suitable experimental setup that incudes muscles is not trivial, and so very few are the attempts made in this direction [70] [71].

### 2.2.2 Numerical studies

Numerical investigation for spinal applications is a powerful tool, as it overcomes several complications related to just treated experimental procedures. Also, a numerical model allows a parametric study, useful for isolating the effect of a specific variable on a certain phenomenon. For these reasons, several research groups around the world have developed their own finite element model of the spine.

This kind of model must reproduce as close as possible all the characteristics of a real spine, in terms of material properties, geometry, parts interaction and loading conditions (fig. 2.12). It is easy to see that the result will not be a simple model, as it is intended to reproduce a complex struc-

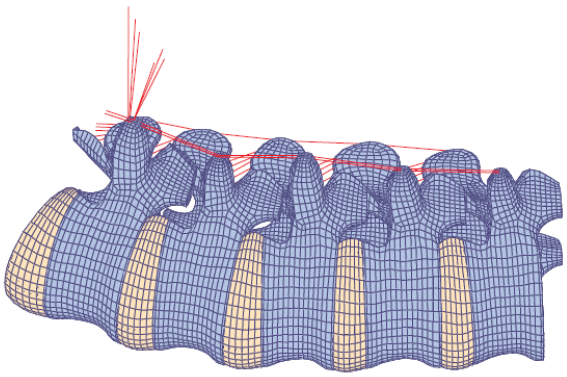

*Figure 2.12: Example of a finite elements model of the spine [11]*

ture by itself, but also because of the difficulty of collecting precise data on the spine. In fact, it must be considered the great inter-subject variability of this, that may differ because of age, gender, height, pathological condition and many other aspects between patients [13] [55]. Thus, a unique geometries and mechanical properties for the model cannot be identified as perfectly representative of the whole population, although in general acceptable for the intended purposes.

The complexity of any finite element model (FEM) depends on the specific aspect it is meant to describe. Highly complex FEM describing only one vertebra or few functional spinal units (FSUs) could be used to investigate, for instance, the failure mechanisms involving damage at trabeculae-cement interface for augmented vertebrae [72]. Bigger models, comprehensive of all the lumbar vertebrae, are instead used to study pathologies and surgery effects on the spine. Also in this case different methodologies exist: if the kinematic alone is to be studied, a solution is to create a simplified multi-segmental structure [12]. With this approach, the complex geometry of the spinal structure, as well as their precise material properties, are neglected: the overall shape of the spine is represented by a series of rigid beams, each representing a single vertebra, connected through deformable elements that act as the intervertebral disc would do, allow-

ing relative rotations between the segments (fig. 2.13). Applying loads to this beam-rigid body model allows to study the displacements of the spine, with non-negligible approximation, but with much reduced computational effort.

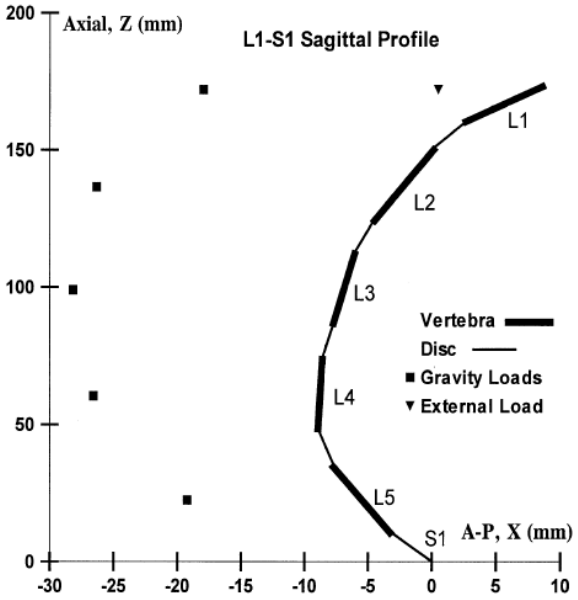


*Figure 2.13: A simplified beam-rigid body model; the points anterior to the spine represent where the gravity forces are applied [12]*

When higher precision is required and if some other variables are needed as an output form the model, the building of a model more representative of reality is made. In this case details on the various involved elements are needed and so, for the reconstruction of the spine, anatomy-matching approaches have been followed, based on in-vivo imaging (typically CT-scan) [73] [74] [75] [13]. Though the modelling techniques may vary between studies, a general trend can be found between models available in literature; most commonly, the spinal structure is divided in the following elements:

- Vertebral body: composed of a cortical bone shell, a cancellous bone

interior part and a superior and an inferior endplate;

- Posterior vertebral elements: these include all bony elements posterior to the vertebral body, and are modelized with mechanical properties that differ from the anterior bony structures;
- Intervertebral disc: composed of the inner nucleus pulposus, surrounded by the annulus fibrosus, whose combined properties show much lower rigidity than the vertebrae;
- Facet cartilage: this are typically built so that, in an undeformed configuration they present a 5 mm distance, and under specific loading condition come in contact generating a local contact force;
- Ligaments: the complex ligamentous structure is modelled as a set of springs whose extremities coincide with the anatomical location of insertions and origins.

A recent review of some amongst the most acknowledged models available in literature [13] collected the material properties implemented in these (fig. 2.14). A table reassuming these data is presented in 2.15.

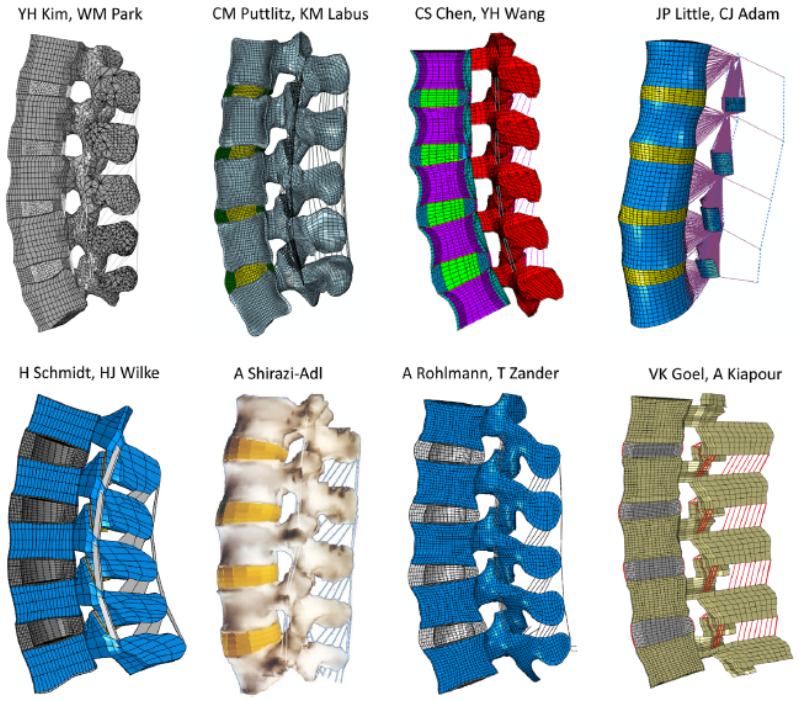


*Figure 2.14: Eight Finite Elements models analized by Dreischarf in his study [13]*

**Table 1**
Mechanical properties of different finite element models.

| Component | Kim and Park | Puttlitz and Labus | Chen and Wang | Little and Adam | Schmidt and Wilke | Shirazi-Adl | Rohlmann and Zander | Goel and Kiapour |
|---|---|---|---|---|---|---|---|---|
| Cortical bone | $E$=12,000 MPa<br>$\nu$=0.3 | $E_{11}$=8000 MPa<br>$E_{22}$=8000 MPa<br>$E_{33}$=12,000 MPa<br>$\nu_1$=0.4<br>$\nu_2$=0.35<br>$\nu_3$=0.3 | $E_1$=22,000 MPa<br>$E_2$=11,300 MPa<br>$\nu_1$=0.484<br>$\nu_2$=0.203 | $E$=11,300 MPa<br>$\nu$=0.2 | $E_1$=22,000 MPa<br>$E_2$=11,300 MPa<br>$\nu_1$=0.484<br>$\nu_2$=0.203 | Rigid | $E$=10,000 MPa<br>$\nu$=0.3 | $E$=12,000 MPa<br>$\nu$=0.3 |
| Cancellous bone | $E$=100 MPa<br>$\nu$=0.2 | Based on CT images | $E_1$=200 MPa<br>$E_2$=140 MPa<br>$\nu_1$=0.45<br>$\nu_2$=0.315 | $E$=140 MPa<br>$\nu$=0.2 | $E_1$=200 MPa<br>$E_2$=140 MPa<br>$\nu_1$=0.45<br>$\nu_2$=0.315 | Rigid | $E_1$=200 MPa<br>$E_2$=140 MPa<br>$\nu_1$=0.45<br>$\nu_2$=0.315 | $E$=100 MPa<br>$\nu$=0.2 |
| Posterior bony elements | $E$=3500 MPa<br>$\nu$=0.25 | $E$=3500 MPa<br>$\nu$=0.3 | $E$=3500 MPa<br>$\nu$=0.25 | Quasi-rigid | $E$=3500 MPa<br>$\nu$=0.25 | Rigid, attached to vertebral body by two deformable beams | $E$=3500 MPa<br>$\nu$=0.25 | $E$=3500 MPa<br>$\nu$=0.25 |
| Ground substance of annulus bulk | Hyperelastic<br>Mooney-Rivlin<br>$c_1$=0.18<br>$c_2$=0.045 | HyperelasticYeoh<br>$c_{10}$=0.0146<br>$c_{20}$=−0.0189<br>$c_{30}$=0.041 | Hyperelastic<br>Mooney-Rivlin<br>$c_1$=0.42<br>$c_2$=0.105 | Hyperelastic<br>Mooney-Rivlin<br>$c_1$=0.7<br>$c_2$=0.2 | Hyperelastic<br>Mooney-Rivlin<br>$c_1$=0.56<br>$c_2$=0.14 | Linear hypoelastic<br>$E$=4.2 MPa<br>$\nu$=0.45 | Hyperelastic<br>Neo-Hookean<br>$c_1$=0.3448<br>$c_2$=0.3 | Hyperelastic<br>Neo-Hookean<br>$c_1$=0.3448<br>$c_2$=0.3 |
| Nucleus pulposus | Incompressible fluid-filled cavity | $E$=1.0 MPa<br>$\nu$=0.49 | Incompressible fluid | Incompressible fluid | Incompressible fluid-filled cavity | Incompressible fluid | Incompressible fluid-filled cavity | Incompressible fluid |
| Fibers of annulus | Non-linear, dependant on distance from disc center, 6 layers - criss-cross pattern, | Non-linear, two families of fibers<br>$A_3$=0.03 (MPa)<br>$b_3$=120.0 (unitless) | Non-linear, 12 layers -criss-cross pattern, | Tension-only, embedded linear elastic elements, 8 layers with alternating orientation | Non-linear stress-strain curve ,<br>16 layers - criss-cross pattern | 8 layers of fiber-reinforced membranes with through annulus depth-dependent thickness and nonlinear | Non-linear, dependant on distance from disc center, 14 layers – criss-cross pattern | 8 layers of fiber-reinforced continuum elements with criss-cross pattern |
| Ligaments | Non-linear stress-strain curve | Exponential force-displacement curves | Linear stress-strain curve | Piecewise nonlinear elastic with individual ligament lengths at each spinal level | Non-linear stress-strain curve | Collection of uniaxial elements with nonlinear properties | Non-linear stress-strain curve | Uniaxial 2D elements with theoretically defined cross-sectional area with nonlinear hypoelastic properties |
| Cartilage of facet joints | Hard frictionless contact, Young's Modulus: 11 MPa, Poisson's ratio: 0.4, Initial gap: 0.5 mm | neo-Hookean,<br>$c_{10}$=2 | Soft contact, Friction coef: 0.1,<br>Initial gap: 0.5 mm | Finite-sliding, frictionless tangential contact with 'softened', exponential normal contact,<br>Initial gap: 0.8 mm | Hard frictionless contact, Young's Modulus: 35 MPa, Poisson's ratio: 0.4<br>Initial gap: 0.4 mm | Soft frictionless contact with variable gap distances and a gap limit for contact initiation of 1.25 mm | Soft frictionless contact,Initial gap: 0.5 mm | Soft frictionless contact using gap elements with initial clearance of 0.5 mm |
| Employed data for validation | Panjabi et al. (1994)<br>Guan et al. (2007) | Panjabi et al. (1994)<br>Niosi et al. (2008)<br>Sawa and Crawford (2008) Ayturk (2007) | Atlas and Deyo (2001)<br>Lin et al. (2013)<br>McMillan et al. (1996)<br>Yamamoto et al. (1989)<br>Shirazi-Adl (1994c)<br>Chen et al. (2001) | Pearcy (1985)<br>Nachemson (1960) | Heuer et al. (2007b)<br>Heuer et al. (2007a)<br>Rohlmann et al. (2001b) Heuer et al. (2008) | Shirazi-Adl (1994b)<br>Shirazi-Adl (1994c) | Heuer et al. (2007b)<br>Brinckmann and Grootenboer (1991)<br>Rohlmann et al. (2001b) Wilson et al. (2006) Rohlmann et al. (2001a) Wilke et al. (2003) | Kiapour and Goel (2009) Goel et al. (2005)<br>Goel et al. (2007)<br>Kiapour et al. (2012b) |
| Solver | Abaqus 6.10[a] | Abaqus 6.11[a] | ANSYS 11.0[b] | Abaqus 6.9.1[a] | Abaqus 6.10[a] | In-house FE solver | Abaqus 6.10[a] | Abaqus 6.10[a] |

*Figure 2.15: Material properties for the models considered in [13]*

### 2.2.3 Loads for finite element models

In general, a numerical model is able to represent different scenarios with relative simplicity, proving to be more flexible than an experimental one [14]. In particular, comparison between several loading conditions can be made with lower time costs, and always higher complexities can be added to the model. According to this, to better understand the choices made for numerical simulations, more detailed considerations on the acting loads can be made.

The lumbar section of the spine supports the weight of all the above segments: head, neck, the two upper extremities and both the cervical and thoracic parts of the torso. Data on the relative weight of these can be found in literature [76]. An even further partitioning can be made, dividing the total mass of the torso in horizontal slices corresponding to each vertebral, whose inertial properties has been calculated by Pearsall et al. [19]. The effect of the upper body weight distribution results in a vertical gravity force that acts slightly anteriorly to the spine and that would cause flexion to the spine (with reference to figure 2.13, in each point anterior to the spine, representing a specific centre of mass, a vertical force is applied). Here lays the importance of the trunk muscles, as their activation acts as a counterpoise to gravity, re-extending the spine during standing. In the case muscular activity is intended to generate movement of the body, the force magnitude of the single muscles will change, and some districts will result more involved than others. As for experimental studies, also in finite elements analysis modelling of the spinal musculature is complex, in particular because of the choice of the fascicles to be included in the model and of their exact positioning. In fact, in many cases, loads have been simulated similarly to those applied in-vitro, using different forces and moments to compress the spine and to reproduce movements. The combinations of these vary depending on the situation to be simulated.

### 2.2.4 Simulations for standing conditions

This kind of simulations is aimed at representing a standing condition, with the subject in neutral posture and the spine assuming a physiological curvature, that result in a slightly more emphasized that in supine lying.
We summarize the modelling methods that appear in literature, when such a posture is to be simulated with models not comphensive of muscles, referring to the study carried on by Rohlmann et al. [11], who tested different loading and boundary conditions for standing on a finite element model. Figure 2.16 shows the possibilities for such simulations: modes a, b and c consist in the application of a vertical force that results mainly in compression, coupled with different constraints imposed on the top of L1 (angular, translational and both constraints). Compression is also obtained by applying the force via a rigid wedged fixture (mode d) or with a follower-load (mode e) defined as it was for in-vitro tests. Notice that, in general, for numerical studies the application of a follower load of 500 N is a very common choice, as it is considered a simple and repeatable way of estimating the total loads acting on the spine, and due to the good results it has proven to return, if compared to experimental data [11]. A different approach is instead mode f, in which a follower-load together with an eccentric vertical force produce a compression and a flexion of the spine, while a rough approximation of the erector muscles (a force applied posteriorly to the spine) acts to extend the structure.

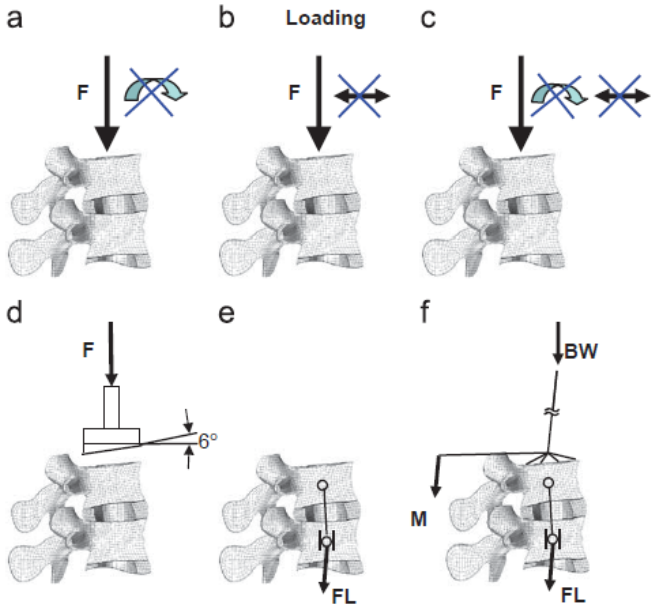


*Figure 2.16: Loading conditions tested by Rohlmann [11]*

### 2.2.5 Simulations for upper body bending

Interesting for studying the stress the spine is subjected to in everyday life are all the movements that imply a change in posture, often performed by high level of activation of the whole trunk muscles. For flexion and extension we refer to a study performed again by Rohlmann et al. [14]. As shown in figure 2.17, in which loading conditions for flexion are represented, bending can be achieved with the application of forces and moments. Forces are similar to those applied for standing, but the intervention of abdominal muscles occur in this case to flex the spine [77]. Being these muscles anteriorly positioned with respect to the spine, their resultant effect is simulated with a flexion moment applied on the top of L1 in modes A, C and D. in the remaining ones forces are applied with lever arms and magnitudes such that the equivalent moment calculated on L1 result again in flexion.

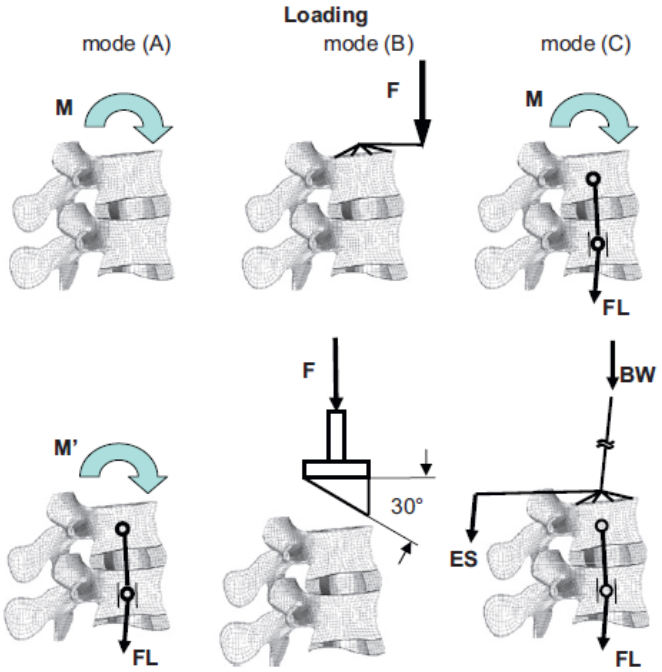


*Figure 2.17: Six different modalities for obtaining upper body bending, as performed by Rohlmann et al. [14]*

In the end, Rohlmann concluded that for optimal results in terms of kinematic and pressures within the discs, the introduction of a force simulating muscles contribution is to be preferred; on the other hand also the simpler condition with pure moment and follower load provided acceptable results.

### 2.2.6 Modelling of the spinal musculature

Adding trunk musculature to a finite element model increases the degree of complexity of the study, but can be very interesting for research aims. On the one hand authors have been discouraged in applying muscle loads, as data on the spinal musculature activation are hard to obtain from in-vivo measurements without incurring in ethical issues. On the other hand, muscle-comprehensive models are believed to provide better data [78]. Co-

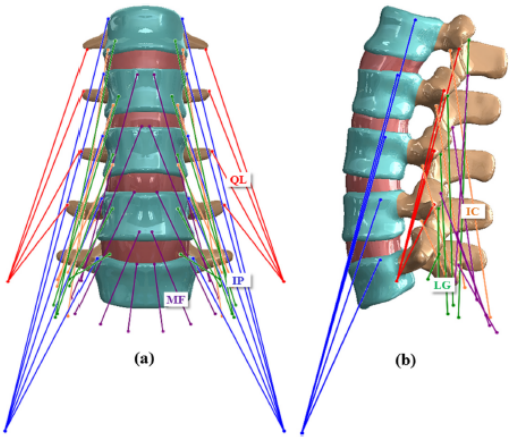


*Figure 2.18: A typical choice for spinale muscles modelling, with the inclusion of the five aforementioned groups [15]*

ordinates for muscles positioning are taken form anatomic descriptions [78] but for the numerical reconstruction several factors must be considered: first, more muscles act on the same vertebral level, each with different direction, length and cross-sectional area. Moreover, a single muscle consists of more than one fascicle, that in turn are oriented differently in space. Including every existing fascicle in the model is hardly a feasible approach, so a selection of the most influential ones has to be made. In most studies, authors chose to reproduce five muscle groups [18] [12] [78]: multifidus, iliocostalis, quadratus lumborum, iliopsoas and longissimus dorsalis (fig. 2.18). Notice instead that the choice of the fascicle of each muscle group to be modelled is not univocal: Stokes et al., for example, included in their model twenty fascicles for the multifidus [16], while Shirazi et al. modelled only five [12].

Beyond this, another clarification on the muscles positioning is to be made: insertions and origins of a fascicle are not precise points, but rather a muscle attaches to bone on a surface; the choice of a single spatial coordinate representative of the origin or insertion of the muscle is then made following an average method (fig. 2.19). Similarly, fascicles are not bi-

dimensional straight structure, as they are modelled numerically, but their path may be curved, or even change according to a specific motory task, while their cross-sectional area may vary along their length. Also for these, regressions methods and average values are used. Therefore a complex muscle can be modelled as a straight wire connecting insertions to origins.

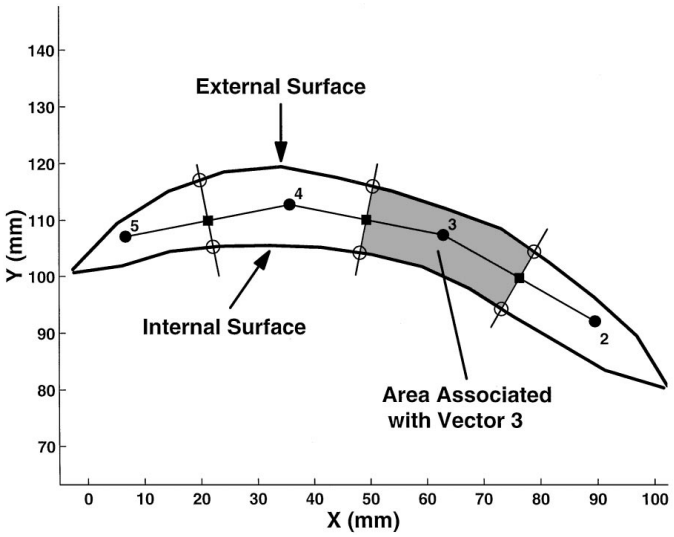


*Figure 2.19: The cross-sectional area of the internal oblique muscle, with data collected by [16]; from this three-dimensional fascicle, a numerical 2-D wire element has to be built*

### 2.2.7 Evaluation of loads to be applied on muscles-compehensive models

The discussion of muscle force magnitudes deserves a separate speech; for muscles positioning, in-vivo data are available and easily accessible, so, considering the previously mentioned approximations, an acceptable geometry can be built. For the forces values to be applied to each fascicle instead, no in-vivo data have been collected so far: the only non-invasive approach to obtain information on rector muscles activation, in fact, is EMG testing. This procedure is able to qualitatively estimate the level of activa-

tion of muscles, but cannot return precise values for very single muscle force [78]. EMG data are then often employed as validation for the outputs obtained from numerical models [79] [16] [80] [21]. As already stated, trunk muscles act as a resistance to gravity loads that would cause upper body to bend; if the analysed subject is carrying weights, loads increase and so do erector muscles forces, as confirmed by EMG signals. Whatever the total load to resist, muscles activate in synergy, each fascicle contracting to generate a force. Being high the number of muscle contributions, to achieve equilibrium a redundancy of solutions exists, and different methods have been used to determine them [21]:

- Reduction methods: in this way, an estimate of the trunk muscle forces is given considering a net total load the spine is subjected to in various postures; these correspond to three moments and three forces, each directed as the x,y and z axis. To simplify the resolution of the static problem so obtained, muscles are grouped or relation between them are introduced, so that the redundancy of solution can be decreased. Then, given the directions along which muscle forces act, local values are calculated by solving the equilibrium equations [81];

- Optimization methods: with this approach, a solution if found basing on a cost-efficiency function. Basically with these methods an inverse dynamics problem is solved, starting from kinematics data obtained experimentally by movement analysis. A simplified beam-rigid model, thus introducing non-negligible approximations, if often employed and the obtained muscle forces are then used in a complete finite element one. The equilibrium equation in this case is solved also considering an estimate of the energy spent by each single muscle: this parameter is minimized, so as it is supposed to happen in-vivo to maintain a correct posture [12];

- EMG-assisted models: here forces are determined using kinematics as an input and weighting each muscle contribution basing on its EMG activity and structure (cross-sectional area, length and contraction velocity). A gain factor is assigned to each muscle and so equilibrium is computed at each level [82].

- Hybrid optimization-EMG-assisted method: this is a combination of the two described method, in which the EMG-based gain factor for each muscle is used to satisfy global moment equilibrium in all the planes.

It is to be noticed that very often the lumbar section of the spine is the main object of investigations, as it represents the most frequently affected area for spinal pathologies [83]. On the other hand, the spine is a complex and rather extended structure, whose functions have repercussions form the higher to lo the lower levels of the human body. Likewise, most spinal muscles extend along the whole spine and their effect is not is isolable for a single vertebral level. For this reason, some authors extended their models so to recreate both the thoracic and lumbar sections of the spine [79] [84] [20] [21]. In this case a more complete trunk musculature is considered; considering the work performed by Shirazi et al. [17], the modelled musculature was divided in two groups: local muscles and global muscles (fig. 2.21 and 2.20). The former are comprehensive of the previously mentioned five muscles (iliocostalis, multifidus, iliopsoas, longissimus and quadratus lumborum), that attach to the pelvis and the lumbar vertebrae (apart from iliopsoas that inserts on the femur), and are responsible for the equilibrium of the lower coulumn. The latter consist of muscles attaching to the thoracic cage and whose total action contribute to the stability of upper spine: these muscles are external oblique, rectus abdominis, internal oblique and the thoracic part of both iliocostalis and longissimus.

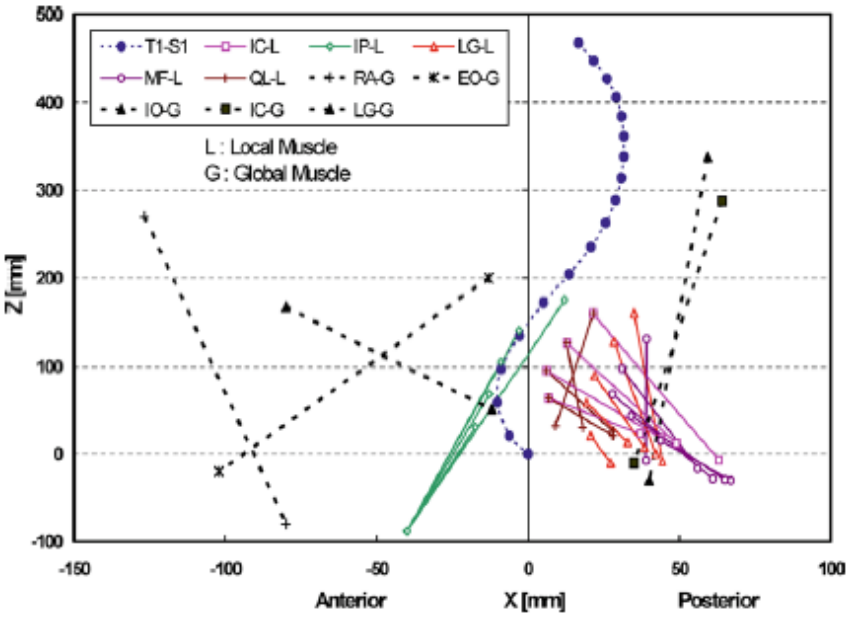


*Figure 2.20: Sagittal view of the spine model of Shirazi [17]*

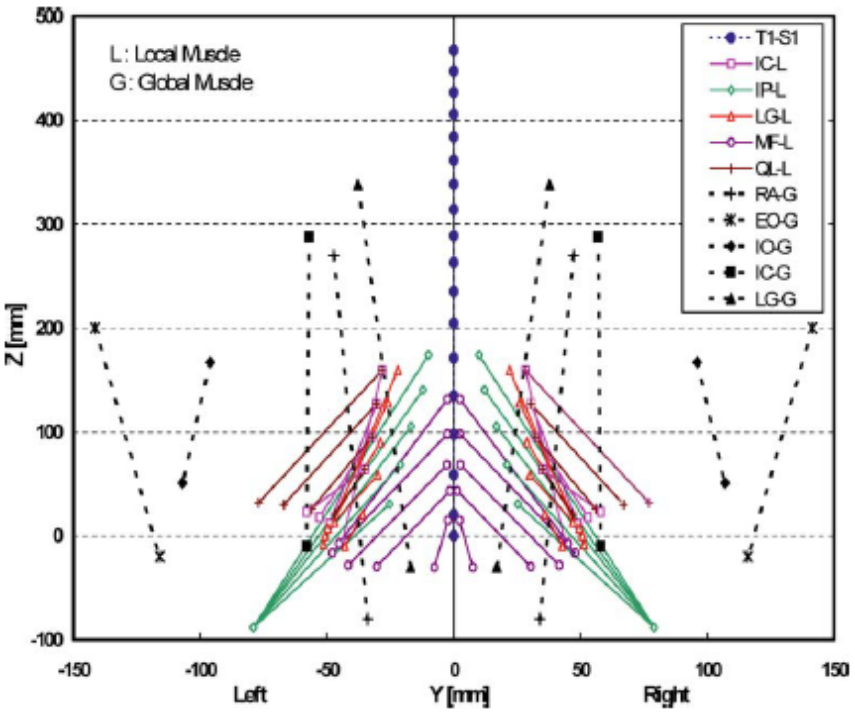


*Figure 2.21: Frontal view of the spine model of Shirazi [17]*

# Chapter 3

# MATERIALS AND METHODS

## 3.1 Finite element model

For this work, we employed as a starting model the one developed by Ottardi [72], available for the LaBS department in Politecnico di Milano. Its main features are reported in the following sections.

### 3.1.1 Geometry

The geometry of the model is referred to a healthy human male aged 40, on whom an in-vivo imaging process was performed. The images are 512x512 pixels/slice, with slice thickness of 0.625 mm, and are obtained from CT scans using a BrightSpeed scanner (General Electric Medical System). The patient during CT was in supine position resulting in a spinal curvature, location and orientation of the vertebral structures modified with respect to the physiological ones. The vertebrae were realized imposing a threshold on the grey scale values with the software Mimics 17.0 (Materialise, Leuven, Belgium) and were divided into a vertebral body made of trabecular and cortical bone, and the posterior elements. All the materials were assumed elastic isotropic except the trabecular bone that was modelled as transverse isotropic. The cortical bone layer is 1-1.2 mm in thickness,

while that of the endplates is 0.7 mm. The intervertebral discs were built in the space between two adjacent vertebrae using Rhinoceros 4.0 Evaluation CAD (McNeel and Associates, Indianapolis, IN, USA). The height of each disc is in good agreement with measurements found in literature [85]. Each disc was divided into the annulus fibrosus and the nucleus pulposus, located slightly posterior from the center [86]. The volumetric ratio between annulus and nucleus was considered 3:7 as shown in literature [87]. For the endplates no cartilaginous parts were included but only bony parts [88] [89].

### 3.1.2 Discretization

The discretization was performed using the software ICEM CFD 14.0 (ANSYS Inc). The mesh of the posterior elements of the vertebrae and the sacrum was done using 4-nodes linear tetrahedral elements (C3D4), whereas the vertebral bodies and the intervertebral discs were modelled with 8-nodes linear hexahedral elements (C3D8). The collagen fibers inside the annulus of the intervertebral disc are represented with four composite rebar layers of S4R elements embedded in the isotropic solid matrix (fig. 3.1). In particular, in each rebar layer, the fibers are modelled with two bundles of tension-only linear elastic fibers, oriented with an angle of $\pm 30^{\circ}$ with respect to the local horizontal plane, considering the center of the disc [90]. A local coordinate system was used to define the orientation of the fibers and the horizontal and tangential directions were specified for each shell element of the rebar. The fiber were characterized by a cross sectional area of 0.1 $mm^2$ [88]. The cortical bone was represented with shell elements (S4R) with a thickness between 1.5 and 2.5 mm. In order to mimic the facet joints, a cartilage layer of approximately 0.2 mm was created surrounding the bone, extruding the mesh of the posterior process elements (linear wedge elements, C3D6), obtaining a gap between the contact surfaces of

about 0.6 mm [88].

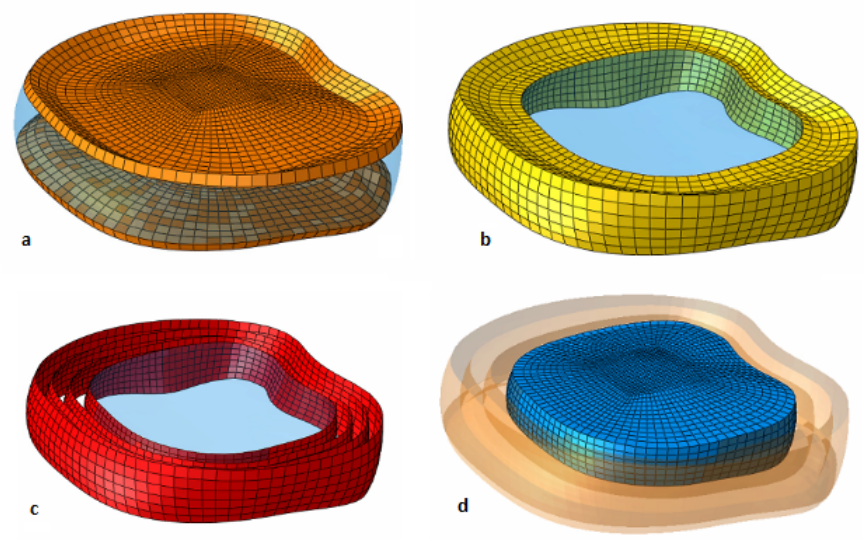


*Figure 3.1: Figure showing the meshes that compose the intervertebral disc of our model: endplates (a), annulus matrix (b) nucleus (c) and fibers (d)*

We specify in table 3.1 the mechanical properties assigned to the materials composing the model.

| | | E (MPa) | $\nu$ |
|---|---|---|---|
| Vertebrae | Cortical bone | 12000 | 0.3 |
| | Trabecular bone | 140,140, 200 | 0.45, 0.315, 0.315 |
| | Posterior process | 3500 | 0.25 |
| IVD | Annulus: fibers | 300 | 0.3 |
| | annulus: Ground substance | 2 | 0.45 |
| | Endplates | 100 | 0.28 |
| | Nucleus polposus | 1 | 0.49 |

*Table 3.1: Material properties of the parts composing the finite element model*

### 3.1.3 Assembly

The model, shown in figure 3.2, was assembled using the software Abaqus 6.12-3 (Dassault Systèmes, Simulia, Johnston, RI, USA) and tension-only linear spring elements (SPRINGA) were used to create the seven groups of ligaments of the spine: anterior longitudinal (ALL), posterior longitudinal (PLL), intertransverse (ITL), flavum (FL), capsular (FC), interspinous (IL) and supraspinous (SL). The initial stiffness values of the ligaments were taken from literature [91], then were rescaled considering the difference in the initial length and readjusted within the validation step, in order to match available literature data in terms of range of motion (ROM). Due to the high number of structures of the model, it was important to find a good compromise between the accuracy of the solution and the computational effort. Thus, a sensitivity analysis was performed by monitoring the stresses especially on the endplates, following the application of pure moments. Within all the mesh created with different seedings, the one that guaranteed less than 5% of difference in terms of stresses when doubling or halving the number of elements was chosen. The total number of elements and nodes of the model is 382989 and 266543 respectively. Several interactions and contacts were defined: between the surface of each couple of vertebral endplates and discs a tie interaction was used, in order to have a solid connection between the nodes of each structure, regardless of the mesh differences. In correspondence of each facet joint, a surface-to-surface contact was imposed, and a coupling constraint was defined between a reference node and the upper surface of the first lumbar vertebra (L1), to enable the application of forces and moments.

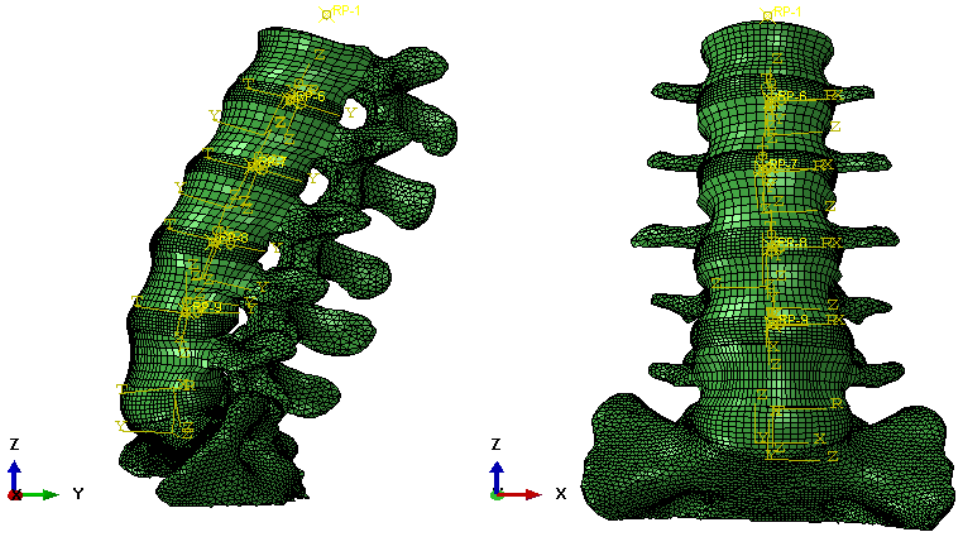


*Figure 3.2: Sagittal and frontal view of the starting finite element model*

## 3.2 Validation of the model with simplified loading conditions

Before the application of lumbar musculature to the model, this was validated by applying simplified loads. As recurs in literature, test were performed to simulate flexion and extension in the sagittal plane (one of the most common loading conditions for verifying resultant rotations and pressures), and standing, as this represents the main condition of interest for our study. This last situation was obtained with the application of a follower load of 500 N. For motion in the sagittal plane, simulations were made with combinations of pure moments of 7.5 Nm (both for flexion and extension) and follower load of 500 N (1175 N in one case). All these loading conditions were suggested by literature, both for numerical and experimental studies [11] [14] [13] [31] [29] [32].

## 3.3 Addition of the spinal musculature

### 3.3.1 Definition of the spatial coordinates

The addition of muscles to the model was preceded by a literature review, aimed at identifying the most common and suitable ways of implementing musculature. In first instance, only lumbar spine models were considered, as models extended to the thoracic part include other muscle groups, not incorporable in our one. Among these we focused on muscles that are most commonly reproduced, and on the fascicles they are composed of. In accordance with the most frequent choices seen in literature [18] [12] [53] we decided to model five muscle groups: iliopsoas (IP), multifidus (MF), iliocostalis (IC), quadratus lumborum (QL) and longissimus lumborum (LG). How to model single muscles, on the contrary, required a more complex analysis, as authors are not in agreement regarding the number of fascicles of each muscle and their origin and insertion coordinates. Coordinates for muscles attachments to bony structures were taken from Chuang et al. [18], as this model provided information both on muscles location and the relative force values to be applied. This lead to model muscles as:

- Multifidus, Iliopsoas and Longissimus Lumborum: each divided in five fascicles, and each of them acting on a different lumbar vertebra;
- Iliocostalis and Quadratus Lumborum: each divided in four fascicles, acting on the upper lumbar vertebrae, but not on L5.

In our intention, these data were scaled to fit our own model and thus providing comparable results to the author's. However, this source alone proved to be not sufficient for the above purpose, as the lack of data on the position of vertebrae in space did not allow us to properly scale the problem. For this reason, Chuang's data were coupled with the ones provided by Stokes et al. [16]: this last study included high precision information

on a thoraco-lumbar model of the spine, showing data both on vertebral centroids location and on origins and insertions of muscles. On the other hand, it was chosen not to use the Stokes' muscles, as the study included a much higher number of fascicles than we required, resulting in a high level of complexity and an increased computational effort for modelling the problem. Tables 3.2 and 3.3 report data from both the articles.

| Muscle Group | Vertebral Level | Force [N] | Origin [mm] | | | | Insertion [mm] | | | |
|---|---|---|---|---|---|---|---|---|---|---|
| | | | X_left | X_right | Y | Z | X_left | X_right | Y | Z |
| IP | L1 | 1,3 | 21,3 | -21,3 | 37,5 | 166,6 | 80 | -80 | -25 | -70 |
| | L2 | 0,5 | 23,9 | -23,9 | 27,7 | 134,9 | 80 | -80 | -25 | -70 |
| | L3 | 5,8 | 24,6 | -24,6 | 20,9 | 99,4 | 80 | -80 | -25 | -70 |
| | L4 | 13,5 | 25 | -25 | 18,3 | 63,5 | 80 | -80 | -25 | -70 |
| | L5 | 10 | 27,6 | -27,6 | 18,1 | 29,2 | 80 | -80 | -25 | -70 |
| MF | L1 | 11,2 | 4,8 | -4,8 | 67 | 135,4 | 37 | -37 | 60 | 17 |
| | L2 | 11,1 | 2,2 | -2,2 | 58,6 | 105,7 | 42 | -42 | 72 | 7 |
| | L3 | 9,2 | 6,5 | -6,5 | 52 | 67,8 | 40 | -40 | 77 | -2 |
| | L4 | 0 | 3,6 | -3,6 | 60,9 | 45 | 26 | -26 | 79 | -8 |
| | L5 | 6,9 | 5 | -5 | 61,9 | 26,5 | 10 | -10 | 83 | -12 |
| LG | L1 | 0,1 | 17,3 | -17,3 | 66,7 | 154,9 | 51 | -51 | 61 | -4 |
| | L2 | 0,1 | 15,3 | -15,3 | 54,9 | 122,9 | 52 | -52 | 58 | 3 |
| | L3 | 1,1 | 18,6 | -18,6 | 51 | 89,4 | 50 | -50 | 55 | -2 |
| | L4 | 50,6 | 18,8 | -18,8 | 49,8 | 58,5 | 43 | -43 | 50 | 14 |
| | L5 | 53,4 | 20,4 | -20,4 | 50 | 32,3 | 43 | -43 | 44 | 18 |
| IC | L1 | 10 | 21,5 | -21,5 | 57,9 | 149,8 | 44 | -44 | 80 | -3 |
| | L2 | 12,3 | 18,5 | -18,5 | 50,2 | 118,1 | 50 | -50 | 66 | 14 |
| | L3 | 15,9 | 18,9 | -18,9 | 42,5 | 83,7 | 50 | -50 | 60 | 18 |
| | L4 | 86,9 | 29,2 | -29,2 | 42 | 52,2 | 44 | -44 | 55 | 22 |
| QL | L1 | 0,2 | 34,1 | -34,1 | 62,4 | 150,1 | 79 | -79 | 28 | 17 |
| | L2 | 1 | 36,1 | -36,1 | 54 | 126,3 | 79 | -79 | 28 | 17 |
| | L3 | 1,1 | 37,7 | -37,7 | 48,5 | 91,8 | 79 | -79 | 28 | 17 |
| | L4 | 0 | 44,8 | -44,8 | 48,5 | 61 | 79 | -79 | 28 | 17 |

*Table 3.2: Muscles coordinates as reported by Chuang et al. [18]*

| Lumbar Multifidus | | | | | | | | | |
|---|---|---|---|---|---|---|---|---|---|
| | | Origin | | | | Insertion | | | |
| name | PCSA | X | Y | Z | UP att | X | Y | Z | LOW att |
| m1s | 40 | 3,2 | -47,9 | 130,8 | L1 | 23,3 | -13,4 | 76,4 | L4 |
| m1t1 | 42 | 2,5 | -54,5 | 129 | L1 | 29,3 | -19,7 | 43,6 | L5 |
| m1t2 | 36 | 2,5 | -54,5 | 129 | L1 | 28,2 | -18,5 | 20 | S/P |
| m1t3 | 60 | 2,5 | -54,5 | 129 | L1 | 45,2 | -49,8 | -7,4 | S/P |
| m2s | 39 | 2,2 | -38 | 106,1 | L2 | 29,3 | -19,7 | 43,6 | L5 |
| m2t1 | 39 | 2,5 | -44,9 | 100,8 | L2 | 28,2 | -18,5 | 20 | S/P |
| m2t2 | 49,5 | 2,5 | -44,9 | 100,8 | L2 | 47,9 | -47,9 | -16,5 | S/P |
| m2t3 | 49,5 | 2,5 | -44,9 | 100,8 | L2 | 47,6 | -47,6 | -3,8 | S/P |
| m3s | 54 | 2,2 | -22,6 | 72,4 | L3 | 28,2 | -18,4 | 20 | S/P |
| m3t1 | 52,3 | 2,8 | -29,5 | 66 | L3 | 41,6 | -49,6 | -28,3 | S/P |
| m3t2 | 52,3 | 2,8 | -29,5 | 66 | L3 | 43,4 | -51,5 | -21,4 | S/P |
| m3t3 | 52,3 | 2,8 | -29,5 | 66 | L3 | 44,8 | -51,5 | -15,3 | S/P |
| m4s | 46,5 | 1,8 | -18,6 | 51,2 | L4 | 33,7 | -29 | 2,4 | S/P |
| m4t1 | 46,5 | 1,4 | -26,5 | 48,6 | L4 | 30,4 | -47,2 | -29,5 | S/P |
| m4t2 | 46,5 | 1,4 | -26,5 | 48,6 | L4 | 31,9 | -42,9 | -19,1 | S/P |
| m4t3 | 46,5 | 1,4 | -26,5 | 48,6 | L4 | 33,5 | -37,2 | -9,1 | S/P |
| m5s | 22,5 | 2,3 | -25,7 | 26,7 | L5 | 10,5 | -20,9 | 0,1 | S/P |
| m5t1 | 22,5 | 2,3 | -31,9 | 22,9 | L5 | 7,6 | -45,4 | -30,4 | S/P |
| m5t2 | 22,5 | 2,3 | -31,9 | 22,9 | L5 | 9,1 | -40 | -19,2 | S/P |
| m5t3 | 22,5 | 2,3 | -31,9 | 22,9 | L5 | 9,9 | -31,1 | -9,9 | S/P |
| Longissimus pars Lomborum | | | | | | | | | |
| | | Origin | | | | Insertion | | | |
| name | PCSA | X | Y | Z | UP att | X | Y | Z | LOW att |
| l1 | 79 | 22,1 | -38,3 | 154,8 | L1 | 51,3 | -44,3 | -8,4 | S/P |
| l2 | 91 | 26 | -27,6 | 127,1 | L2 | 50,7 | -42,1 | 0,1 | S/P |

| | | | | | | | | | |
|---|---|---|---|---|---|---|---|---|---|
| l3 | 103 | 28,9 | -13,6 | 93,2 | L3 | 49,6 | -38,4 | 7,3 | S/P |
| l4 | 110 | 30 | -3,2 | 64,5 | L4 | 47,1 | -32,9 | 13,3 | S/P |
| l5 | 116 | 36 | -10,6 | 31,7 | L5 | 42,9 | -27,2 | 17,6 | S/P |
| Iliocostalis pars Lomborum | | | | | | | | | |
| | | Origin | | | | Insertion | | | |
| name | PCSA | X | Y | Z | UP att | X | Y | Z | LOW att |
| i1 | 108 | 41,7 | -34,8 | 154 | L1 | 52,6 | -46,1 | 8,6 | S/P |
| i2 | 154 | 49,5 | -25,2 | 126,7 | L2 | 57,1 | -37,6 | 20,6 | S/P |
| i3 | 182 | 51,2 | -9,2 | 92,4 | L3 | 59,6 | -32,9 | 26,5 | S/P |
| i4 | 189 | 48,8 | -0,8 | 64,6 | L4 | 61,2 | -27 | 30,6 | S/P |
| Iliopsoas | | | | | | | | | |
| | | Origin | | | | Insertion | | | |
| name | PCSA | X | Y | Z | UP att | X | Y | Z | LOW att |
| pL1VB | 211 | 19,5 | -26,3 | 171,3 | L1 | 73,2 | 51,4 | -21,1 | S/P |
| pL1TP | 40,7 | 22,8 | -31,9 | 154,9 | L1 | 73,2 | 51,4 | -21,1 | S/P |
| pL12D | 211 | 21,6 | -7,5 | 145,2 | L1/L2 | 73,2 | 51,4 | -21,1 | S/P |
| pL2TP | 84,2 | 28 | -21,2 | 126 | L2 | 73,2 | 51,4 | -21,1 | S/P |
| pL23D | 161 | 23,8 | 7,4 | 109,2 | L2/L3 | 73,2 | 51,4 | -21,1 | S/P |
| pL3TP | 173 | 35,8 | -5,7 | 92 | L3 | 73,2 | 51,4 | -21,1 | S/P |
| pL34D | 191 | 25,6 | 20,7 | 68,7 | L3/L4 | 73,2 | 51,4 | -21,1 | S/P |
| pL4TP | 120 | 31,2 | 2,7 | 63,1 | L4 | 73,2 | 51,4 | -21,1 | S/P |
| pL45D | 119 | 25,8 | 17 | 37 | L4/L5 | 73,2 | 51,4 | -21,1 | S/P |
| pL5TP | 24 | 39,8 | -1,5 | 31,3 | L5 | 73,2 | 51,4 | -21,1 | S/P |
| pL5VB | 39,5 | 24 | 9,3 | 19,6 | L5 | 73,2 | 51,4 | -21,1 | S/P |
| Quadratus Lumborum | | | | | | | | | |
| | | Origin | | | | Insertion | | | |
| name | PCSA | X | Y | Z | UP att | X | Y | Z | LOW att |
| QLT12 | 128 | 55,1 | -34,6 | 159,8 | T12 | 82,9 | -13,1 | 15,7 | S/P |
| QLL1 | 88 | 35,8 | -38,1 | 154,6 | L1 | 82,9 | -13,1 | 15,7 | S/P |

| | | | | | | | | | |
|---|---|---|---|---|---|---|---|---|---|
| QLL2 | 80 | 37 | -27,8 | 127 | L2 | 82,9 | -13,1 | 15,7 | S/P |
| QLL3 | 75 | 39,4 | -12,6 | 92,8 | L3 | 82,9 | -13,1 | 15,7 | S/P |
| QLL4 | 70 | 38,2 | -1 | 64,4 | L4 | 82,9 | -13,1 | 15,7 | S/P |

*Table 3.3: Muscles coordinates as reported in by Stokes et al. [16]*

We show below (fig. 3.3, 3.4, 3.5 and 3.6) the position of muscles in the sagittal and frontal planes, both for Chuang and Stokes (in the frontal plane muscles on one side only are shown, as symmetry is assumed in the medio-lateral direction); for Stokes' coordinates, also the centroids of the lumbar vertebrae are reported. Notice that the x,y and z-axes are directed laterally, posteriorly and upward respectively.

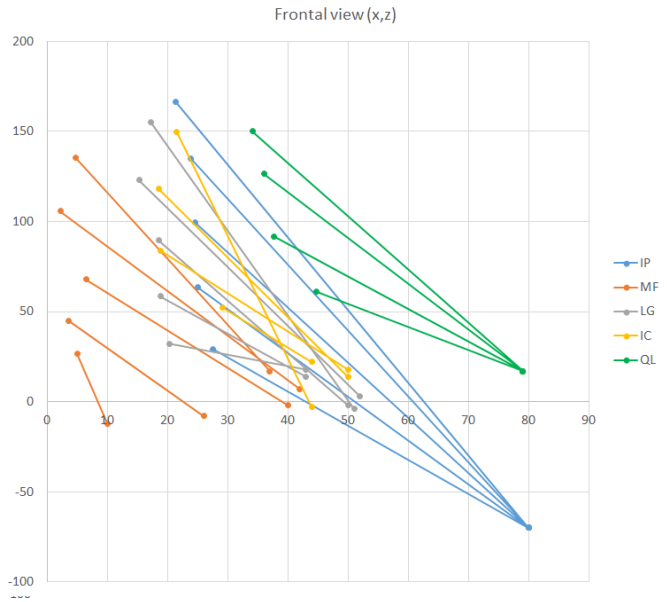


*Figure 3.3: Frontal view of the muscle considered by Chuang et al. [18]*

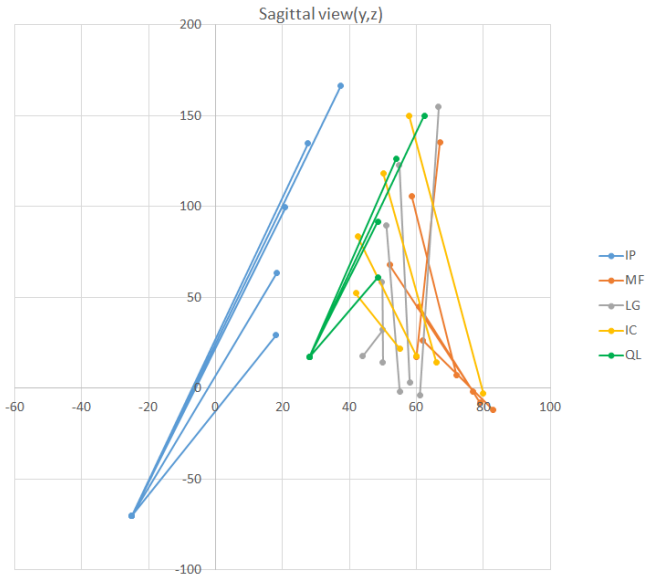


*Figure 3.4: Sagittal view of the muscle considered by Chuang et al. [18]*

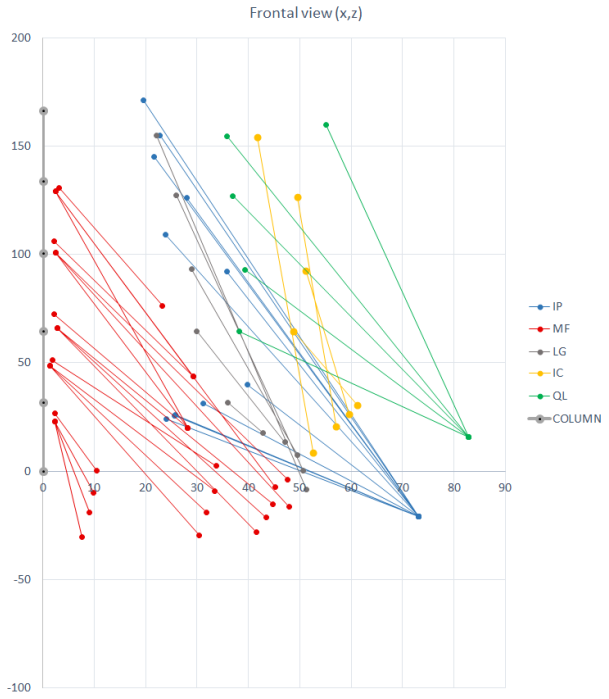


*Figure 3.5: Frontal view of the muscle considered by Stokes et al. [16]*

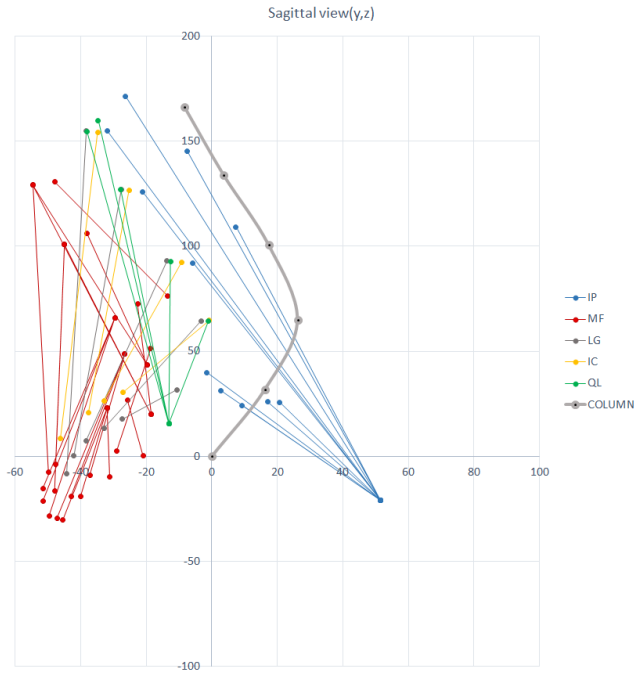


*Figure 3.6: Sagittal view of the muscle considered by Stokes et al. [16]*

The availability of both Chuang's and Stokes' data, allowed us to perform a scaling of the spatial coordinates to the model; as we referred to different studies, in which the geometries are different with respect to our one, this step is necessary for an optimal fitting of muscles on our spine. Were considered variations in terms of height, width and length of the lumbar section (meaning dimensions along the x,y and z-axes), as well as a tilt angle of the sacrum with respect to the vertical axis. During this phase, were also considered the differences in curvature that holds between the analyzed models (fig. 3.7); the latter, as an aproximation of the lordosis, was calculated as the line joining the vertebral centroids in its undeformed shape; As models were built basing on patients in-vivo imaging, intersubject variability occurred and differences in the measured curvature were present; this phenomenon was impossible to be scaled, as this would have implied to change the basis of our model, so in subsequent analyzes it was

taken into account.

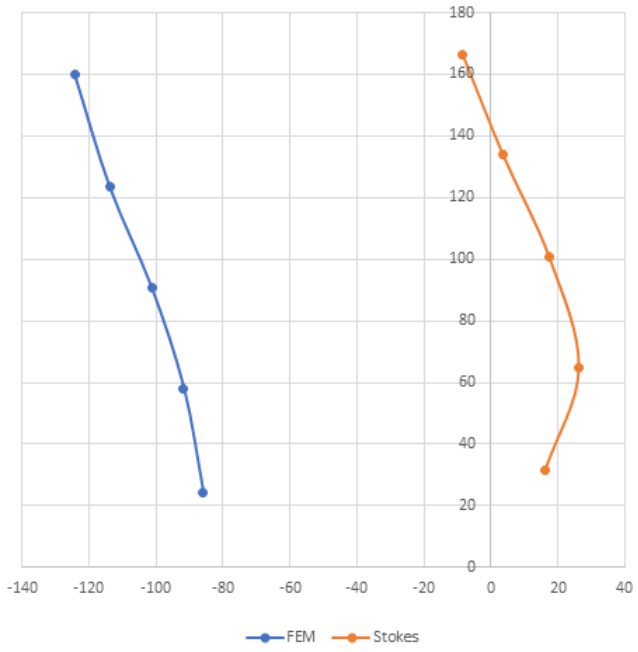


*Figure 3.7: Sagittal view of the spine, in which the difference in curvature between Stokes' spine and our model's is shown*

After evaluating the aforementioned differences, this phase was organized in two steps: first muscles data by Chuang have been scaled on the spine provided by Stokes, employing musculature's positions as an index of the overall extension of the models. This allowed to have a model comprehensive of all the information needed for the second step: the previously obtained muscles' coordinates were adapted to our spine, this time basing on the extension of the spine intended as the relationship between the positions of the lumbar vertebrae centroid. Here we explain in detail the choices we made for the whole scaling process:

- Proportion between Stokes' and Chuang's musculature: this consisted in calculating the extension in the three dimensions of the whole considered muscles, and for each axis a different parameter was used:

- For the medio-lateral direction the most and less lateral x-coordinate of any muscle insertion was evaluated; the first was the insertion point of QL for Stokes and of IP for Chuang, while the latter coincided to a MF fascicle for both. A difference between the maximum and minimum x values for each model ($\Delta$x) was then calculated and the ratio between $\Delta$x of Chuang and Stokes was evaluated (Rx);
- In the sagittal plane, differences along the y-axis were considered by selecting the maximum and minimum attachment point for any muscle: the most anterior point was the insertion of IP for both, while the most posterior resulted in an insertion of IC for Chuang and of MF for Stokes. The $\Delta$y and Ry parameters were then calculated similarly to those in the x direction;
- For height, maximum and minimum points were again selected, but not for the entire musculature, but rather on the only multifidus. This choice was made following the fact that the lowest muscle attachment at all would have been IP for both the models; this muscle however inserts on the femur, resulting in the insertion point reported by the authors as an approximation of the location in which it comes in contact with the pelvis. We considered this approach to be too rough for our aims, and then decided to base on MF as it is a muscle that extends through the whole posterior spine, thus providing a good knowledge on the vertical extension of the lumbar spine. Again, basing on these, we obtained a Rz value for the vertical fitting.

Once obtained these constants, the proportion was calculated by dividing each x,y and z coordinate from Chuang's data by the correspondent ratio (Rx, Ry, Rz); this was done both for insertions and for origins of each fascicle.

- Symmetry with respect to the z-axis: this operation was performed, as the data related to Chuang's and Stokes' spines were referred to a lordosis curvature directed in the opposite y direction; we then simply applied a symmetry to the previously obtained data;
- Translation in the sagittal plane: as the coordinates from literature were referred to different reference systems, with origins of the axis positioned differently, we had to adjust them; to do this we chose to make the highest point of the musculature coincide, which meant to perform a translation along the y and z axis so that the origins of IPL1 had the same coordinates;
- Rotation in the sagittal plane: as the curvature of our model was different from Stokes', we performed a rotation in the yz plane, so that the two spines could be as coincident as possible. We then calculated an angle such that the total distance between the vertebral centroids of the two models was minimized and rotated all the muscles coordinates of this value;
- Symmetry with respect to the z-axis: the opposite step as the previous symmetry was made, so to go back to lumbar curvature directed as in our model;
- Translation in the antero-posterior direction: this last operation was made, as the origins of the reference systems of our model was placed anteriorly to the spine; to do this, we calculated the magnitude of the translations such that the distance between the centroid of L2 and the origin of IPL2 was the same both in Stokes' and in our model.

We now report in table 3.4 the data obtained after the whole scaling process; coordinates deriving from the single steps are instead reported in Appendix A. In figure 3.8 we show how the model appears after the application of muscle connectors.

| Muscle Group | Vertebral Level | Origin [mm] | | | | Insertion [mm] | | | |
|---|---|---|---|---|---|---|---|---|---|
| | | X_left | X_right | Y | Z | X_left | X_right | Y | Z |
| IP | L1 | 22,31 | -22,31 | 135,45 | 167,44 | 83,80 | -83,80 | 49,12 | -58,96 |
| | L2 | 25,04 | -25,04 | 122,49 | 137,26 | 83,80 | -83,80 | 49,12 | -58,96 |
| | L3 | 25,77 | -25,77 | 112,05 | 103,01 | 83,80 | -83,80 | 49,12 | -58,96 |
| | L4 | 26,19 | -26,19 | 105,66 | 67,93 | 83,80 | -83,80 | 49,12 | -58,96 |
| | L5 | 28,91 | -28,91 | 101,78 | 34,17 | 83,80 | -83,80 | 49,12 | -58,96 |
| MF | L1 | 5,03 | -5,03 | 160,85 | 133,58 | 38,76 | -38,76 | 141,32 | 17,70 |
| | L2 | 2,30 | -2,30 | 149,48 | 105,21 | 44,00 | -44,00 | 151,94 | 6,57 |
| | L3 | 6,81 | -6,81 | 138,97 | 68,58 | 41,90 | -41,90 | 155,85 | -2,82 |
| | L4 | 3,77 | -3,77 | 145,20 | 45,18 | 27,24 | -27,24 | 157,16 | -8,95 |
| | L5 | 5,24 | -5,24 | 144,19 | 26,85 | 10,48 | -10,48 | 160,62 | -13,31 |
| LG | L1 | 18,12 | -18,12 | 162,65 | 152,81 | 53,43 | -53,43 | 140,04 | -3,09 |
| | L2 | 16,03 | -16,03 | 147,72 | 122,55 | 54,47 | -54,47 | 137,87 | 4,12 |
| | L3 | 19,48 | -19,48 | 140,32 | 89,97 | 52,38 | -52,38 | 134,40 | -0,49 |
| | L4 | 19,69 | -19,69 | 135,83 | 59,66 | 45,04 | -45,04 | 131,25 | 15,80 |
| | L5 | 21,37 | -21,37 | 133,21 | 33,83 | 45,04 | -45,04 | 125,83 | 20,38 |
| IC | L1 | 22,52 | -22,52 | 153,53 | 148,73 | 46,09 | -46,09 | 158,67 | -4,13 |
| | L2 | 19,38 | -19,38 | 142,62 | 118,32 | 52,38 | -52,38 | 146,84 | 14,10 |
| | L3 | 19,80 | -19,80 | 131,42 | 85,26 | 52,38 | -52,38 | 141,43 | 18,68 |
| | L4 | 30,59 | -30,59 | 127,55 | 54,28 | 46,09 | -46,09 | 136,98 | 23,15 |
| QL | L1 | 35,72 | -35,72 | 157,95 | 148,54 | 82,76 | -82,76 | 110,13 | 21,10 |
| | L2 | 37,82 | -37,82 | 147,20 | 125,99 | 82,76 | -82,76 | 110,13 | 21,10 |
| | L3 | 39,49 | -39,49 | 138,14 | 92,60 | 82,76 | -82,76 | 110,13 | 21,10 |
| | L4 | 46,93 | -46,93 | 134,83 | 62,26 | 82,76 | -82,76 | 110,13 | 21,10 |

*Table 3.4: Final coordinates for muscles origins and insertions, obtained after the whole scaling process*

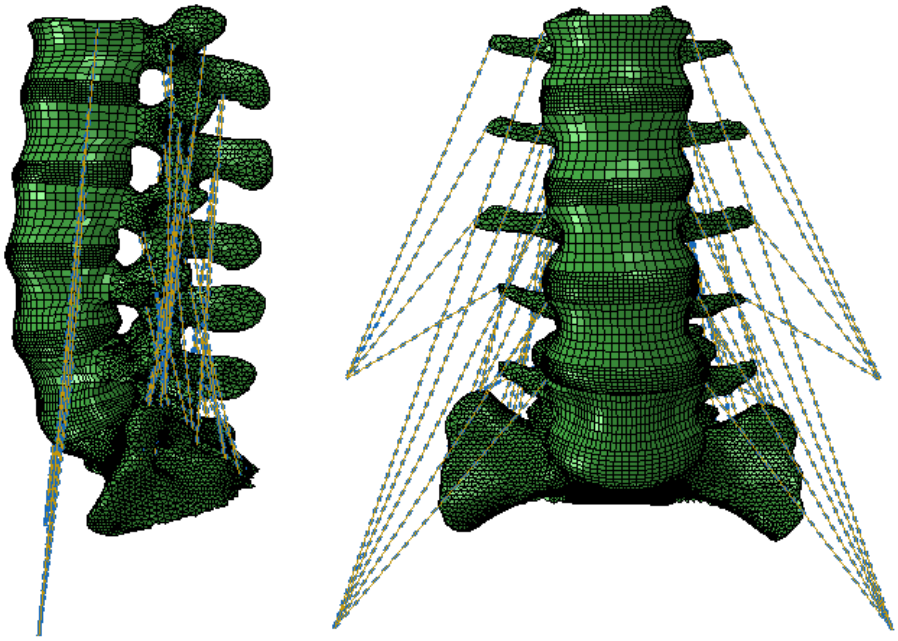

*Figure 3.8: The model after the implementation of lumbar muscles (represented by blue dashed lines)*

### 3.3.2 Boundary conditions and connectors

Having now available the coordinates for muscle attachments, these were implemented in Abaqus; as we expected, we had to adjust several insertion and origin points, to better adapt them to the spine. This step was made so that muscles could attach to the bony structures of the model as prescribed by anatomical evidences: the origins of the iliopsoas were placed laterally on the vertebral body, and each point was constrained via a continuum distribution coupling to the adjacent mesh surfaces. The insertions of IP, instead, were not modified from the obtained data, as they represent an attachment to the pelvis, absent in our model, and these points were then encastred. For the same reason, encastres were placed also on the insertions of QL. All the other points were attached on the adequate anatomical region, and continuum distribution couplings were again made, joining each point

with the adjacent mesh nodes. For each fascicle, wires were created joining the insertion and origin points and connectors properties were assigned to each. Axial connectors were chosen, with a linear elastic behaviour and a stiffness value of $10^{-5}$.

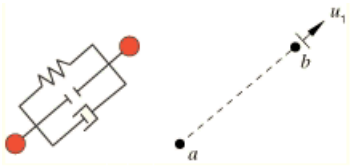


*Figure 3.9: Axial connector assignment*

## 3.4 Loading conditions

The model of this work, with respect to literature, focuses in reproducing in a high realistic way not only the muscular action but also the acting gravity loads. For this aim, we referred to El-Rich et al. [21], who simulated standing under gravity loads with and without additional external loads. For the definition of gravity loads, he refers to Kiefer et al. [20] and Pearsall et al. [19], as did in this study. This authors present an approach for simulating gravity of the upper body by applying concentrated forces in specific points, the centres of mass (CM), that are divided between lumbar centres of mass (ranging from L1 to L5) and centres of mass of the upper body (T1 to T12 contributions, as well as those deriving from head, neck and arms). The direction corresponding to the gravity force is parallel to the line joining the L1 and L5 vertebral centroids, considered as the direction of the gravitational acceleration.

### 3.4.1 Upper body loads

The centre of mass of the body parts above the lumbar section of the spine was considered as a single point, in accordance with other studies [12] [18];

were chose to calculate all the resultant loads as applied in the centroid of the first lumbar vertebra. In this point were applied an equivalent moment and a force deriving from the upper body weight, as done by El-Rich et al. [21], these account for the weight of head, neck, and arms, for the compression force exerted by some global extensors muscles (iliocostalis pars thoracis and longissimus pars thoracis) and for the weight of the thoracic section of the spine. As already mentioned, the CT scan images of the vertebrae for our model were taken from a healthy adult man aged 40. Therefore, all the calculations were made supposing an average weight of the European men of 70.8 Kg [92]. Kiefer et al. [84] chose to assign, for a 75 Kg man, 40 Kg to the toraco-lumbar spine; this were divided in 7.5 Kg for the arms, 8 Kg for the head, and the remaining 24.5 Kg were distributed between the spine slices. Each slice represents a cross-sectional part of the spine in the horizonatal plane, with height approximately as that of a single vertebra; each slice is assigned a weight value that represents the contribution of the whole bony and soft tissues present in it (fig. 3.10). These values were also calculated by Pearsall et al. [19] using the pixel intensity values of CT scans images, correlated to tissue densities. He provides the gravity loads for each of the trunk slices (of a 70.8 Kg man) from the thoracic spine to the pelvis.

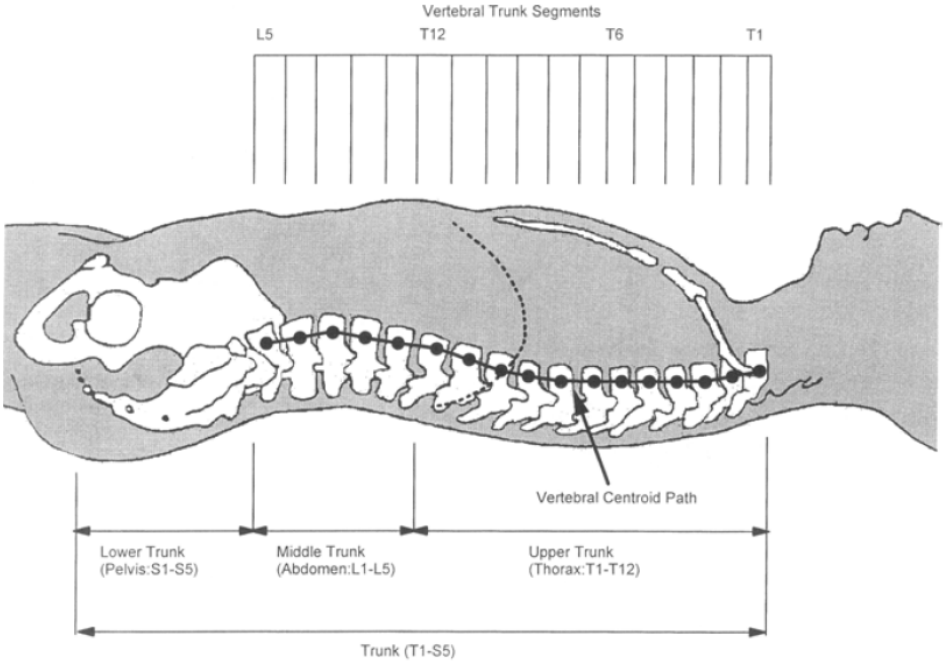


*Figure 3.10: Pearsall's division into slices of the trunk, ranging from T1 to L5; each of this slices is assigned a weight value [19]*

For a 70.8 Kg man, the values for the different parts are slightly inferior: from Pearsall's data it can be concluded that 37.31 Kg have to be assigned to the thoraco-lumbar spine (slighly inferior to the previous 40 Kg) dividing them into 21.81 Kg assigned to the trunk slices, and 7.5 Kg and 8 Kg for arms head and neck respictevely. Then for the thoracic spine the gravity force for each slice (T1-T12, derived from El-Rich et al. [21]), the compression force of the global muscles (IC and LG) and the gravity force of arms, head and neck, expressed in Newton, are the following (tab. 3.5):

| T1 | T2 | T3 | T4 | T5 | T6 | T7 | T8 | T9 | T10 | T11 | T12 | Arms | Head & Neck | IC | LG |
|---|---|---|---|---|---|---|---|---|---|---|---|---|---|---|---|
| 7,95 | 7,65 | 9,57 | 9,02 | 9,27 | 9,14 | 9,58 | 10,29 | 10,75 | 13,92 | 14,51 | 17,33 | 73,57 | 78,48 | 14 | 34 |

*Table 3.5: Force values applied as external loads to the model (in Newton)*

The lever arms of these loads are calculated from a known spinal curva-

ture obtained from literature (again from El-Rich et al. [21]), as our model does not account for the upper levels of the spine; the consequent equivalent moment to be applied in L1 is then found. In El-Rich's work, a deformed shape, deriving from the application of gravity loads on a stress-free configuration, in obtained such that *"the rotations prescribed in the model were* [...] *selected in a manner as to yield deformed postures in general agreement with measured sagittal profile of all subjects rather than attempting to simulate a specific subject profile"*. The positions of the global muscles in the deformed configuration have also been extrapolated from El-Rich's data. Head and neck were located in the centre of T1 [84]. The arms contribution was divided in three levels, equally distributed 3 cm posteriorly to T2, T3 and T4 [77]. The loads of the slices were positioned in the centre of mass given prescribed by Pearsall's study: given the vertebral centre at each level, the CM is at a known distance. The position of the overall gravity loads are represented in the picture below (fig. 3.11).

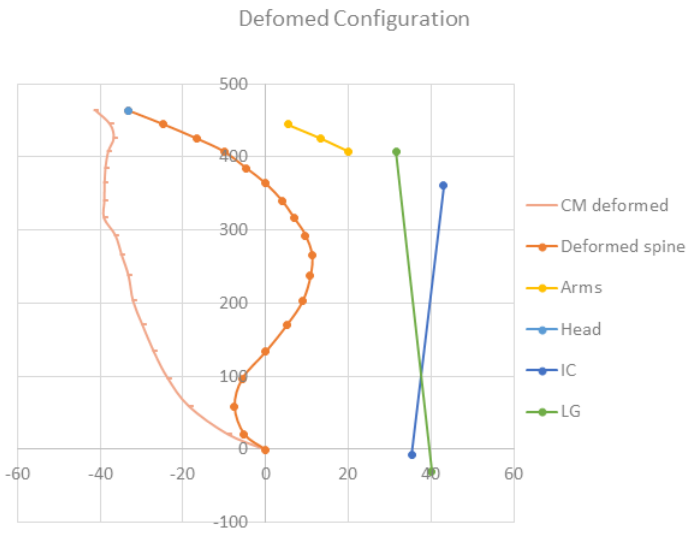


*Figure 3.11: Sagittal view of the deformed profile of the spine on which the positions of gravity loads (deriving from thoracic slices centres of mass, arms, head and neck) and of global muscles (IC and LG) were defined*

The contribution of all the forces was evaluated, and resultant vertical force and flexion moment were calculated; the values are shown in table 3.6.

| Force [N] | Moment [Nmm] |
|---|---|
| 329 | 6000 |

*Table 3.6: Equivalent vertical force and flexion moment to be applied on L1; we recall that the vertical direction was chosen parallel to the line joining the L1 and L5 centroids*

### 3.4.2 Lumbar centres of mass

The lumbar centres of mass positions are calculated from the data given by Pearsall et al. [19]. For each level, the centre of mass is positioned anteriorly to the vertebral centroid of a prescribed value, that vary for each vertebra; the values of both the vertebral centroids and the lumbar CM are reported in table 3.7.

| VERTEBRAL CENTROIDS | | | CENTRES OF MASS | | |
|---|---|---|---|---|---|
| level | y | z | level | y | z |
| L1 | -124,29 | 160,08 | CML1 | 89,69 | 173,22 |
| L2 | -113,82 | 123,44 | CML2 | 86,71 | 133,73 |
| L3 | -101,31 | 90,71 | CML3 | 85,42 | 96,74 |
| L4 | -91,69 | 57,97 | CML4 | 82,34 | 61,52 |
| L5 | -85,94 | 24,33 | CML5 | 83,33 | 26,46 |

*Table 3.7: Coordinates for vertebral centroid and the correspondent CM*

The load values to be applied for each centre of mass are again reported by Pearsall et al., and are reassumed below (tab. 3.8).

| level | Mass [g] | Force [N] |
|---|---|---|
| L1 | 1677,2 | 16,45 |
| L2 | 1688,7 | 16,57 |
| L3 | 1669,7 | 16,38 |
| L4 | 1799,1 | 17,65 |
| L5 | 1823,8 | 17,89 |

*Table 3.8: Values of mass and force for each lumbar CM*

In figure 3.12 we show the model, highlighting the point in which the gravity loads are applied as red dots.

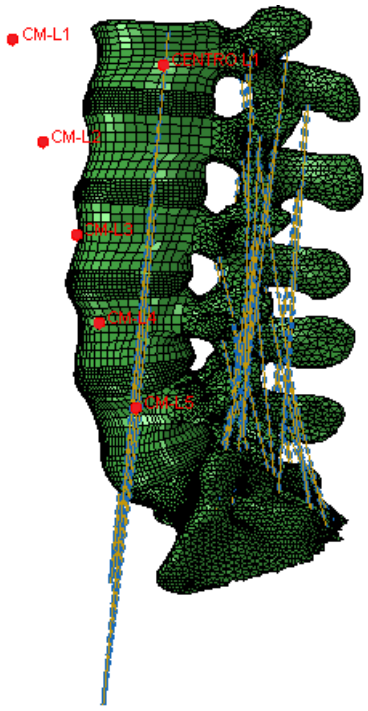


*Figure 3.12: The model after the implementation of the centres of mass (represented by red dots)*

### 3.4.3 Muscle forces evaluation

The determination of the forces associated to muscles is not a trivial issue, as the involved fascicle that act as stabilizers are several and the equilibrium could be achieved with a redundancy of solutions. In past studies a solution was found basing on the minimization of a cost function representing the total expended energy, but these were simplified beam-rigid models, able to represent an approximate kinematics of the spine [20] [77] [21]. In this work, we tried to directly employ the non-linear three-dimensional finite element model we possess, to find suitable results for a standing condition. Again, this was made following a literature review of the possibilities for muscle force implementation. As shown in figure 3.13 and 3.14, where a collection of some data on muscle forces from literature is presented, few correspondence can be found between authors: there are great variations both in the magnitude of the total force generated by muscles and on the distribution between the fascicles. Moreover a wide variation in muscle force activation per spinal level and muscle group was found.

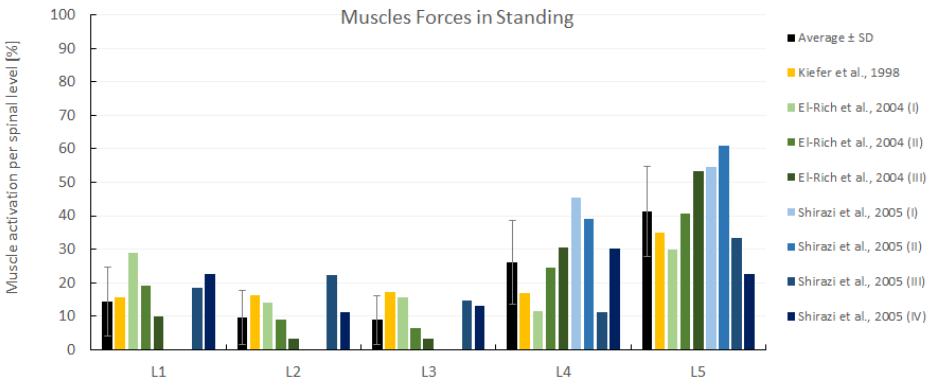


*Figure 3.13: Muscles force grouped by level of application of some models found in literature [20] [21] [17]; El-Rich (I) simulates pure standing, while in (II) and (III) co-activation of abdominal muscles is also added; Shirazi (I) to (IV) present different prescribed kinematics and co-activation levels*

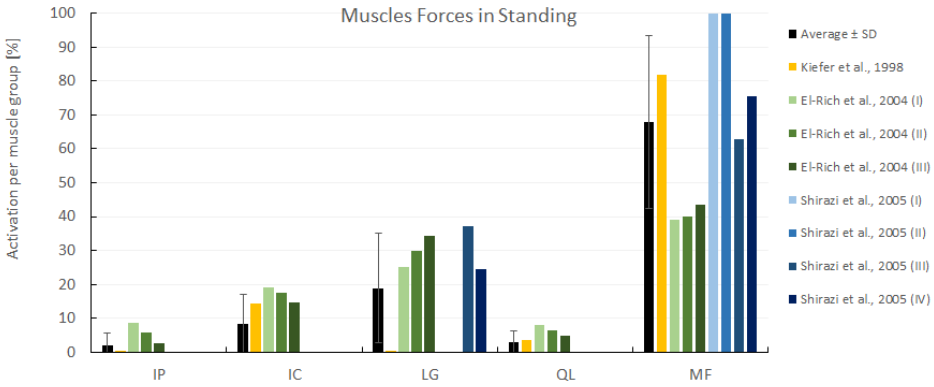


*Figure 3.14: Muscles force grouped by muscle of some models found in literature [20] [21] [17]; El-Rich (I) simulates pure standing, while in (II) and (III) co-activation of abdominal muscles is also added; Shirazi (I) to (IV) present different prescribed kinematics and co-activation levels*

Being this issue also strongly dependant on the model employed, it became difficult to identify a priori a proper muscles load distribution for our case. After evaluating the possibilities, we decided to follow the approach proposed by Kiefer et al. [20]: in this study a contribution for each fascicle

was found, weighted on the total force applied on muscles. Notice that, in the model used by the author, iliocostalis was modeled as composed of five fascicle, while in our one, only four were considered; we then neglected the additional contribution given by Kiefer's ICL5, resulting in the data shown in table 3.9.

| | IC | IP | LG | MF | QL |
|---|---|---|---|---|---|
| L1 | 0.5 | 0 | 0 | 13.8 | 1.2 |
| L2 | 0.1 | 0 | 0 | 15.3 | 0.9 |
| L3 | 0 | 0 | 0.2 | 16.4 | 0.7 |
| L4 | 0 | 0 | 0.2 | 15.9 | 0.7 |
| L5 | - | 0.1 | 0 | 20.3 | - |

*Table 3.9: Values of the rate of activation ($a_i$) for each muscle fascicle expressed as percentage*

With this approach the proportions of activation were fixed for each single fascicle, knowing the percentage of the total force to apply to each of them. In this way, a multi-parametric equilibrium problem, in which the solution depended on 23 forces (one for each fascicle, assuming symmetry between left and right), was reduced to the finding of the only value of the total applied force. For this aim, we introduced the parameter $k$, that, multiplied by the percentage of activation ($a_i$) given in table 3.9 of each fascicle, returns the correspondent force acting on the connector:

$$F_i = a_i k$$

The total force resulted then to be the sum of the single contributions:

$$F_{tot} = \sum_{i=1}^{23} F_i$$

Simulations were then made, assigning different values of $k$, and results were evaluated in terms of kinematics and intradiscal pressures. A

first-attempt value for the total force was found by making the total flexion moment applied in L1 (deriving from the contribution of all the forces present in the model) equal zero. This returned a value for $k$ of 1.39. From this, moving towards both higher and lower values, with a step size of 0.01, all possibilities were simulated, and the upper and lower limits were found: 1.45 and 1.31 respectively; above and below these values, the model was no longer able to correctly complete simulations due to computational issues. Reassuming, in table 3.10 are reported the total force cases simulated:

| Lower Limit | $k$ values | | | | | | | | | | | | | Upper Limit |
|---|---|---|---|---|---|---|---|---|---|---|---|---|---|---|
| 1.31 | 1.32 | 1.33 | 1.34 | 1.35 | 1.36 | 1.37 | 1.38 | 1.39 | 1.40 | 1.41 | 1.42 | 1.43 | 1.44 | 1.45 |

*Table 3.10: Considered values for k*

## 3.5 Variables of interest

Here we briefly list the variables that were extrapolated from simulations, to be compared with experimental and numerical studies:

- Vertebral rotations (VR): these are defined as the difference between the inclination angle of a single vertebra in the deformed and undeformed configuration in the sagittal plane;
- Intervertebral rotations (IVR): these are obtained as differences between VR of a vertebra and the just below one, representing the relative rotation between them;
- Intervertebral angles (IVA): these are the absolute angles between adjacent vertebrae, defined between vertebral axis; differently from IVR and VR, these care proper of each configuration, even if no motion occurs;

*Figure 3.15: Example of how IVA are taken (yellow angle) [22]*

- Angles between endplates: they are taken between the inferior endplate of a vertebra and the superior endplate of the just below one (fig. 3.16)

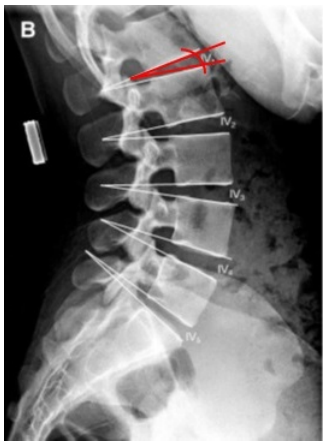


*Figure 3.16: Example of how angles between endplates are taken (red angle) [22]*

- Lordosis: this is a typical clinical estimate of the curvature of the lumbar spine; it can be defined as the angle between the superior endplate of L1 and the inferior of L5, or as the angle between the inferior endplate of L1 and the superior of S1 (fig. 3.17);


*Figure 3.17: Example of evaluation of lordosis as the angle between the superior endplate of L1 and the inferior endplate of L5 and example of evaluation of the lumbosacral angle calculated as the angle between L5 and S1 anterior faces directions. [23]*

- Lumbosacral angle: this angle is defined between the anterior faces of L5 and S1 and is an estimate of the tilting of the pelvis (fig. 3.17);
- Intradiscal pressure: this is the pressure present within the intervertebral discs when the spine is loaded. We will present these data as boxplots. This choice is due to the fact that a unique value is not easily identifiable for numerical simulations, while it is, on the contrary, for in-vivo testing: experimentally, the pressure value is registered with a transducer that reads a single value, as pressure is uniformly distributed within the disc, being this mainly composed of liquid. In our model the disc nucleus is modeled as an elastic solid, thus, in general, it presents a non-uniformly distributed pressure. With a boxplot we then analyze the results as a statistical distribution of pressure on all the mesh nodes composing the nucleus.

# Chapter 4

# RESULTS AND DISCUSSION

## 4.1 Results for validation with simplified loading conditions

### 4.1.1 Undeformed geometry

In this section we report data on the overall curvature of the model, evaluated through the lorodsis angle; figures 4.1 and 4.2 show a comparison between the model lordosis and that evaluated by in-vivo and numerical studies. In figure 4.1, the angle is measured between superior endplate of L1 and the the inferior endplate of L5; in figure 4.2 it is evaluated between the superior endplates both in L1 and S1.

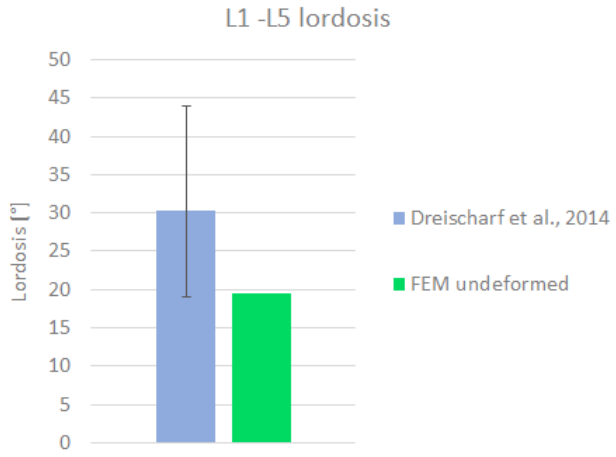


*Figure 4.1: Comparison of the lordosis angle with numerical studies [13]*

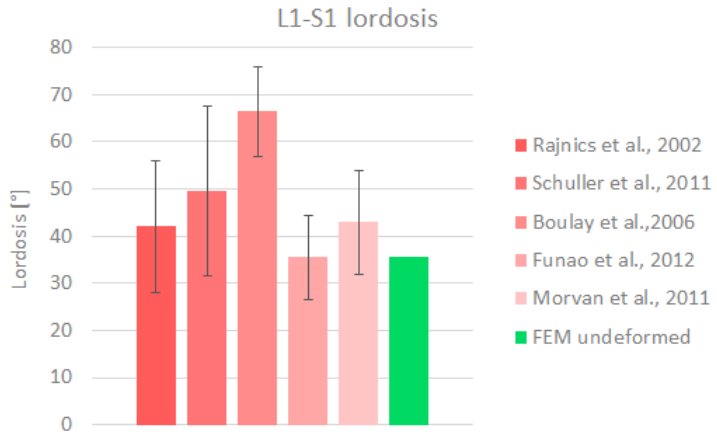


*Figure 4.2: Comparison of the lordotic angle evaluated by some in-vivo studies [24] [25] [26] [27] [28]*

The results reflect the geometry of the model: as it was built on images of a lying patient, the curvature of the spine is quite different from a physiological one. A low lordotic angle highlights from L1 to L5, but a more accentuated one occurs between L5 and S1; this brings the whole final lordosis in range, though in the near lower limit, with other studies.

### 4.1.2 Flexion-extension

We report in this section the results of simulations for movements in the sagittal plane: a pure moment was applied, directed as the x-axis, also in combination with a follower load, directed, for each level, as the line joining the centroids of adjacent vertebrae. Moments were applied both in flexion and extension, and results are compared with numerical, in-vivo and in-vitro studies. The following graphs (fig. 4.3, 4.4, 4.5 and 4.6) report values for intervertebral rotations (IVR). In figure 4.5 instead, the total range of motion (sum of the IVR of all the vertebral levels) is shown.

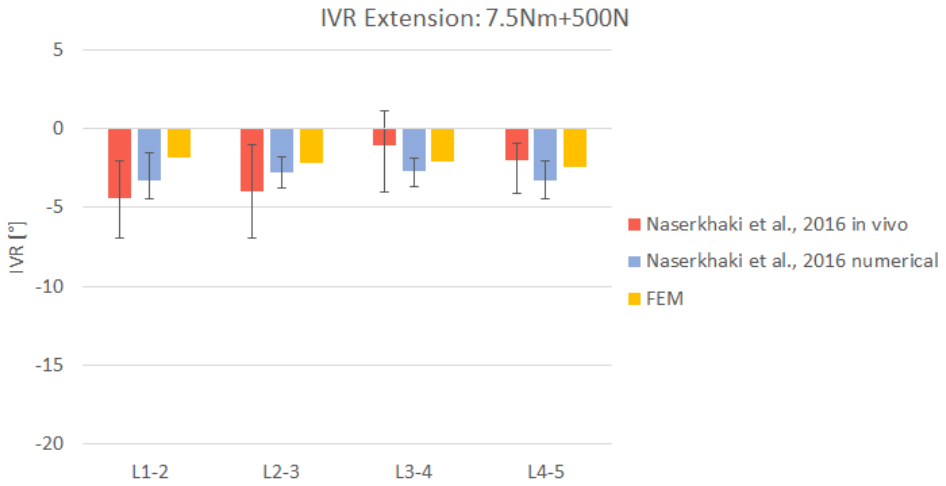


*Figure 4.3: Results for IVR obtained with the application of a flexion moment of 7.5 Nm and a follower load of 500 N; comparison made with data from studies by Naserkhaki et al. [29]*

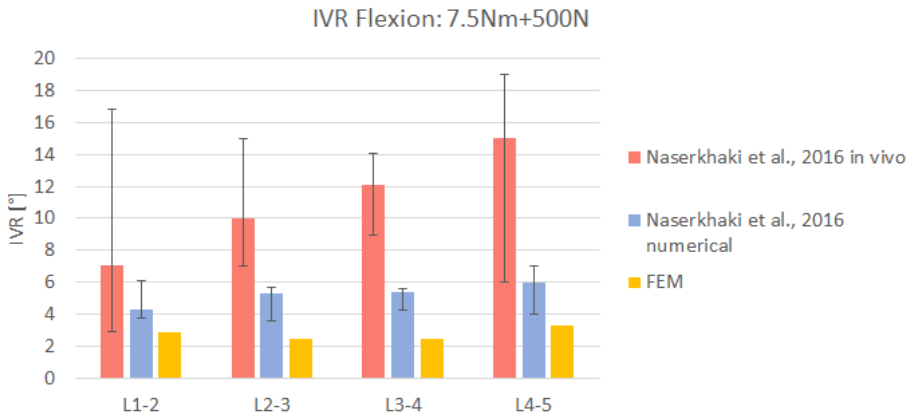


*Figure 4.4: Results for IVR obtained with the application of a extension moment of 7.5 Nm and a follower load of 500 N; comparison made with data from studies by Naserkhaki et al. [29]*

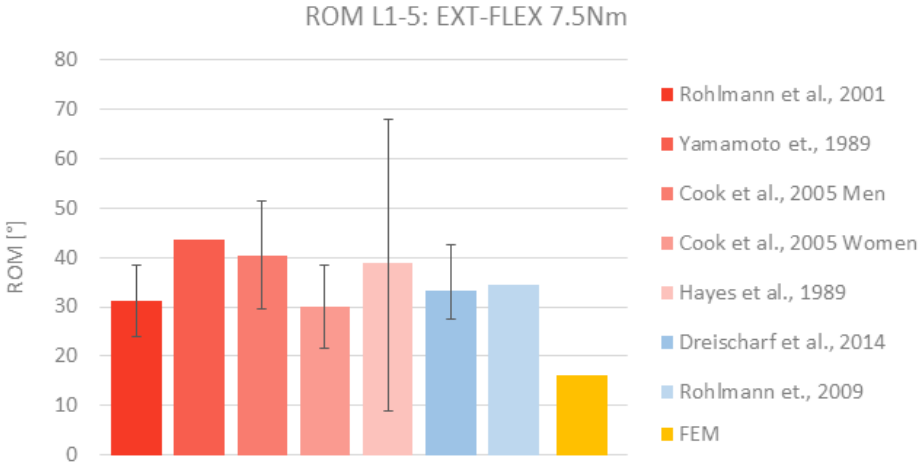


*Figure 4.5: Comparison for the total range of motion (flexion-extension) obtained by the application of pure moments only (7.5 Nm) with both experimental [30] [31] [32] [33] and numerical [13] [14] studies*

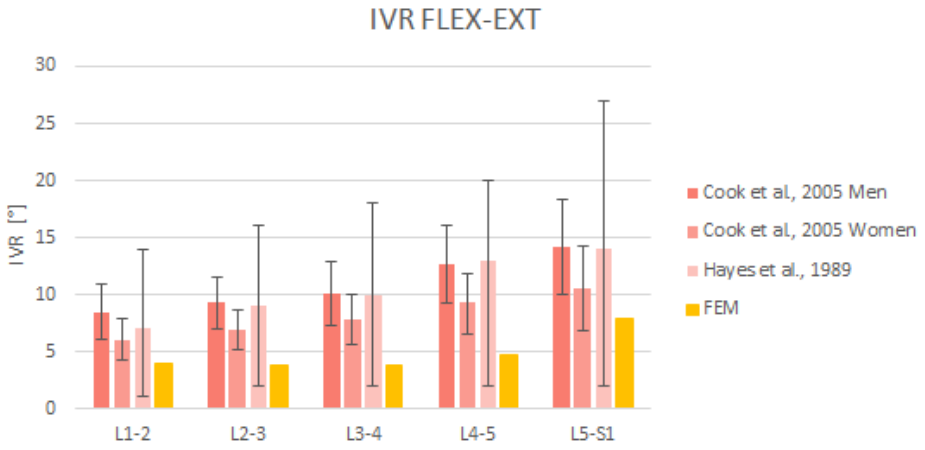


*Figure 4.6: IVR for flexion-extension (pure moments only of 7.5 Nm) compared with Cook et al. [32] and Hayes et al. [33] studies*

Below (fig. 4.7) we show an additional result, obtained with an increased follower load magnitude of 1175 N, which represents a simulation condition proposed by Rohlmann et al. [14] for a more realistic representation of the total trunk loads.

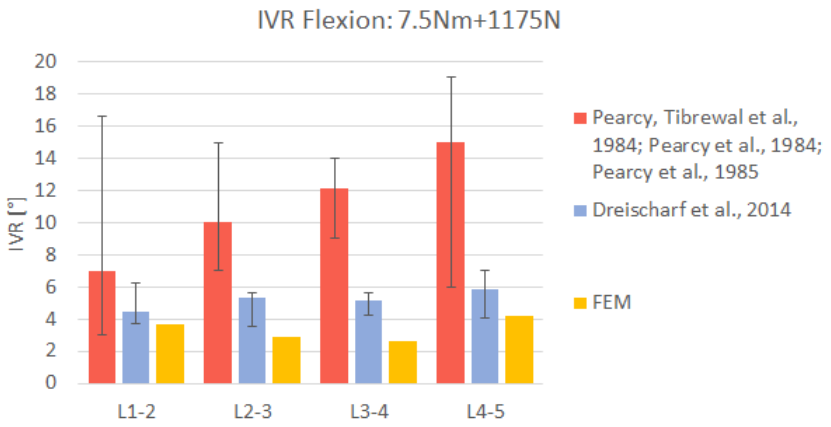


*Figure 4.7: Results for IVR obtained with the application of a flexion moment of 7.5 Nm and a follower load of 1175 N; comparison made with data from Pearcy et al. [34] and Dreischarf et al. [13]*

ROMs and IVRs of our model are in good agreement with numerical data, while they show more discrepancy with in vivo and in vitro models. The low level of the FEM kinematic values can be associated to the particular lordosis of the spine, slightly too erected than the expected physiological one.

The IDP of the model is compared with literature in the following figures (fig. 4.8, 4.9, 4.10,4.11 and 4.12) and is represented by boxplots. Flexion and extension were simulated with 7.5 Nm pure moment and 7.5 Nm moment combined with a 500 N follower load.

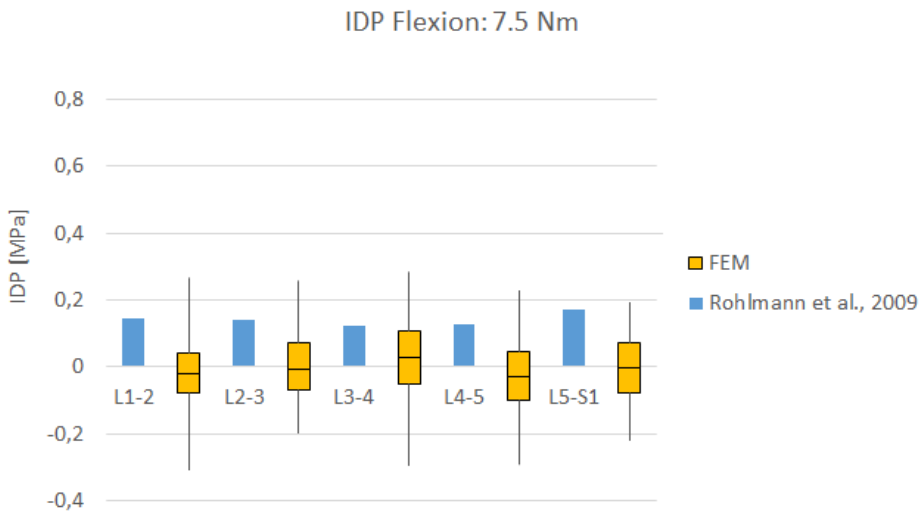


*Figure 4.8: IDP for pure flexion compared to Rohlmann et al. [14]*

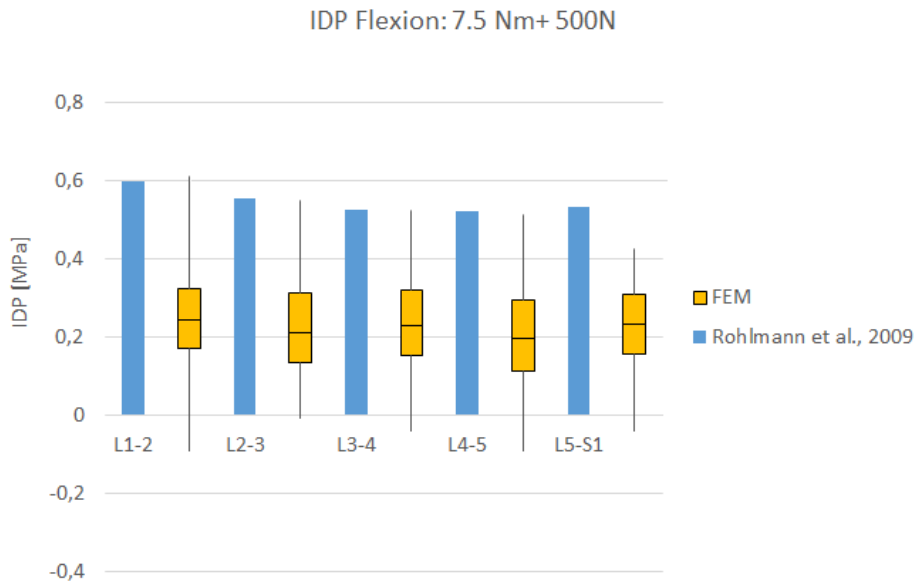


*Figure 4.9: IDP for flexion combined with follower load compared with Rohlmann et al. [14]*

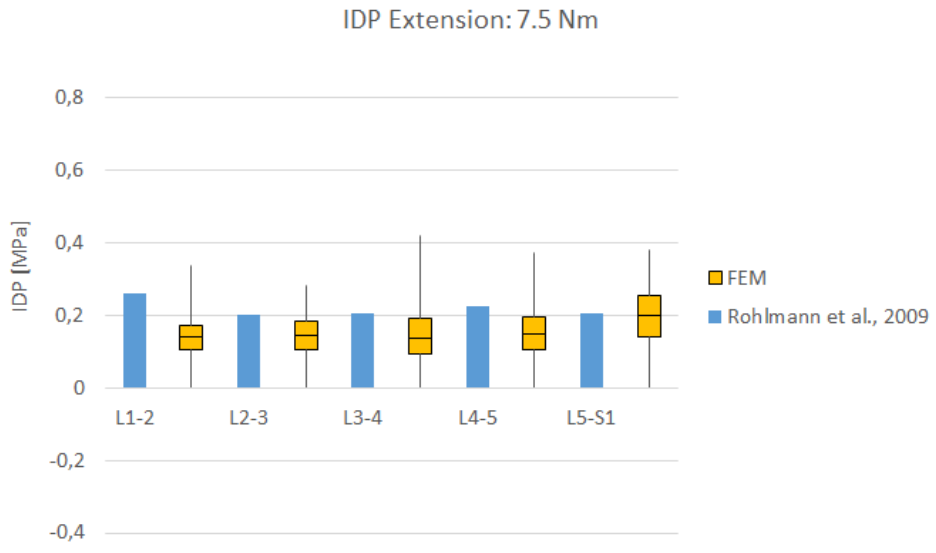


*Figure 4.10: IDP for pure extension compared with Rohlmann et al. [14]*

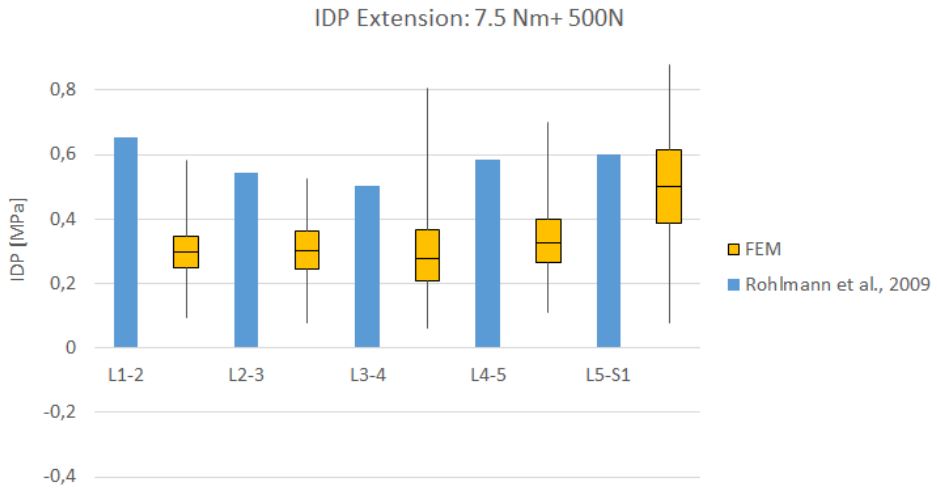


*Figure 4.11: IDP for extension with follower load compared with Rohlmann et al. [14]*

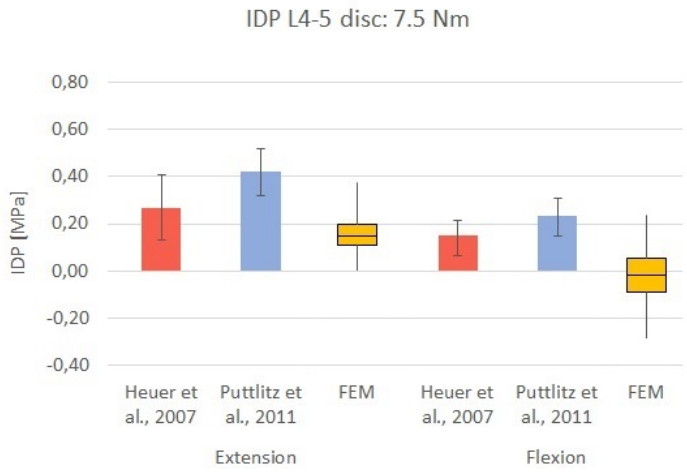


*Figure 4.12: IDP for pure flexion and extension compared with literature [35][36]*

As the interpretation of the results is not an easy issue, considering the median value, few correspondence can be found with numerical data, while, they show good agreement with experimental ones obtained by Heuer et al. [36] (fig. 4.12). Also, it must be noticed the lack of experimental data for IDP for vertebral levels other than L3-L4 and L4-L5, as most of the literature on this issue report pressure values only for this levels [44] [81] [43].

### 4.1.3 Standing

The standing condition is not as common as flexion and extension to be simulated in numerical studies, as it represents a low stress condition for the spine with respects to motions. In finite element models it is often simulated by the sole application of a follower load. Here we present a comparison with studies by Rohlmann et al. [11] (fig. 4.13).

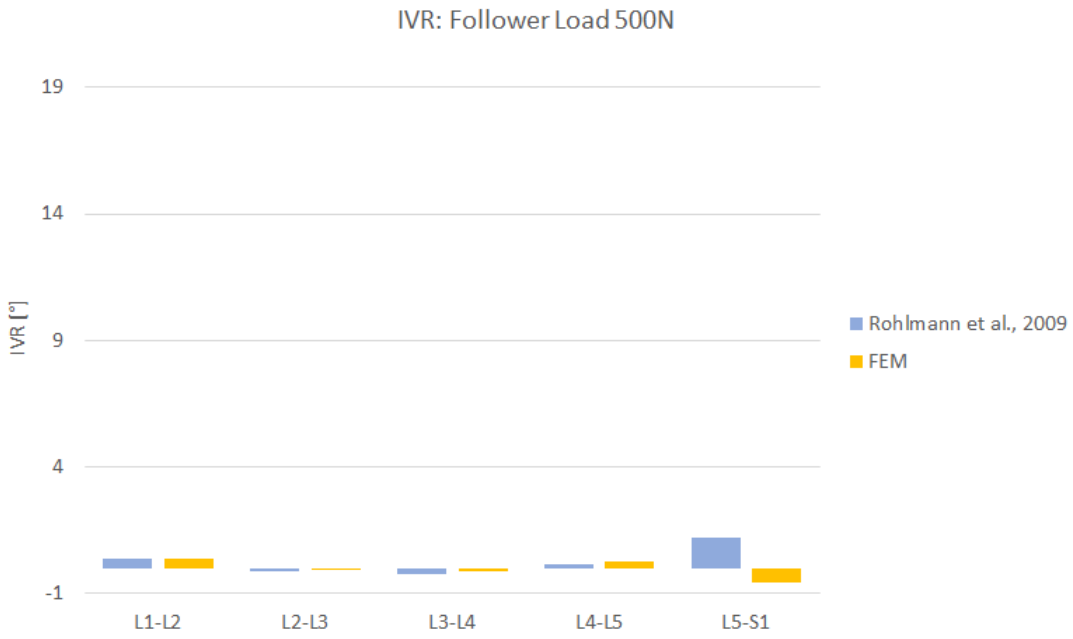


*Figure 4.13: IVR for simulations with a follower load value of 500 N [11]*

IDP of the model for the simulation of upright standing is presented in figure 4.14 and 4.15: in the first a comparison between the boxplots and a numerical study by Rohlmann et al. [11] is made, while in the second the median value obtained from our simulation is compared with a collection of numerical data carried out by Dreischarf et al. [13].

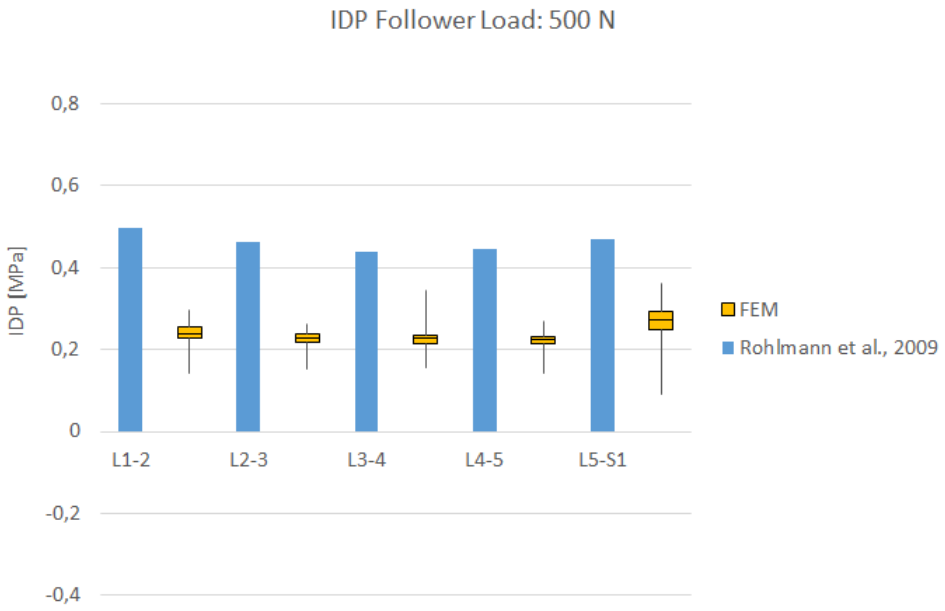


*Figure 4.14: IDP for simulations with a follower load value of 500 N. Comparison with literature is shown [11]*

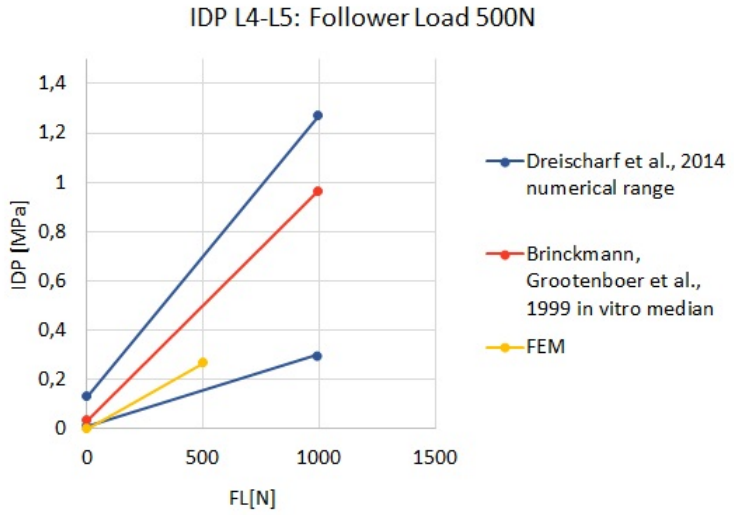


*Figure 4.15: IDP is compared Dreischarf et al. [13] and Brinckmann, Grootenboer et al. [37]*

## 4.2 Variation of $k$ value

### 4.2.1 Energy estimate

In this part of the chapter, we present the results of the simulations performed with all the muscles forces values presented in the previous chapter. At first, figure 4.16 reports data on the energy expended by musculature. This was estimated as the strain energy stored in all the connectors, and represents the total energetic expenditure of posterior muscles, necessary to resist the gravity loads that would cause excessive flexion of the spine.

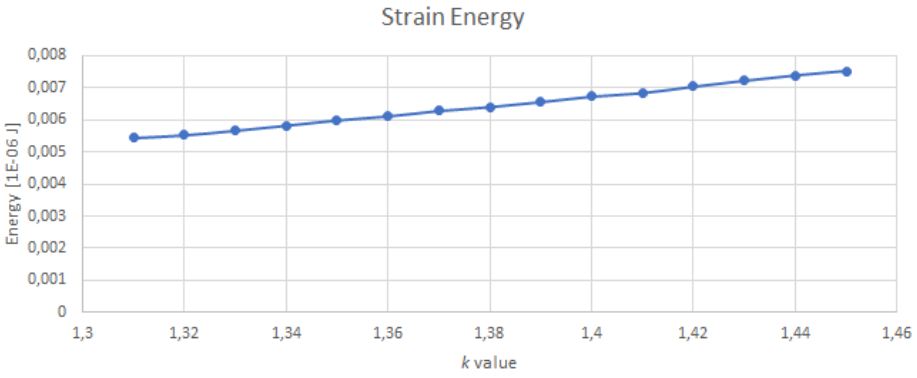


*Figure 4.16: Trend of the strain energy of muscles*

It can be observed that a linear trend exist on the resultant curve: as the $k$ values increases (proportional to the total muscle force), so does the total energy and the slope remains almost constant. This means that no stiffening effects of the structure occurs in the whole simulation campaign.

### 4.2.2 Angles and rotations

The application of muscle forces, intended for counterbalancing the flexion of the spine derived from gravity loads, resulted in a change of the lumbar curvature. At first, we report the intervertebral rotation that occurred for all the $k$ values (fig. 4.17).

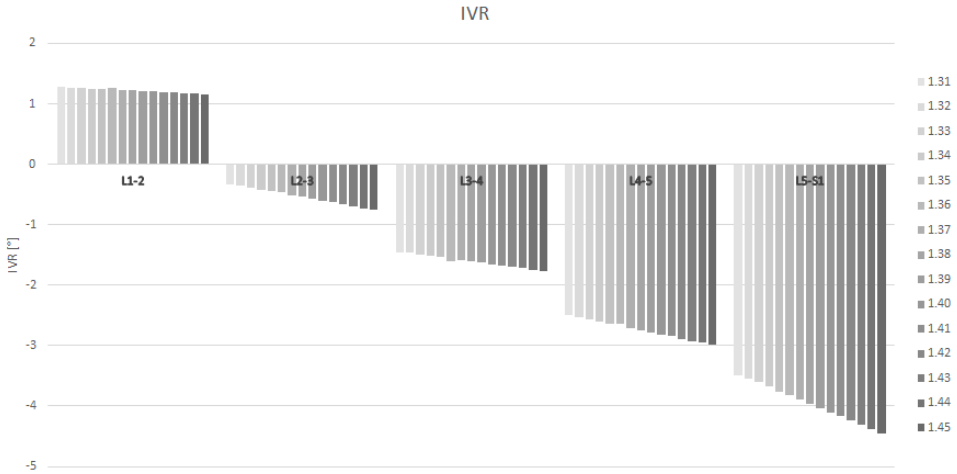


*Figure 4.17: Intervertebral rotations for each vertebral joint*

Positive angles mean that flexion occurred, while negative angles represent extension. It can be observed that anterior rotation appears only on the first joint; the overall effect is however of extension on the whole spine, resulting in a more accentuated lumbar lordosis. From data on rotations, knowing the angles between the vertebrae in the undeformed configuration, the final geometry (in terms of intervertebral angles, IVA) can be calculated. IVA are then reported in figure 4.18 for each value of $k$.

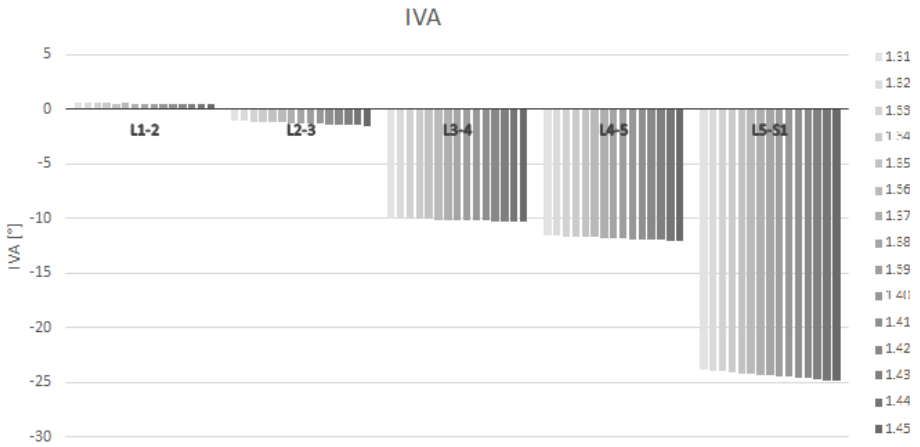


*Figure 4.18: Intervertebral angles for each vertebral joint*

From the presented data, it is clear that linearity occurs both in terms of rotations and angles. Increasing the muscles forces applied to the model results in an accentuation of the lordotic curve. In this regard, it is interesting reminding that the initial model presented a small lordotic angle, close to the lower limit of a physiological curvature; the action of musculature tends to extend the spine, increasing lordosis and making it closer to average values.

### 4.2.3 Intradiscal pressure

As already mentioned, for the evaluation of intradiscal pressures, were performed a statistical analysis of data obtained on the whole nucleus of the intervertebral disc. We recall that values were extrapolated from all the nodes composing each disc, in particular from 78384 nodes on each of L1-L2, L2-L3 and L3-L4, from 73968 nodes on L4-L5 and from 49776 nodes on L5-S1. Boxplots for the maximum and minimum $k$ values are presented in figure 4.19, for all the five intervertebral discs.

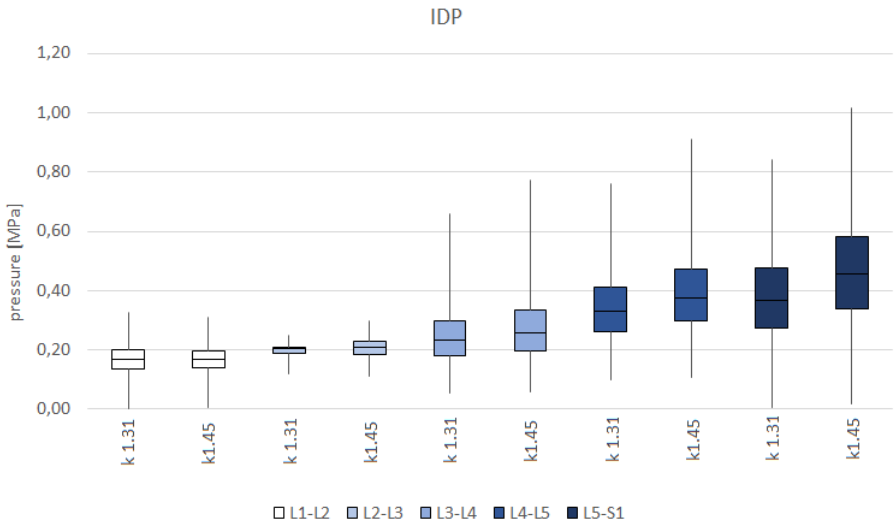


*Figure 4.19: Boxplot for pressure values on all the intervertebral discs, for different k 1.31 and 1.45*

Complete results for for $k$ values form 1.31 to 1.45, with increments of 0.01, are reported in appendix B, in terms of average and median values, standard deviation (SD) and of an rough average approximation value obtained as $\frac{p_{max}-p_{min}}{2}$. Moreover, boxplots for all $k$ values and all intervertebral discs are reported there.

A general quasi-linear trend can be recognized, as $k$ increases; this is particularly evident with respect to the median and average pressure values within the disc: small non linearities can be seen for the lower values of $k$, only on the first two intervertebral disc, possibly due to the particular gravity loads that are applied on the top of the model. Nevertheless, a linear interpolation seemed to properly fit the data also for these levels.

### 4.2.4 Linearity of the results

The results presented so far are a collection of the output parameters considered of interest for comparison with data from literature and give an overview of the trend at the variation of $k$. Both for pressure and deformed geometry a linear trend can be observed, with increasing IDP and decreasing IVA (meaning increasing extension) for higher values of $k$. For this reason, to avoid redundancy of data, from now on we will report results only for the upper and lower values of $k$ (1.45 and 1.31 respectively), knowing that, for intermediate values, the model behavior will be in between the two.

## 4.3 Rotations

### 4.3.1 Comparison with numerical simulations

In figure 4.20 the rotations of each vertebra, expressed in degree, are presented. They are compared with numerical data only, since in-vivo data are not avaible. The sacrum is fixed to the ground, therefore, all the rotations are calculated with respect to it. In the follower load condition, as calculated by Rohlmann et al. [11] and in our model, small rotations are obtained. Results are different for the simulations with musculature: the muscle action opposes to the flexural contribution of body weight, providing a final spinal rotation in extension. This can reach up to 10 degree of rotation for L2 with *k* 1.45.

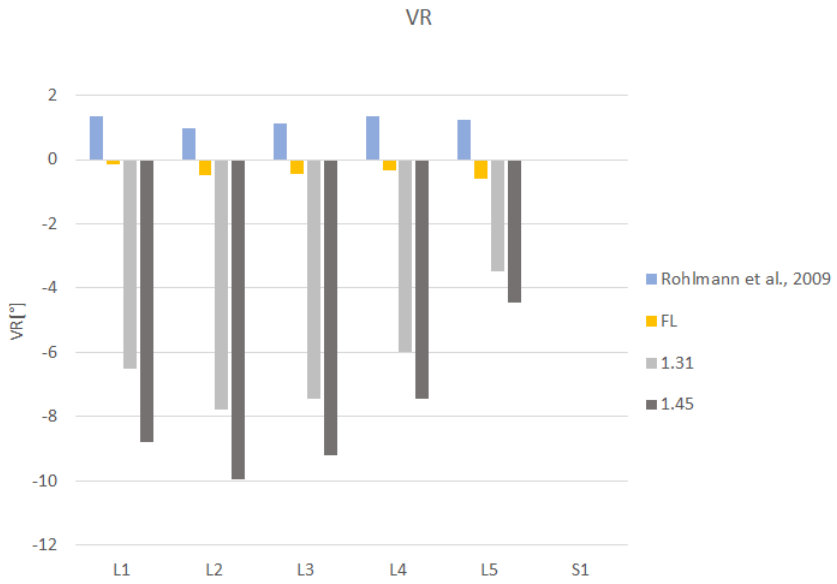


*Figure 4.20: VR of the model for k maximum and minimum and 500 N follower load compared with a follower load of 500N simulated by Rohlmann et al. [11]*

In figure 4.21 the intervertebral rotation of each joint are presented. For simulations with *k*, L1 appears to flex with respect to L2. The reason for

this is that in L1 are applied the force and flexor moment of the upper body weight, producing a lesser extensory effect for this vertebra than on the others, that instead show a posterior rotation. For the follower load simulations, the intervertebral rotations are smaller than the previous ones. Rotations alone cannot allow definitive conclusions on which loading condition should be preferred, but further investigation on the obtained curvature can be made studying the resultant intervertebral angles.

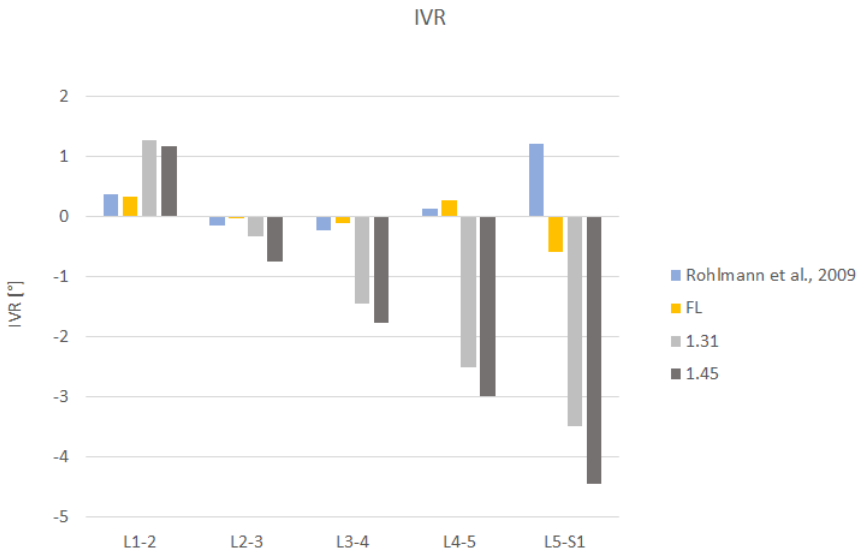


*Figure 4.21: Intervertebral rotations of the model for k maximum and minimum and model with a follower load of 500N compared with a follower load of 500N simulated by Rohlmann et al. [11]*

## 4.4 Intervertebral angles

### 4.4.1 Comparison with undeformed configuration and follower load

The values obtained simulating muscles forces and then follower load are similar for the upper level, while more discrepancy can be observed in the

last vertebral levels (fig. 4.22); its trend, as expected, is that the higher is the lumbar extensory rotation induced, the higher is the angle between L5 and S1.

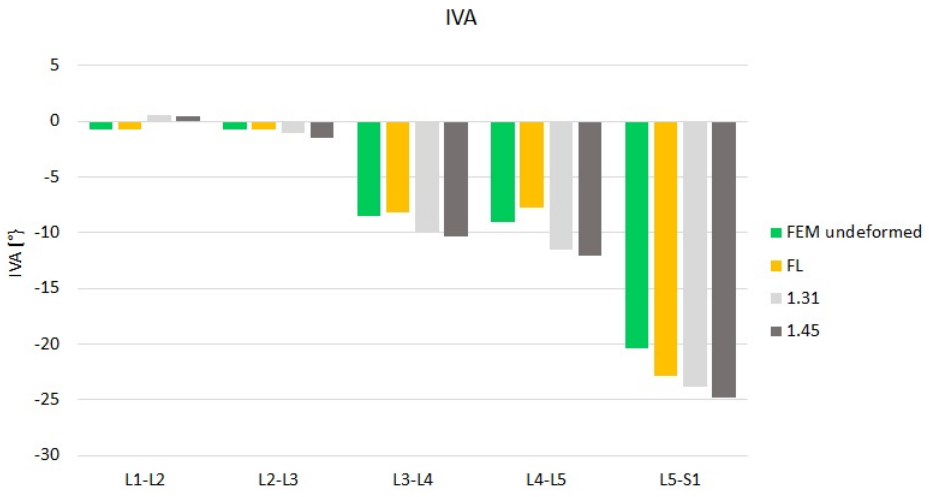


*Figure 4.22: Numerical data of IVA*

### 4.4.2 Comparison with experimental data

For the evaluation of the results in terms of intervertebral angles, experimental studies of Bernhardt et al., [39], Stagnara et al., [40] and Jackson et al., [38] were taken as comparison. In particular, Jackson has been analized 100 standing lateral radiographs of volunteers and 100 standing lateral radiographs of patients with low back pain. Figure 4.23 shows that the results of the model are in good agreement with literature's standard deviation for most of the levels.

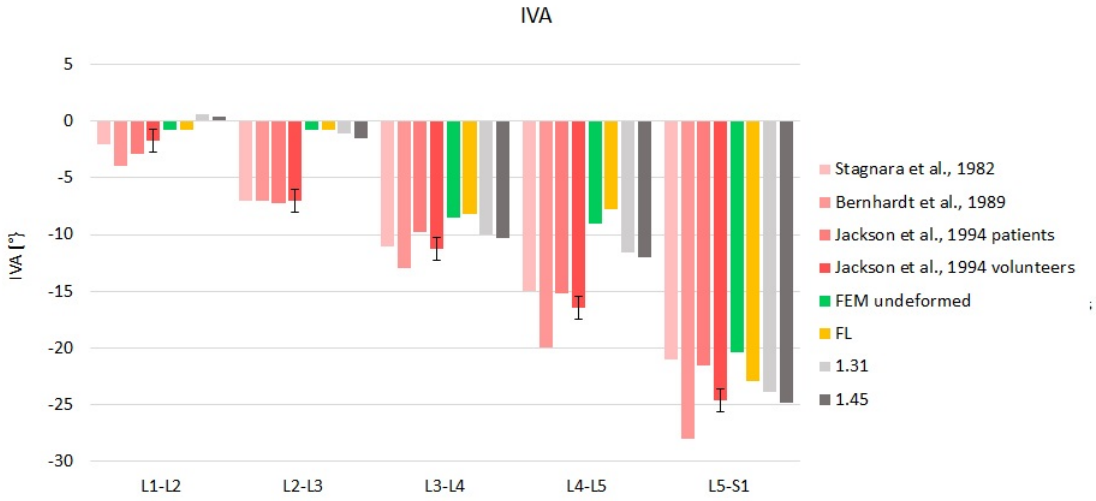


*Figure 4.23: Model's IVA compared with literature [38], [39], [40]*

Only L2-3 and L4-5 show different values but they are not abnormal values as they are included in the maximum and minimum values registered by Jackson et al. (table 4.1).

| | | L1-2 | L2-3 | L3-4 | L4-5 | L5-S1 |
|---|---|---|---|---|---|---|
| IVA [°] | max | 11 | 5 | 0 | 3 | -11 |
| | min | -12 | -18 | -19 | -28 | -39 |

*Table 4.1: Maximum and Minimum values for IVA reported by Jackson et al. [38]*

For further evaluations, a calculation of the difference between the average value of Jackson's study and the model's results were made (table 4.2). Moreover, the sum of the differences for each vertebral joint is reported.

From table 4.2, it appears that the lowest difference is for the simulation with $k$= 1.45, while the highest occurs for the follower load case.

| | | L1-2 | L2-3 | L3-4 | L4-5 | L5-S1 |
|---|---|---|---|---|---|---|
| IVA [°] | Jackson et al., 1994 | -1,7±4, 2 | -7±4, 3 | -11,3±3, 8 | -16,5±5, 0 | -24,6±6, 2 |
| | 1.31 | 0,56 | -1,09 | -9,98 | -11,56 | -23,88 |
| | 1.45 | 0,44 | -1,51 | -10,30 | -12,06 | -24,84 |
| | FL | -0,38 | -0,79 | -8,65 | -8,80 | -20,97 |
| difference[°] | 1.31 | 2,26 | 5,91 | 1,32 | 4,94 | 0,72 |
| | 1.45 | 2,14 | 5,49 | 1,00 | 4,44 | -0,24 |
| | FL | 1,32 | 6,21 | 2,65 | 7,70 | 3,63 |
| diff. sum[°] | 1.31 | 15,14 | | | | |
| | 1.45 | 12,84 | | | | |
| | FL | 21,50 | | | | |

*Table 4.2: Comparison for IVA between experimental data by Jackson et al. [38] and simulation performed with muscles and follower load; differences are calculated between simulations and experimental data for each level and then summed up*

## 4.5 Angles between endplates

### 4.5.1 Comparison with numerical simulations

As for the previous results, the simulations in figure 4.25 shows similar trends in terms of angles. Only L2-3 has an opposite trend beacuse the L2 inferior endplate has a more horizontal direction with respect to the other as can be seen from the figure 4.24.

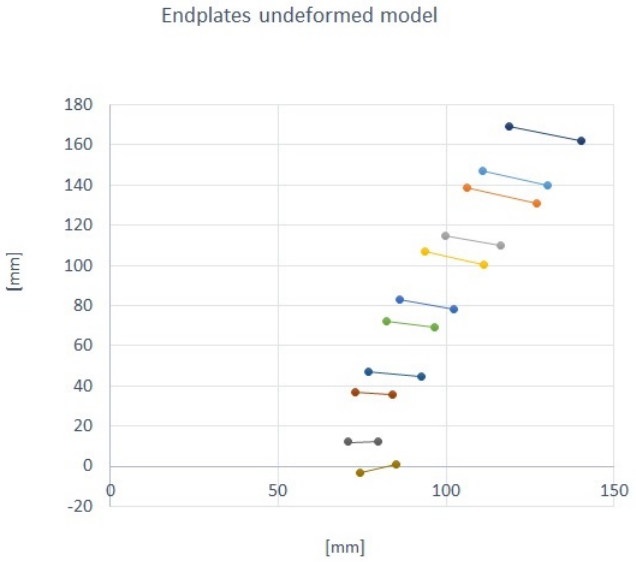


*Figure 4.24: Endplates directions in the undeformed configuration of the FEM model*

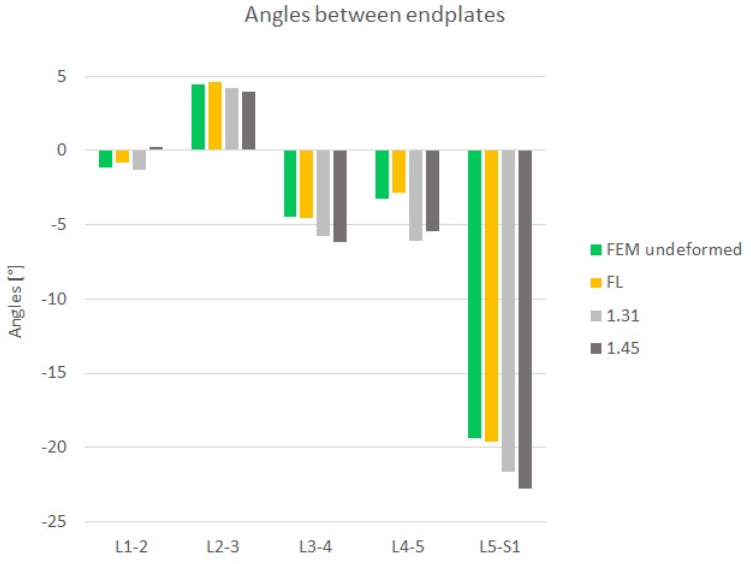


*Figure 4.25: Angles between the endplates of the numerical simulations on the model*

### 4.5.2 Comparison with experimental data

Results compared with other experimental data are here reported, for the angles between endplates (fig. 4.26). Only for L1-2, L3-4 the results fall in the range of Viggiani et al. [22]. Also for these results a comparison of the calculated differences between numerical and in vivo data were made, and are reported in table 4.3.

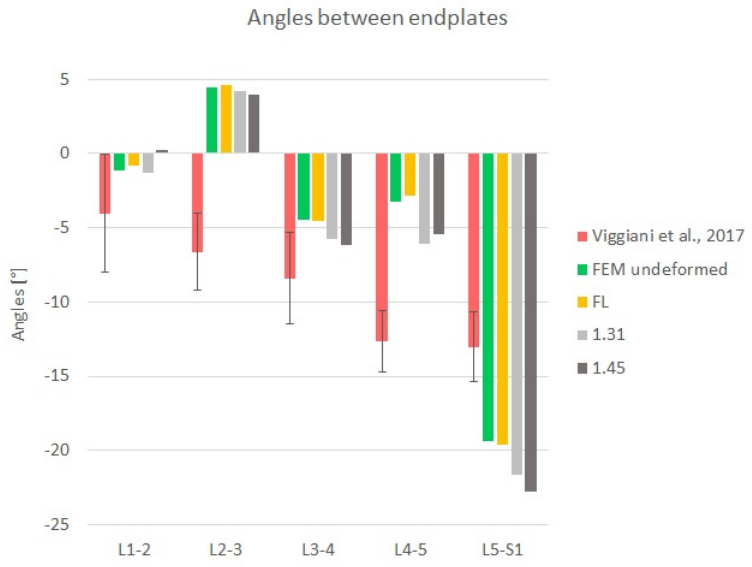


*Figure 4.26: Angles between endplates of the model compared with literature [22]*

Again, the lowest difference value is obtained for the simulation with $k$= 1.45. The sums of the angles reported in figure 4.27, indicate that the simulations with $k$ = 1.31 and 1.45 fall in the in vivo range while FL simulations has inferior values.

| | | L1-2 | L2-3 | L3-4 | L4-5 | L5-S1 |
|---|---|---|---|---|---|---|
| angles [°] | Viggiani et al., 2017 | 4,01±3,9 | 6,62±2,5 | 8,40±3 | 12,64±2 | 13,01±2,3 |
| | 1.31 | 1,26 | -4,22 | 5,73 | 6,05 | 21,67 |
| | 1.45 | -0,25 | -3,96 | 6,17 | 5,43 | 22,76 |
| | FL | 0,78 | -4,65 | 4,51 | 2,87 | 19,58 |
| difference[°] | 1.31 | 2,75 | 10,84 | 2,67 | 6,59 | -8,66 |
| | 1.45 | 4,27 | 10,57 | 2,23 | 7,21 | -9,75 |
| | FL | 3,23 | 11,27 | 3,89 | 9,77 | -6,57 |
| diff. sum[°] | 1.31 | 14,18 | | | | |
| | 1.45 | 14,53 | | | | |
| | FL | 21,59 | | | | |

*Table 4.3: Comparison for angles between endplates with experimental data by Viggiani et al. [22] and simulation performed with muscles and follower load; differences are calculated between simulations and experimental data for each level and then summed up*

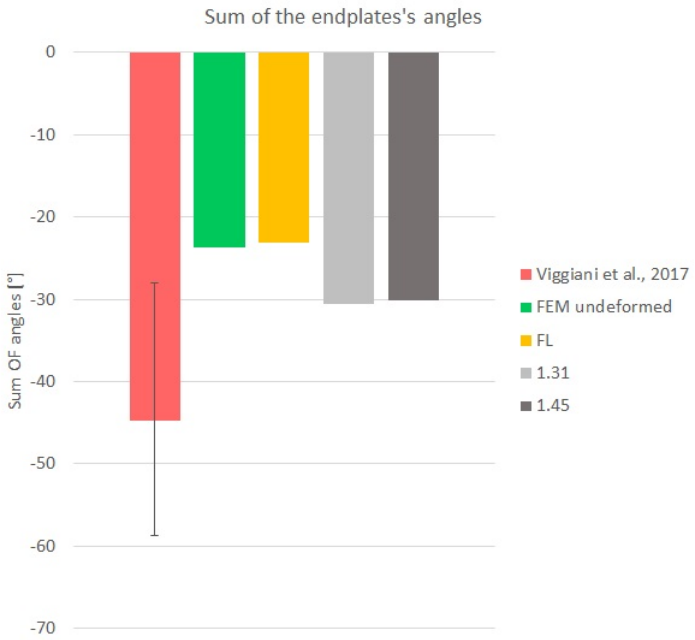


*Figure 4.27: Sum of the angles between endplates compared with literature [22]*

Also for the sum of the angles between endplates, a better correspondance with in vivo data are shown for the muscle forces simulations ($k$=1.31 and $k$=1.45).

## 4.6 Lordosis and lumbosacral angle

The lordosis has been evaluated from L1 to L5 and from L1 to S1 in figures 4.28 and 4.29. The L1-L5 lordosis is a low value for the column with respect to literature while for L1-S1 lordosis the values are more in accordance with the Tarantino's range. This prove that the model has a small curvature from L1 to L5 but a more accentuated lordosis is present between L5 and S1. This is confirmed by the analysis of the lumbosacral angle: the angle of the model is lower than the one of literature, meaning that L5 and S1 are more inclined between them.

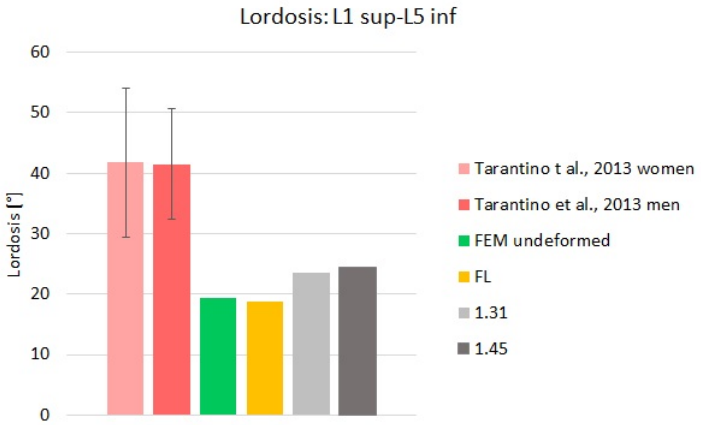


*Figure 4.28: Lumbar lordosis calculated as the angle between the superior endplate of L1 and the inferior endplate of L5. Comparisons with literature have been made. [23]*

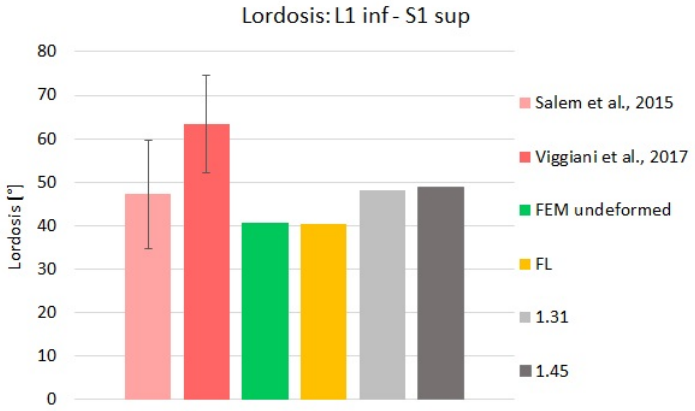


*Figure 4.29: Lordosis calculated from the inferior endplate of L1 and the superior endplate of S1 compared to Viggiani et al. [22] and Salem et al. [41]*

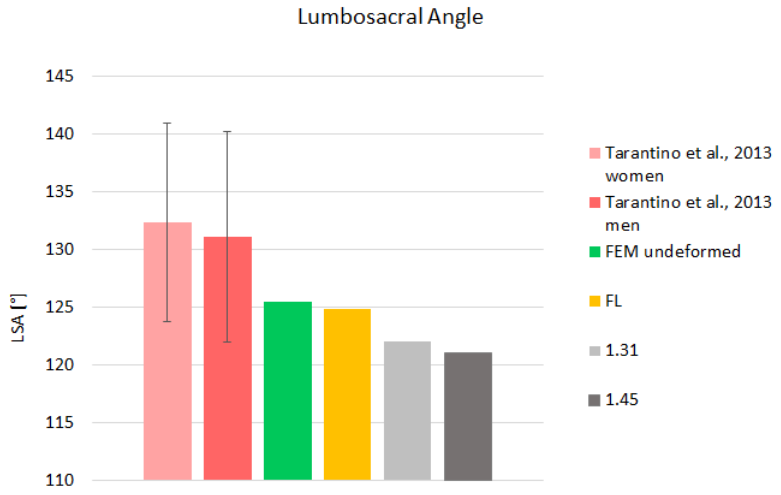


*Figure 4.30: Lumbosacral angle compared with Tarantino [23]*

## 4.7 Intradiscal pressure

### 4.7.1 Comparison with numerical simulations

For pressure data obtained within the intervertebral discs, boxplots have been built; this operation is not feasible with data from literature, as authors provide a single values for IDP. On the contrary, the operation could

be done with pressures obtained from the model before the implementation of musculature, in the case the standing condition was simulated via the application of a follower load of 500 N. Comparisons have been made with literature, with data provided by Rohlmann et al. [11]. Here a 500 N follower load is applied again. In figure 4.31 box plots of data from our model are presented along with Rohlmann's.

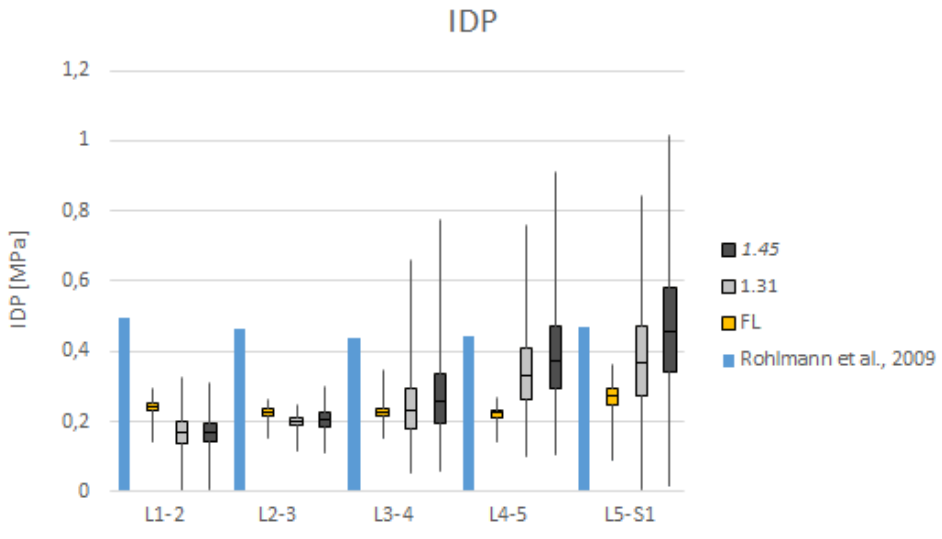


*Figure 4.31: Comparison of pressure values with numerical data by Rohlmann et al. [11] for all intervertebral discs*

From the graphs it can be deduced that in the case of follower load application a more uniform pressure distribution occurs, while the application of muscles forces results in a wider curve with increased standard deviation. This fact can be explained as the follower loads provides an almost purely compressive action on each vertebral joint, while the simulated condition, with complex loads both from muscles and gravity loads, results in less predictable dynamics on the single level, though the overall action on the lumbar spine can be considered axial.

### 4.7.2 Comparison with experimental data

In this section pressure data are compared with in-vivo measurement. As already mentioned, the comparison with such experimental data suffer some limitations, due to the availability of IDP values only for the L3-L4 and L4-L5 intervertebral discs. Nevertheless, being these the most stressed of the lumbar spine, interesting considerations can be made basing on these sole data. In figures 4.32 and 4.33 IDP registered in-vivo are presented together with data from our model, both in the follower load case and with the addition of muscles.

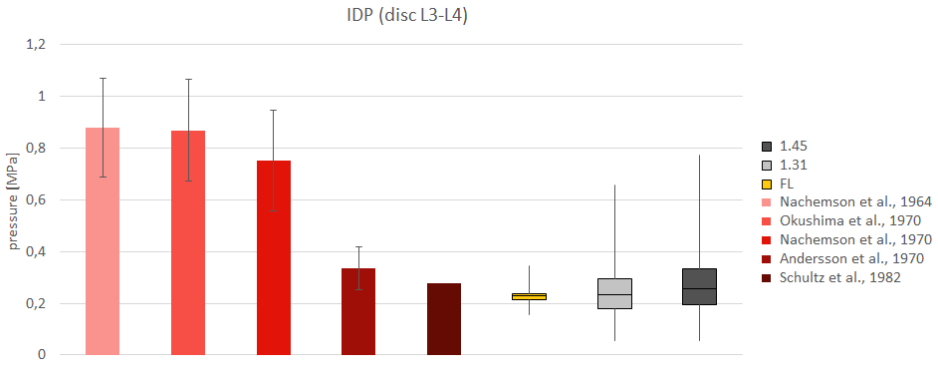


*Figure 4.32: Comparison of pressure values for the L3-L4 disc with in-vivo data from literature [42] [43] [44] [45] [46]*

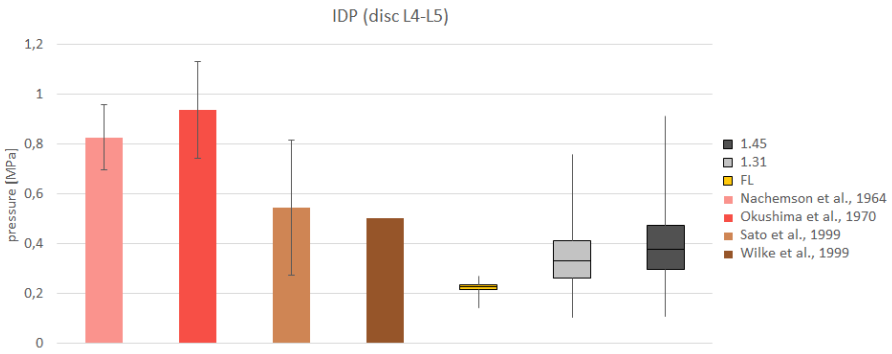


*Figure 4.33: Comparison of pressure values for the L4-L5 disc with in-vivo data from literature [42] [43] [47] [48]*

It must be noticed that data reported from literature present non negligible variations: IDP recorded in the disc L4-L5 varies of 0.6 MPa between the maximum and minumum reported values, while for L5-S1 the variation is about 0.4 MPa. However, it can be observed the simulations performed with follower load tend to give as an output a pressure value inferior to the experimental one; the application of muscles forces increases IDP, making its median value closer to that reported by the most recent studies. It is interesting noticing that, for the FL case on the L4-L5 disc, also the maximum pressure value does not reach the magnitude expected form literature.

# Chapter 5

# CONCLUSIONS AND FUTURE DEVELOPMENTS

In this last chapter we discuss the presented results and make considerations on the possible further developments of the model.
Before this study, a finite element model of the lumbar spine already existed in our department, and was employed for several aims, but performing simulations only with simplified loading conditions. In particular we refer to the application of a follower load, commonly considered in literature as one the most efficient way of simulating standing [11]. Its reliability lays in particular in the simplicity of modelling it, both experimentally and for numerical testing. An almost totally axial action of 500 N between each vertebral joint is accepted as representative of the overall effect of gravitational components, that alone would flex the spine, and local musculature, mainly positioned posteriorly and then resulting in an extension effect. Modelling standing in such a way results in an almost unchanged lumbar curvature with respect to the unloaded configuration, as reported by Rohlmann et al. [11] and confirmed by simulations made on our model. On the other hand, it is evident that the dynamic situation on the spine is much more complex than that proposed by a follower load application: on

a single vertebra act several muscles, each with a different attachment site and a different force direction, resulting in a specific kinematic contribution in space. Moreover, also loads deriving from gravity act differently on each spinal level, resulting in specific contributions of flexion for each vertebra. In this study we tried to reach a more precise level of modellization of the whole loads acting on the lumbar spine, both for muscles forces and gravitational loads. In our aim this would result in more attainable data in terms of rotations, angles and pressures. The determination of forces acting on each fascicle resulted to be the real issue of the work. Once stated that standing would have been the situation to be simulated, it was clear that no univocal solution could be found. This both because different targets could be identified as objective functions (moment equilibrium, null shear forces, minimum of energy expenditure, ...) and because of the multitude of forces in action, that resulted in a redundancy of the solutions. Possibly, one choice rather than another one could have brought to different results; this fact also maintains open the possibility for further optimization of muscles forces.

We base our considerations on the resultant kinematics on two variables: the rotation that occurred between unloaded and loaded configuration, and the consequent angles between the vertebrae. For rotations, in-vivo data are hardly obtainable: an unloaded spine, in fact, exists only in the testing process and in reality, on a standing subject, the effects of gravity and musculature cannot be avoided. Intervertebral rotations can then be compared only with in-vitro and numerical simulations, then recurring in the simplifications on loads naturally introduced with these approaches. Numerical evidences, in particular, register rotations around zero, being the follower action prevalently axial. With the loading conditions we introduced, we got instead an overall effect of posterior rotation (extension), limited to a total of $9^\circ$ on L1. Thus, the purely axial effect obtainable with a follower

load does not occurs any more with our loading conditions, but a shear and moment contribution inevitably arise.
On the other hand, if comparison with in-vivo data is to be made, one should rely on angles, easily obtainable via radiographic analysis on a standing subject [38] [22]. In these regard, we noticed that the unloaded geometry of our model presented a low lordotic angle, barely in range with physiological values. This situation remained unchanged after the application of a follower load, being almost null the rotations. On the contrary, the extension effect induced by the new loading condition had the effect of accentuating the spinal curvature, with the result of decreasing the gap between physiological average values and our model's intervertebral angle.
The last parameter to be studied was intradiscal pressure. In literature it is not clear which value should be reported for IDP within the disc for computational studies: numerical models often make use of solid elastic materials for modelling the nucleus, resulting in a non-uniform distribution on it. Reporting the maximum rather than the average or median value means presenting a completely different scenario, so we decided to present data in the form of boxplots, so that the entire behaviour could be visualized. A comparison with the follower load case indicated that a wider spreading of pressure values occurs if applying complex loading conditions. This is explainable as an extension moment contribution exists, and so the most posterior points of the nucleus are subjected to a higher compression than the anterior ones, resulting in a higher pressure value for the former and a lower one for the latter.
Given the availability of data explained, comparison with in-vivo data can be made only for the L3-L4 and L4-L5 discs. For the first, the follower load case shows low pressure both in terms of maximum and median, remaining out of the ranges proposed by the studies of Nachemson et al. [42] [44] and Okushima et al. [43], but close to those of Anderrson et al. [45] and Schultz

et al. [46]. The complex loading condition shows similar median values, though the data are more spread, and the highest values get closer in range with the standard deviation of Nachemson et al. [42] [44] and Okushima et al.[43]. For the L4-L5 disc, the follower load values appear lower than those reported by all the considered studies. The new loading condition, in this case, is instead able to return higher pressures both in terms of median and maximum values. This distributions seems to be much closer to all the in-vivo studies than the follower load.

Reassuming all the above considerations, it has been noticed that the addition of muscles forces and complex gravity loads introduce rotations that a follower load does not present. These rotations, however had the effect of extending the spine, leading to a final spinal curvature closer to a physiological average value, considering that the undeformed geometry showed a hypolordotic profile. For pressures, reminding the ambiguity in the IDP values, clear evidences can be made on the L4-L5 disc, on which registered values tend to better represent those reported by in-vivo studies.

To be further investigated is how the model behaviour would change if different targets should be posed for the search of muscles forces values. Other studies implemented algorithms so that the overall effect of loads could be compared to the axial action typical of the follower load [93] [94]. This would likely reduce the rotation of the vertebrae, but on the other hand would leave the model curvature straightened. Different forces values should be implemented on the model, having in mind the main goal of the simulation to be performed, knowing that different dynamic conditions could lead to much different scenarios. Moreover, in this study we limited to simulating a standing condition, while it would be of course interesting testing also to flexion and extension. In regard to this, a possible implementation of further muscles could be made: the main role in anterior flexion of the body, in fact, is of the global muscles that are not included in our

model (rectus abdominus and internal and external oblique) and then they would result crucial for simulating new motions in space. The implementation of more extended musculature would then allow the simulation of more complex condition, always considering that, for acceptable results, a suitable algorithm for muscles forces optimization must be implemented.

# Bibliography


[1] Dr. Chris. Parts of the spine: Anatomy, picture, spinal column, backbone. http://www.healthhype.com/parts-of-the-spine-anatomy-picture-spinal-column-backbone.html.

[2] MHA Stephen Kishner, MD. Lumbar spine anatomy. https://www.google.it/url?sa=i&rct=j&q=&esrc=s&source=images&cd=&cad=rja&uact=8&ved=0ahUKEwiMw9-DvbTXAhWCPhQKHV88DDcQjRwIBw&url=http%3A%2F%2Femedicine.medscape.com%2Farticle%2F1899031-overview&psig=AOvVaw2kfjNj0FsnkL-BX_2Aekja&ust=1510419437646467.

[3] Ella Been, Asier Gómez-Olivencia, and Patricia A Kramer. Brief communication: Lumbar lordosis in extinct hominins: implications of the pelvic incidence. *American journal of physical anthropology*, 154(2):307–314, 2014.

[4] Assit. Professor at Padmashree Dr. D.Y. Biomechanics of lumbar spine. https://www.slideshare.net/venus88/biomechanics-of-lumbar-spine.

[5] Dale Reese Tom G.Mayer MD, Eric A.K. Mayer MD. Lumbar musculature: Anatomy and function. https://www.google.it/url?sa=i&rct=j&q=&esrc=s&source=

images&cd=&cad=rja&uact=8&ved=0ahUKEwiymZyN3p_WAhVNL1AKHW1jD3oQjhwIBQ&url=https%3A%2F%2Fclinicalgate.com%2Flumbar-musculature-anatomy-and-function%2F&psig=AFQjCNFkZ-z3mYugVTjC6En9QB7JIAsLKg&ust=1505308697671408.

[6] The lumbar muscles and their fasciae. https://www.google.it/url?sa=i&rct=j&q=&esrc=s&source=images&cd=&cad=rja&uact=8&ved=0ahUKEwj40autu6LWAhVPZ1AKHYjpBYUQjhwIBQ&url=https%3A%2F%2Fclinicalgate.com%2Fthe-lumbar-muscles-and-their-fasciae%2F&psig=AFQjCNGC2-OlBJ9qIpiswcldL0IWy9d9WA&ust=1505402424603894.

[7] NPMHG Bogduk, M Pearcy, and G Hadfield. Anatomy and biomechanics of psoas major. *Clinical Biomechanics*, 7(2):109–119, 1992.

[8] Interspinales. http://body-disease.com/interspinales/.

[9] H-J Wilke, A Rohlmann, S Neller, F Graichen, L Claes, and G Bergmann. Issls prize winner: a novel approach to determine trunk muscle forces during flexion and extension: a comparison of data from an in vitro experiment and in vivo measurements. *Spine*, 28(23):2585–2593, 2003.

[10] H-J Wilke, K Wenger, and L Claes. Testing criteria for spinal implants: recommendations for the standardization of in vitro stability testing of spinal implants. *European Spine Journal*, 7(2):148–154, 1998.

[11] A Rohlmann, T Zander, M Rao, and G Bergmann. Applying a follower load delivers realistic results for simulating standing. *Journal of biomechanics*, 42(10):1520–1526, 2009.

[12] A Shirazi-Adl, S Sadouk, M Parnianpour, D Pop, and M El-Rich. Muscle force evaluation and the role of posture in human lumbar spine under compression. *European spine journal*, 11(6):519–526, 2002.

[13] M Dreischarf, T Zander, A Adl, CM Puttlitz, CJ Adam, CS Chen, VK Goel, A Kiapour, YH Kim, KM Labus, et al. Comparison of eight published static finite element models of the intact lumbar spine: predictive power of models improves when combined together. *Journal of biomechanics*, 47(8):1757–1766, 2014.

[14] A Rohlmann, T Zander, M Rao, and G Bergmann. Realistic loading conditions for upper body bending. *Journal of Biomechanics*, 42(7):884–890, 2009.

[15] Shih-Hao Chen, Zheng-Cheng Zhong, Chen-Sheng Chen, Wen-Jer Chen, and Chinghua Hung. Biomechanical comparison between lumbar disc arthroplasty and fusion. *Medical engineering & physics*, 31(2):244–253, 2009.

[16] Ian AF Stokes and Mack Gardner-Morse. Quantitative anatomy of the lumbar musculature. *Journal of biomechanics*, 32(3):311–316, 1999.

[17] A Shirazi-Adl, M El-Rich, DG Pop, and M Parnianpour. Spinal muscle forces, internal loads and stability in standing under various postures and loads: application of kinematics-based algorithm. *European spine journal*, 14(4):381–392, 2005.

[18] Wen-Hsien Chuang, Shang-Chih Lin, Shih-Hao Chen, Chih-Wei Wang, Wen-Chi Tsai, Yeung-Jen Chen, and Jiun-Ren Hwang. Biomechanical effects of disc degeneration and hybrid fixation on the transition and adjacent lumbar segments: trade-off between junctional problem, motion preservation, and load protection. *Spine*, 37(24):E1488–E1497, 2012.

[19] David J Pearsall, J Gavin Reid, and Lori A Livingston. Segmental inertial parameters of the human trunk as determined from computed tomography. *Annals of biomedical engineering*, 24(2):198–210, 1996.

[20] Alexander Kiefer, A Shirazi-Adl, and M Parnianpour. Synergy of the human spine in neutral postures. *European Spine Journal*, 7(6):471–479, 1998.

[21] Marwan El-Rich, Aboulfazl Shirazi-Adl, and Navid Arjmand. Muscle activity, internal loads, and stability of the human spine in standing postures: combined model and in vivo studies. *Spine*, 29(23):2633–2642, 2004.

[22] Daniel Viggiani, Kaitlin M Gallagher, Michael Sehl, and Jack P Callaghan. The distribution of lumbar intervertebral angles in upright standing and extension is related to low back pain developed during standing. *Clinical Biomechanics*, 49:85–90, 2017.

[23] Umberto Tarantino, Ezio Fanucci, Riccardo Iundusi, Monica Celi, Simone Altobelli, Elena Gasbarra, Giovanni Simonetti, and Guglielmo Manenti. Lumbar spine mri in upright position for diagnosing acute and chronic low back pain: statistical analysis of morphological changes. *Journal of Orthopaedics and Traumatology*, 14(1):15–22, 2013.

[24] Péter Rajnics, Alexandre Templier, Wafa Skalli, Francois Lavaste, and Tamás Illés. The association of sagittal spinal and pelvic parameters in asymptomatic persons and patients with isthmic spondylolisthesis. *Clinical Spine Surgery*, 15(1):24–30, 2002.

[25] Sébastien Schuller, Yann Philippe Charles, and Jean-Paul Steib. Sagittal spinopelvic alignment and body mass index in patients with degenerative spondylolisthesis. *European Spine Journal*, 20(5):713–719, 2011.

[26] C Boulay, C Tardieu, J Hecquet, C Benaim, B Mouilleseaux, C Marty, D Prat-Pradal, Jean Legaye, Ginette Duval-Beaupère, and J Pélissier. Sagittal alignment of spine and pelvis regulated by pelvic incidence:

standard values and prediction of lordosis. *European Spine Journal*, 15(4):415–422, 2006.

[27] Haruki Funao, Takashi Tsuji, Naobumi Hosogane, Kota Watanabe, Ken Ishii, Masaya Nakamura, Kazuhiro Chiba, Yoshiaki Toyama, and Morio Matsumoto. Comparative study of spinopelvic sagittal alignment between patients with and without degenerative spondylolisthesis. *European Spine Journal*, 21(11):2181–2187, 2012.

[28] Gérard Morvan, Philippe Mathieu, Valérie Vuillemin, Henri Guerini, Philippe Bossard, Frédéric Zeitoun, and Marc Wybier. Standardized way for imaging of the sagittal spinal balance. *European Spine Journal*, 20(5):602, 2011.

[29] Sadegh Naserkhaki, Jacob L Jaremko, Samer Adeeb, and Marwan El-Rich. On the load-sharing along the ligamentous lumbosacral spine in flexed and extended postures: Finite element study. *Journal of biomechanics*, 49(6):974–982, 2016.

[30] Antonius Rohlmann, Sylvia Neller, Lutz Claes, Georg Bergmann, and Hans-Joachim Wilke. Influence of a follower load on intradiscal pressure and intersegmental rotation of the lumbar spine. *Spine*, 26(24):E557–E561, 2001.

[31] Isao Yamamoto, Manohar M Panjabi, Trey Crisco, and TOM Oxland. Three-dimensional movements of the whole lumbar spine and lumbosacral joint. *Spine*, 14(11):1256–1260, 1989.

[32] Daniel J Cook, Matthew S Yeager, and Boyle C Cheng. Range of motion of the intact lumbar segment: a multivariate study of 42 lumbar spines. *International journal of spine surgery*, 9, 2015.

[33] Mark A Hayes, Thomas C Howard, Curtis R Gruel, and Joseph A

Kopta. Roentgenographic evaluation of lumbar spine flexion-extension in asymptomatic individuals. *Spine*, 14(3):327–331, 1989.

[34] MJ Pearcy and SB Tibrewal. Axial rotation and lateral bending in the normal lumbar spine measured by three-dimensional radiography. *Spine*, 9(6):582–587, 1984.

[35] Ugur M Ayturk and Christian M Puttlitz. Parametric convergence sensitivity and validation of a finite element model of the human lumbar spine. *Computer methods in biomechanics and biomedical engineering*, 14(8):695–705, 2011.

[36] Frank Heuer, Hendrik Schmidt, Lutz Claes, and Hans-Joachim Wilke. Stepwise reduction of functional spinal structures increase vertebral translation and intradiscal pressure. *Journal of biomechanics*, 40(4):795–803, 2007.

[37] Paul Brinckmann and Henk Grootenboer. Change of disc height, radial disc bulge, and intradiscal pressure from discectomy an in vitro investigation on human lumbar discs. *Spine*, 16(6):641–646, 1991.

[38] Roger P Jackson and Anne C McManus. Radiographic analysis of sagittal plane alignment and balance in standing volunteers and patients with low back pain matched for age, sex, and size: A prospective controlled clinical study. *Spine*, 19(14):1611–1618, 1994.

[39] Mark Bernhardt and Keith H Bridwell. Segmental analysis of the sagittal plane alignment of the normal thoracic and lumbar spines and thoracolumbar junction. *Spine*, 14(7):717–721, 1989.

[40] Peirre Stagnara, Jean Claude De Mauroy, Georges Dran, Georges P Gonon, Giuseppe Costanzo, Joannes Dimnet, and Annick Pasquet. Reciprocal angulation of vertebral bodies in a sagittal plane: approach to

references for the evaluation of kyphosis and lordosis. *Spine*, 7(4):335–342, 1982.

[41] Walid Salem, Ysaline Coomans, Jean-Michel Brismée, Paul Klein, Stéphane Sobczak, and Pierre-Michel Dugailly. Sagittal thoracic and lumbar spine profiles in upright standing and lying prone positions among healthy subjects: Influence of various biometric features. *Spine*, 40(15):E900–E908, 2015.

[42] Alf Nachemson. The influence of spinal movements on the lumbar intradiscal pressure and on the tensile stresses in the annulus fibrosus. *Acta Orthopaedica Scandinavica*, 33(1-4):183–207, 1963.

[43] H Okushima. Study on hydrodynamic pressure of lumbar intervertebral disc. *Nihon geka hokan. Archiv fur japanische Chirurgie*, 39(1):45, 1970.

[44] Alf Nachemson and GOSTA Elfstrom. Intravital dynamic pressure measurements in lumbar discs. *Scand J Rehabil Med*, 2(suppl 1):1–40, 1970.

[45] BJ Andersson and R Ortengren. Lumbar disc pressure and myoelectric back muscle activity during sitting. ii. studies on an office chair. *Scandinavian Journal of rehabilitation medicine*, 6(3):115, 1974.

[46] Albert Schultz, Gunnar Andersson, R Ortengren, K Haderspeck, and A Nachemson. Loads on the lumbar spine. validation of a biomechanical analysis by measurements of intradiscal pressures and myoelectric signals. *JBJS*, 64(5):713–720, 1982.

[47] Katsuhiko Sato, Shinichi Kikuchi, and Takumi Yonezawa. In vivo intradiscal pressure measurement in healthy individuals and in patients with ongoing back problems. *Spine*, 24(23):2468, 1999.

[48] Hans-Joachim Wilke, Peter Neef, Marco Caimi, Thomas Hoogland, and Lutz E Claes. New in vivo measurements of pressures in the intervertebral disc in daily life. *Spine*, 24(8):755–762, 1999.

[49] Christian Wong, John Rasmussen, Erik Simonsen, Lone Hansen, Mark de Zee, and Sebastian Dendorfer. The influence of muscle forces on the stress distribution in the lumbar spine. *Open Spine J*, 3:21–26, 2011.

[50] Tonya Hines. Anatomy of the human spine. `https://www.google.it/url?sa=t&rct=j&q=&esrc=s&source=web&cd=7&cad=rja&uact=8&ved=0ahUKEwjPl7j2kt7XAhURpaQKHY6fDiYQFgg3MAY&url=https%3A%2F%2Fwww.spineuniverse.com%2Fanatomy%2Fspinal-cord-ligaments-muscles-blood-supply&usg=AOvVaw3zCFEpCMs-kDHfI57480YJ`.

[51] Riza Bayoglu, Leo Geeraedts, Karlijn HJ Groenen, Nico Verdonschot, Bart Koopman, and Jasper Homminga. Twente spine model: A complete and coherent dataset for musculo-skeletal modeling of the thoracic and cervical regions of the human spine. *Journal of biomechanics*, 2017.

[52] Francisco Ezquerro, Antonio Simón, María Prado, and Ana Pérez. Combination of finite element modeling and optimization for the study of lumbar spine biomechanics considering the 3d thorax–pelvis orientation. *Medical engineering & physics*, 26(1):11–22, 2004.

[53] Kao-Shang Shih, Pei-Wei Weng, Shang-Chih Lin, Yi-Tzu Chen, Cheng-Kung Cheng, and Chian-Her Lee. Biomechanical comparison between concentrated, follower, and muscular loads of the lumbar column. *Computer methods and programs in biomedicine*, 135:209–218, 2016.

[54] A Shirazi-Adl and M Parnianpour. Load-bearing and stress analysis of

the human spine under a novel wrapping compression loading. *Clinical Biomechanics*, 15(10):718–725, 2000.

[55] Ella Been and Leonid Kalichman. Lumbar lordosis. *The Spine Journal*, 14(1):87–97, 2014.

[56] PhD Huei-Ming Chai, PT. Sacral angle. `http://www.pt.ntu.edu.tw/hmchai/hGlossary/SacralAngle.htm`.

[57] Thomas M. Gavin Avinash G. Patwardhan, Kevin P. Meade. Biomechanics of the spine. `https://musculoskeletalkey.com/biomechanics-of-the-spine/`.

[58] Dan Washmuth. Multifidus muscle: Origin, insertion and action. `http://study.com/academy/lesson/multifidus-muscle-origin-insertion-action.html`.

[59] MD Keith Bridwell. Spinal muscles: A comprehensive guide. `https://www.spineuniverse.com/anatomy/spinal-muscles-1`.

[60] Chu ML Yazdani-Ardakani and S Gradisar IA Askew MJ. Partitioning of the l4-l5 dynamic moment into disc, ligamentous, and muscular components during lifting 1986 volvo award in biomechanics. *J Biomech*, 19(97):87, 1986.

[61] GA Dumas, MJ Poulin, B Roy, M Gagnon, and M Jovanovic. Orientation and moment arms of some trunk muscles. *Spine*, 16(3):293–303, 1991.

[62] Lone Hansen, Mark De Zee, John Rasmussen, Thomas B Andersen, Christian Wong, and Erik B Simonsen. Anatomy and biomechanics of the back muscles in the lumbar spine with reference to biomechanical modeling. *Spine*, 31(17):1888–1899, 2006.

[63] L Penning. Psoas muscle and lumbar spine stability: a concept uniting existing controversies. *European Spine Journal*, 9(6):577–585, 2000.

[64] Eva Andersson, L Oddsson, H Grundström, and Alf Thorstensson. The role of the psoas and iliacus muscles for stability and movement of the lumbar spine, pelvis and hip. *Scandinavian journal of medicine & science in sports*, 5(1):10–16, 1995.

[65] HF Farfan. Form and function of the musculoskeletal system as revealed by mathematical analysis of the lumbar spine: An essay. *Spine*, 20(13):1462–1473, 1995.

[66] S Gracovetsky. An hypothesis for the role of the spine in human locomotion: a challenge to current thinking. *Journal of biomedical engineering*, 7(3):205–216, 1985.

[67] Phill Pollintine, Patricia Dolan, Jon H Tobias, and Michael A Adams. Intervertebral disc degeneration can lead to stress-shielding of the anterior vertebral body: a cause of osteoporotic vertebral fracture? *Spine*, 29(7):774–782, 2004.

[68] MA Adams, WC Hutton, and JRR Stott. The resistance to flexion of the lumbar intervertebral joint. *Spine*, 5(3):245–253, 1980.

[69] Hans-Joachim Wilke, Antonius Rohlmann, Sylvia Neller, Markus Schulthei, Georg Bergmann, Friedmar Graichen, and Lutz E Claes. Is it possible to simulate physiologic loading conditions by applying pure moments?: A comparison of in vivo and in vitro load components in an internal fixator. *Spine*, 26(6):636–642, 2001.

[70] Manohar Panjabi, Kuniyoshi Abumi, Joanne Duranceau, and Thomas Oxland. Spinal stability and intersegmental muscle forces: A biomechanical model. *Spine*, 14(2):194–200, 1989.

[71] H-J Wilke, L Claes, H Schmitt, and S Wolf. A universal spine tester for in vitro experiments with muscle force simulation. *European Spine Journal*, 3(2):91–97, 1994.

[72] Claudia Ottardi. Strategies for the biomechanical evaluation of spine surgery: computational models and experimental testing. 2015.

[73] C Breau, A Shirazi Adl, and J De Guise. Reconstruction of a human ligamentous lumbar spine using ct images: a three-dimensional finite element mesh generation. *Annals of biomedical engineering*, 19(3):291–302, 1991.

[74] Antonius Rohlmann, Lars Bauer, Thomas Zander, Georg Bergmann, and Hans-Joachim Wilke. Determination of trunk muscle forces for flexion and extension by using a validated finite element model of the lumbar spine and measured in vivo data. *Journal of Biomechanics*, 39(6):981–989, 2006.

[75] Marcel Dreischarf, Antonius Rohlmann, Rui Zhu, Hendrik Schmidt, and Thomas Zander. Is it possible to estimate the compressive force in the lumbar spine from intradiscal pressure measurements? a finite element evaluation. *Medical engineering & physics*, 35(9):1385–1390, 2013.

[76] David A Winter. *Biomechanics and motor control of human movement*. John Wiley & Sons, 2009.

[77] Navid Arjmand and Aboulfazl Shirazi-Adl. Biomechanics of changes in lumbar posture in static lifting. *Spine*, 30(23):2637–2648, 2005.

[78] Nikolai Bogduk, Janet E Macintosh, and Mark J Pearcy. A universal model of the lumbar back muscles in the upright position. *Spine*, 17(8):897–913, 1992.

[79] Babak Bazrgari, Aboulfazl Shirazi-Adl, and Navid Arjmand. Analysis of squat and stoop dynamic liftings: muscle forces and internal spinal loads. *European Spine Journal*, 16(5):687–699, 2007.

[80] Ian AF Stokes and Mack Gardner-Morse. Lumbar spinal muscle activation synergies predicted by multi-criteria cost function. *Journal of biomechanics*, 34(6):733–740, 2001.

[81] Albert B Schultz and Gunnar BJ Andersson. Analysis of loads on the lumbar spine. *Spine*, 6(1):76–82, 1981.

[82] Kevin P Granata and WS Marras. An emg-assisted model of trunk loading during free-dynamic lifting. *Journal of biomechanics*, 28(11):1309–1317, 1995.

[83] Ali M Alshami. Prevalence of spinal disorders and their relationships with age and gender. *Saudi medical journal*, 36(6):725, 2015.

[84] A Kiefer, M Parnianpour, and A Shirazi-Adl. Stability of the human spine in neutral postures. *European Spine Journal*, 6(1):45–53, 1997.

[85] Iris Busscher, Joris JW Ploegmakers, Gijsbertus J Verkerke, and Albert G Veldhuizen. Comparative anatomical dimensions of the complete human and porcine spine. *European Spine Journal*, 19(7):1104–1114, 2010.

[86] Robert Eberlein, Gerhard A Holzapfel, and Markus Fröhlich. Multi-segment fea of the human lumbar spine including the heterogeneity of the annulus fibrosus. *Computational Mechanics*, 34(2):147–163, 2004.

[87] IA Kapandji. The trunk and the vertebral column. *The Physiology of the Joint*, 3:42–119, 1980.

[88] Fabio Galbusera, Chiara Maria Bellini, Federica Anasetti, Cristina Ciavarro, Alessio Lovi, and Marco Brayda-Bruno. Rigid and flexible

spinal stabilization devices: a biomechanical comparison. *Medical engineering & physics*, 33(4):490–496, 2011.

[89] Pasquale Vena, Giampaolo Franzoso, Dario Gastaldi, Roberto Contro, and Villiam Dallolio. A finite element model of the l4–l5 spinal motion segment: biomechanical compatibility of an interspinous device. *Computer methods in biomechanics and biomedical engineering*, 8(1):7–16, 2005.

[90] Danè Dabirrahmani, Stephan Becker, Michael Hogg, Richard Appleyard, Gamal Baroud, and Mark Gillies. Mechanical variables affecting balloon kyphoplasty outcome–a finite element study. *Computer methods in biomechanics and biomedical engineering*, 15(3):211–220, 2012.

[91] Mina Alizadeh, Mohammed Rafiq Abdul Kadir, and Saturnino Saldanha. Biomechanical effects of short construct spine posterior fixation, in thoracolumbar region with l1 burst fracture. In *Biomedical Engineering and Sciences (IECBES), 2010 IEEE EMBS Conference on*, pages 454–459. IEEE, 2010.

[92] Sarah Catherine Walpole, David Prieto-Merino, Phil Edwards, John Cleland, Gretchen Stevens, and Ian Roberts. The weight of nations: an estimation of adult human biomass. *BMC public health*, 12(1):439, 2012.

[93] Kyungsoo Kim and Yoon Hyuk Kim. Role of trunk muscles in generating follower load in the lumbar spine of neutral standing posture. *Journal of biomechanical engineering*, 130(4):041005, 2008.

[94] Kap-Soo Han, Antonius Rohlmann, Seok-Jo Yang, Byeong Sam Kim, and Tae-Hong Lim. Spinal muscles can create compressive follower loads in the lumbar spine in a neutral standing posture. *Medical engineering & physics*, 33(4):472–478, 2011.

# Appendix A

# Appendix A

Here a reported the muscles coordinates obtained after each of the scaling steps explained in Chapter 2. In table A.7 we report instead the final coordinates that were actually used in Abaqus, after fitting the data basing on anatomical evidences.

| Muscle Group | Vertebral Level | Origin [mm] | | | | Insertion [mm] | | | |
|---|---|---|---|---|---|---|---|---|---|
| | | X left | X right | Y | Z | X left | X right | Y | Z |
| IP | L1 | 22,313 | -22,313 | 36,7708 | 165,07 | 83,8046 | -83,8046 | -24,5139 | -69,3572 |
| | L2 | 25,0366 | -25,0366 | 27,1614 | 133,661 | 83,8046 | -83,8046 | -24,5139 | -69,3572 |
| | L3 | 25,7699 | -25,7699 | 20,4936 | 98,4872 | 83,8046 | -83,8046 | -24,5139 | -69,3572 |
| | L4 | 26,1889 | -26,1889 | 17,9442 | 62,9169 | 83,8046 | -83,8046 | -24,5139 | -69,3572 |
| | L5 | 28,9126 | -28,9126 | 17,7481 | 28,9319 | 83,8046 | -83,8046 | -24,5139 | -69,3572 |
| MF | L1 | 5,02828 | -5,02828 | 65,6972 | 134,157 | 38,7596 | -38,7596 | 58,8333 | 16,8439 |
| | L2 | 2,30463 | -2,30463 | 57,4606 | 104,729 | 43,9974 | -43,9974 | 70,6 | 6,93572 |
| | L3 | 6,80913 | -6,80913 | 50,9889 | 67,1774 | 41,9023 | -41,9023 | 75,5028 | -1,98163 |
| | L4 | 3,77121 | -3,77121 | 59,7158 | 44,5868 | 27,2365 | -27,2365 | 77,4639 | -7,92654 |
| | L5 | 5,23779 | -5,23779 | 60,6964 | 26,2567 | 10,4756 | -10,4756 | 81,3861 | -11,8898 |
| LG | L1 | 18,1228 | -18,1228 | 65,4031 | 153,478 | 53,4254 | -53,4254 | 59,8139 | -3,96327 |
| | L2 | 16,0276 | -16,0276 | 53,8325 | 121,771 | 54,473 | -54,473 | 56,8722 | 2,97245 |
| | L3 | 19,4846 | -19,4846 | 50,0083 | 88,5791 | 52,3779 | -52,3779 | 53,9306 | -1,98163 |
| | L4 | 19,6941 | -19,6941 | 48,8317 | 57,9628 | 45,045 | -45,045 | 49,0278 | 13,8714 |
| | L5 | 21,3702 | -21,3702 | 49,0278 | 32,0034 | 45,045 | -45,045 | 43,1444 | 17,8347 |
| IC | L1 | 22,5225 | -22,5225 | 56,7742 | 148,424 | 46,0925 | -46,0925 | 78,4444 | -2,97245 |
| | L2 | 19,3798 | -19,3798 | 49,2239 | 117,016 | 52,3779 | -52,3779 | 64,7167 | 13,8714 |
| | L3 | 19,7988 | -19,7988 | 41,6736 | 82,9314 | 52,3779 | -52,3779 | 58,8333 | 17,8347 |
| | L4 | 30,5887 | -30,5887 | 41,1833 | 51,7207 | 46,0925 | -46,0925 | 53,9306 | 21,798 |
| QL | L1 | 35,7217 | -35,7217 | 61,1867 | 148,722 | 82,7571 | -82,7571 | 27,4556 | 16,8439 |
| | L2 | 37,8168 | -37,8168 | 52,95 | 125,14 | 82,7571 | -82,7571 | 27,4556 | 16,8439 |
| | L3 | 39,4929 | -39,4929 | 47,5569 | 90,957 | 82,7571 | -82,7571 | 27,4556 | 16,8439 |
| | L4 | 46,9306 | -46,9306 | 47,5569 | 60,4399 | 82,7571 | -82,7571 | 27,4556 | 16,8439 |

*Table A.1: Muscles coordinates after the proportion*

| Muscle Group | Vertebral Level | Origin [mm] | | | | Insertion [mm] | | | |
|---|---|---|---|---|---|---|---|---|---|
| | | X left | X right | Y | Z | X left | X right | Y | Z |
| IP | L1 | 22,313 | -22,313 | -36,7708 | 165,07 | 83,8046 | -83,8046 | 24,5139 | -69,3572 |
| | L2 | 25,0366 | -25,0366 | -27,1614 | 133,661 | 83,8046 | -83,8046 | 24,5139 | -69,3572 |
| | L3 | 25,7699 | -25,7699 | -20,4936 | 98,4872 | 83,8046 | -83,8046 | 24,5139 | -69,3572 |
| | L4 | 26,1889 | -26,1889 | -17,9442 | 62,9169 | 83,8046 | -83,8046 | 24,5139 | -69,3572 |
| | L5 | 28,9126 | -28,9126 | -17,7481 | 28,9319 | 83,8046 | -83,8046 | 24,5139 | -69,3572 |
| MF | L1 | 5,02828 | -5,02828 | -65,6972 | 134,157 | 38,7596 | -38,7596 | -58,8333 | 16,8439 |
| | L2 | 2,30463 | -2,30463 | -57,4606 | 104,729 | 43,9974 | -43,9974 | -70,6 | 6,93572 |
| | L3 | 6,80913 | -6,80913 | -50,9889 | 67,1774 | 41,9023 | -41,9023 | -75,5028 | -1,98163 |
| | L4 | 3,77121 | -3,77121 | -59,7158 | 44,5868 | 27,2365 | -27,2365 | -77,4639 | -7,92654 |
| | L5 | 5,23779 | -5,23779 | -60,6964 | 26,2567 | 10,4756 | -10,4756 | -81,3861 | -11,8898 |
| LG | L1 | 18,1228 | -18,1228 | -65,4031 | 153,478 | 53,4254 | -53,4254 | -59,8139 | -3,96327 |
| | L2 | 16,0276 | -16,0276 | -53,8325 | 121,771 | 54,473 | -54,473 | -56,8722 | 2,97245 |
| | L3 | 19,4846 | -19,4846 | -50,0083 | 88,5791 | 52,3779 | -52,3779 | -53,9306 | -1,98163 |
| | L4 | 19,6941 | -19,6941 | -48,8317 | 57,9628 | 45,045 | -45,045 | -49,0278 | 13,8714 |
| | L5 | 21,3702 | -21,3702 | -49,0278 | 32,0034 | 45,045 | -45,045 | -43,1444 | 17,8347 |
| IC | L1 | 22,5225 | -22,5225 | -56,7742 | 148,424 | 46,0925 | -46,0925 | -78,4444 | -2,97245 |
| | L2 | 19,3798 | -19,3798 | -49,2239 | 117,016 | 52,3779 | -52,3779 | -64,7167 | 13,8714 |
| | L3 | 19,7988 | -19,7988 | -41,6736 | 82,9314 | 52,3779 | -52,3779 | -58,8333 | 17,8347 |
| | L4 | 30,5887 | -30,5887 | -41,1833 | 51,7207 | 46,0925 | -46,0925 | -53,9306 | 21,798 |
| QL | L1 | 35,7217 | -35,7217 | -61,1867 | 148,722 | 82,7571 | -82,7571 | -27,4556 | 16,8439 |
| | L2 | 37,8168 | -37,8168 | -52,95 | 125,14 | 82,7571 | -82,7571 | -27,4556 | 16,8439 |
| | L3 | 39,4929 | -39,4929 | -47,5569 | 90,957 | 82,7571 | -82,7571 | -27,4556 | 16,8439 |
| | L4 | 46,9306 | -46,9306 | -47,5569 | 60,4399 | 82,7571 | -82,7571 | -27,4556 | 16,8439 |

*Table A.2: Muscles coordinates after the first symmetry*

| Muscle Group | Vertebral Level | Origin [mm] | | | | Insertion [mm] | | | |
|---|---|---|---|---|---|---|---|---|---|
| | | X left | X right | Y | Z | X left | X right | Y | Z |
| IP | L1 | 22,313 | -22,313 | -26,3 | 171,3 | 83,8046 | -83,8046 | 34,9847 | -63,1274 |
| | L2 | 25,0366 | -25,0366 | -16,6906 | 139,891 | 83,8046 | -83,8046 | 34,9847 | -63,1274 |
| | L3 | 25,7699 | -25,7699 | -10,0228 | 104,717 | 83,8046 | -83,8046 | 34,9847 | -63,1274 |
| | L4 | 26,1889 | -26,1889 | -7,47333 | 69,1467 | 83,8046 | -83,8046 | 34,9847 | -63,1274 |
| | L5 | 28,9126 | -28,9126 | -7,27722 | 35,1617 | 83,8046 | -83,8046 | 34,9847 | -63,1274 |
| MF | L1 | 5,02828 | -5,02828 | -55,2264 | 140,387 | 38,7596 | -38,7596 | -48,3625 | 23,0737 |
| | L2 | 2,30463 | -2,30463 | -46,9897 | 110,959 | 43,9974 | -43,9974 | -60,1292 | 13,1656 |
| | L3 | 6,80913 | -6,80913 | -40,5181 | 73,4073 | 41,9023 | -41,9023 | -65,0319 | 4,24821 |
| | L4 | 3,77121 | -3,77121 | -49,245 | 50,8166 | 27,2365 | -27,2365 | -66,9931 | -1,69669 |
| | L5 | 5,23779 | -5,23779 | -50,2256 | 32,4865 | 10,4756 | -10,4756 | -70,9153 | -5,65996 |
| LG | L1 | 18,1228 | -18,1228 | -54,9322 | 159,707 | 53,4254 | -53,4254 | -49,3431 | 2,26657 |
| | L2 | 16,0276 | -16,0276 | -43,3617 | 128,001 | 54,473 | -54,473 | -46,4014 | 9,2023 |
| | L3 | 19,4846 | -19,4846 | -39,5375 | 94,8089 | 52,3779 | -52,3779 | -43,4597 | 4,24821 |
| | L4 | 19,6941 | -19,6941 | -38,3608 | 64,1927 | 45,045 | -45,045 | -38,5569 | 20,1013 |
| | L5 | 21,3702 | -21,3702 | -38,5569 | 38,2332 | 45,045 | -45,045 | -32,6736 | 24,0646 |
| IC | L1 | 22,5225 | -22,5225 | -46,3033 | 154,654 | 46,0925 | -46,0925 | -67,9736 | 3,25739 |
| | L2 | 19,3798 | -19,3798 | -38,7531 | 123,245 | 52,3779 | -52,3779 | -54,2458 | 20,1013 |
| | L3 | 19,7988 | -19,7988 | -31,2028 | 89,1612 | 52,3779 | -52,3779 | -48,3625 | 24,0646 |
| | L4 | 30,5887 | -30,5887 | -30,7125 | 57,9505 | 46,0925 | -46,0925 | -43,4597 | 28,0278 |
| QL | L1 | 35,7217 | -35,7217 | -50,7158 | 154,952 | 82,7571 | -82,7571 | -16,9847 | 23,0737 |
| | L2 | 37,8168 | -37,8168 | -42,4792 | 131,37 | 82,7571 | -82,7571 | -16,9847 | 23,0737 |
| | L3 | 39,4929 | -39,4929 | -37,0861 | 97,1869 | 82,7571 | -82,7571 | -16,9847 | 23,0737 |
| | L4 | 46,9306 | -46,9306 | -37,0861 | 66,6697 | 82,7571 | -82,7571 | -16,9847 | 23,0737 |

*Table A.3: Muscles coordinates after the first translation*

| Muscle Group | Vertebral Level | Origin [mm] | | | | Insertion [mm] | | | |
|---|---|---|---|---|---|---|---|---|---|
| | | X left | X right | Y | Z | X left | X right | Y | Z |
| IP | L1 | 22,313 | -22,313 | -44,7072 | 167,441 | 83,8046 | -83,8046 | 41,6192 | -58,9647 |
| | L2 | 25,0366 | -25,0366 | -31,7509 | 137,259 | 83,8046 | -83,8046 | 41,6192 | -58,9647 |
| | L3 | 25,7699 | -25,7699 | -21,3109 | 103,014 | 83,8046 | -83,8046 | 41,6192 | -58,9647 |
| | L4 | 26,1889 | -26,1889 | -14,9221 | 67,9298 | 83,8046 | -83,8046 | 41,6192 | -58,9647 |
| | L5 | 28,9126 | -28,9126 | -11,0445 | 34,1661 | 83,8046 | -83,8046 | 41,6192 | -58,9647 |
| MF | L1 | 5,02828 | -5,02828 | -70,1135 | 133,576 | 38,7596 | -38,7596 | -50,578 | 17,6973 |
| | L2 | 2,30463 | -2,30463 | -58,7366 | 105,214 | 43,9974 | -43,9974 | -61,2017 | 6,57245 |
| | L3 | 6,80913 | -6,80913 | -48,2339 | 68,5845 | 41,9023 | -41,9023 | -65,1094 | -2,82366 |
| | L4 | 3,77121 | -3,77121 | -54,4615 | 45,1812 | 27,2365 | -27,2365 | -66,4147 | -8,94606 |
| | L5 | 5,23779 | -5,23779 | -53,45 | 26,8528 | 10,4756 | -10,4756 | -69,8844 | -13,311 |
| LG | L1 | 18,1228 | -18,1228 | -71,9146 | 152,815 | 53,4254 | -53,4254 | -49,2981 | -3,09358 |
| | L2 | 16,0276 | -16,0276 | -56,9765 | 122,549 | 54,473 | -54,473 | -47,1253 | 4,12006 |
| | L3 | 19,4846 | -19,4846 | -49,5782 | 89,9664 | 52,3779 | -52,3779 | -43,6642 | -0,48609 |
| | L4 | 19,6941 | -19,6941 | -45,0909 | 59,6579 | 45,045 | -45,045 | -40,5081 | 15,8049 |
| | L5 | 21,3702 | -21,3702 | -42,4729 | 33,8301 | 45,045 | -45,045 | -35,0889 | 20,3823 |
| IC | L1 | 22,5225 | -22,5225 | -62,789 | 148,726 | 46,0925 | -46,0925 | -67,9263 | -4,1274 |
| | L2 | 19,3798 | -19,3798 | -51,8797 | 118,32 | 52,3779 | -52,3779 | -56,1046 | 14,1049 |
| | L3 | 19,7988 | -19,7988 | -40,6805 | 85,2551 | 52,3779 | -52,3779 | -50,6854 | 18,6823 |
| | L4 | 30,5887 | -30,5887 | -36,8112 | 54,2813 | 46,0925 | -46,0925 | -46,2409 | 23,1535 |
| QL | L1 | 35,7217 | -35,7217 | -67,2077 | 148,544 | 82,7571 | -82,7571 | -19,385 | 21,0974 |
| | L2 | 37,8168 | -37,8168 | -56,4643 | 125,993 | 82,7571 | -82,7571 | -19,385 | 21,0974 |
| | L3 | 39,4929 | -39,4929 | -47,3989 | 92,596 | 82,7571 | -82,7571 | -19,385 | 21,0974 |
| | L4 | 46,9306 | -46,9306 | -44,0921 | 62,2585 | 82,7571 | -82,7571 | -19,385 | 21,0974 |

*Table A.4: Muscles coordinates after the rotation*

| Muscle Group | Vertebral Level | Origin [mm] | | | | Insertion [mm] | | | |
|---|---|---|---|---|---|---|---|---|---|
| | | X left | X right | Y | Z | X left | X right | Y | Z |
| IP | L1 | 22,313 | -22,313 | 44,7072 | 167,441 | 83,8046 | -83,8046 | -41,6192 | -58,9647 |
| | L2 | 25,0366 | -25,0366 | 31,7509 | 137,259 | 83,8046 | -83,8046 | -41,6192 | -58,9647 |
| | L3 | 25,7699 | -25,7699 | 21,3109 | 103,014 | 83,8046 | -83,8046 | -41,6192 | -58,9647 |
| | L4 | 26,1889 | -26,1889 | 14,9221 | 67,9298 | 83,8046 | -83,8046 | -41,6192 | -58,9647 |
| | L5 | 28,9126 | -28,9126 | 11,0445 | 34,1661 | 83,8046 | -83,8046 | -41,6192 | -58,9647 |
| MF | L1 | 5,02828 | -5,02828 | 70,1135 | 133,576 | 38,7596 | -38,7596 | 50,578 | 17,6973 |
| | L2 | 2,30463 | -2,30463 | 58,7366 | 105,214 | 43,9974 | -43,9974 | 61,2017 | 6,57245 |
| | L3 | 6,80913 | -6,80913 | 48,2339 | 68,5845 | 41,9023 | -41,9023 | 65,1094 | -2,82366 |
| | L4 | 3,77121 | -3,77121 | 54,4615 | 45,1812 | 27,2365 | -27,2365 | 66,4147 | -8,94606 |
| | L5 | 5,23779 | -5,23779 | 53,45 | 26,8528 | 10,4756 | -10,4756 | 69,8844 | -13,311 |
| LG | L1 | 18,1228 | -18,1228 | 71,9146 | 152,815 | 53,4254 | -53,4254 | 49,2981 | -3,09358 |
| | L2 | 16,0276 | -16,0276 | 56,9765 | 122,549 | 54,473 | -54,473 | 47,1253 | 4,12006 |
| | L3 | 19,4846 | -19,4846 | 49,5782 | 89,9664 | 52,3779 | -52,3779 | 43,6642 | -0,48609 |
| | L4 | 19,6941 | -19,6941 | 45,0909 | 59,6579 | 45,045 | -45,045 | 40,5081 | 15,8049 |
| | L5 | 21,3702 | -21,3702 | 42,4729 | 33,8301 | 45,045 | -45,045 | 35,0889 | 20,3823 |
| IC | L1 | 22,5225 | -22,5225 | 62,789 | 148,726 | 46,0925 | -46,0925 | 67,9263 | -4,1274 |
| | L2 | 19,3798 | -19,3798 | 51,8797 | 118,32 | 52,3779 | -52,3779 | 56,1046 | 14,1049 |
| | L3 | 19,7988 | -19,7988 | 40,6805 | 85,2551 | 52,3779 | -52,3779 | 50,6854 | 18,6823 |
| | L4 | 30,5887 | -30,5887 | 36,8112 | 54,2813 | 46,0925 | -46,0925 | 46,2409 | 23,1535 |
| QL | L1 | 35,7217 | -35,7217 | 67,2077 | 148,544 | 82,7571 | -82,7571 | 19,385 | 21,0974 |
| | L2 | 37,8168 | -37,8168 | 56,4643 | 125,993 | 82,7571 | -82,7571 | 19,385 | 21,0974 |
| | L3 | 39,4929 | -39,4929 | 47,3989 | 92,596 | 82,7571 | -82,7571 | 19,385 | 21,0974 |
| | L4 | 46,9306 | -46,9306 | 44,0921 | 62,2585 | 82,7571 | -82,7571 | 19,385 | 21,0974 |

*Table A.5: Muscles coordinates after the second symmetry*

| Muscle Group | Vertebral Level | Origin [mm] | | | | Insertion [mm] | | | |
|---|---|---|---|---|---|---|---|---|---|
| | | X left | X right | Y | Z | X left | X right | Y | Z |
| IP | L1 | 22,313 | -22,313 | 135,447 | 167,441 | 83,8046 | -83,8046 | 49,1211 | -58,9647 |
| | L2 | 25,0366 | -25,0366 | 122,491 | 137,259 | 83,8046 | -83,8046 | 49,1211 | -58,9647 |
| | L3 | 25,7699 | -25,7699 | 112,051 | 103,014 | 83,8046 | -83,8046 | 49,1211 | -58,9647 |
| | L4 | 26,1889 | -26,1889 | 105,662 | 67,9298 | 83,8046 | -83,8046 | 49,1211 | -58,9647 |
| | L5 | 28,9126 | -28,9126 | 101,785 | 34,1661 | 83,8046 | -83,8046 | 49,1211 | -58,9647 |
| MF | L1 | 5,02828 | -5,02828 | 160,854 | 133,576 | 38,7596 | -38,7596 | 141,318 | 17,6973 |
| | L2 | 2,30463 | -2,30463 | 149,477 | 105,214 | 43,9974 | -43,9974 | 151,942 | 6,57245 |
| | L3 | 6,80913 | -6,80913 | 138,974 | 68,5845 | 41,9023 | -41,9023 | 155,85 | -2,82366 |
| | L4 | 3,77121 | -3,77121 | 145,202 | 45,1812 | 27,2365 | -27,2365 | 157,155 | -8,94606 |
| | L5 | 5,23779 | -5,23779 | 144,19 | 26,8528 | 10,4756 | -10,4756 | 160,625 | -13,311 |
| LG | L1 | 18,1228 | -18,1228 | 162,655 | 152,815 | 53,4254 | -53,4254 | 140,038 | -3,09358 |
| | L2 | 16,0276 | -16,0276 | 147,717 | 122,549 | 54,473 | -54,473 | 137,866 | 4,12006 |
| | L3 | 19,4846 | -19,4846 | 140,318 | 89,9664 | 52,3779 | -52,3779 | 134,404 | -0,48609 |
| | L4 | 19,6941 | -19,6941 | 135,831 | 59,6579 | 45,045 | -45,045 | 131,248 | 15,8049 |
| | L5 | 21,3702 | -21,3702 | 133,213 | 33,8301 | 45,045 | -45,045 | 125,829 | 20,3823 |
| IC | L1 | 22,5225 | -22,5225 | 153,529 | 148,726 | 46,0925 | -46,0925 | 158,667 | -4,1274 |
| | L2 | 19,3798 | -19,3798 | 142,62 | 118,32 | 52,3779 | -52,3779 | 146,845 | 14,1049 |
| | L3 | 19,7988 | -19,7988 | 131,421 | 85,2551 | 52,3779 | -52,3779 | 141,426 | 18,6823 |
| | L4 | 30,5887 | -30,5887 | 127,551 | 54,2813 | 46,0925 | -46,0925 | 136,981 | 23,1535 |
| QL | L1 | 35,7217 | -35,7217 | 157,948 | 148,544 | 82,7571 | -82,7571 | 110,125 | 21,0974 |
| | L2 | 37,8168 | -37,8168 | 147,205 | 125,993 | 82,7571 | -82,7571 | 110,125 | 21,0974 |
| | L3 | 39,4929 | -39,4929 | 138,139 | 92,596 | 82,7571 | -82,7571 | 110,125 | 21,0974 |
| | L4 | 46,9306 | -46,9306 | 134,832 | 62,2585 | 82,7571 | -82,7571 | 110,125 | 21,0974 |

*Table A.6: Muscles coordinates after the second translation*

| Muscle Group | Vertebral Level | Origin [mm] | | | | Insertion [mm] | | | |
|---|---|---|---|---|---|---|---|---|---|
| | | X left | X right | Y | Z | X left | X right | Y | Z |
| IP | L1 | 21,15 | -21,15 | 133,29 | 161,93 | 83,8 | -83,8 | 49,12 | -58,96 |
| | L2 | 20,87 | -20,87 | 120,08 | 129,15 | 83,8 | -83,8 | 49,12 | -58,96 |
| | L3 | 21,5 | -21,5 | 109,38 | 97,12 | 83,8 | -83,8 | 49,12 | -58,96 |
| | L4 | 22,02 | -22,02 | 96,78 | 64,9 | 83,8 | -83,8 | 49,12 | -58,96 |
| | L5 | 23,645 | -23,645 | 87,3 | 32,695 | 83,8 | -83,8 | 49,12 | -58,96 |
| MF | L1 | 36 | -36 | 153,65 | 148,5 | 82,76 | -82,76 | 110,13 | 21,1 |
| | L2 | 39,375 | -39,375 | 145,18 | 117,9 | 82,76 | -82,76 | 110,13 | 21,1 |
| | L3 | 42,16 | -42,16 | 133,11 | 83,635 | 82,76 | -82,76 | 110,13 | 21,1 |
| | L4 | 37,97 | -37,97 | 121,46 | 55,225 | 82,76 | -82,76 | 110,13 | 21,1 |
| | L5 | 3,345 | -3,345 | 164,31 | 126,37 | 23,08 | -23,08 | 119,57 | 3,73 |
| LG | L1 | 4,01 | -4,01 | 152,44 | 95,035 | 29,435 | -29,435 | 113,61 | -13,095 |
| | L2 | 7,365 | -7,365 | 132,85 | 61,935 | 28,72 | -28,72 | 120,47 | -21,885 |
| | L3 | 1,555 | -1,555 | 130,77 | 33,27 | 23,925 | -23,925 | 122,72 | -29,25 |
| | L4 | 2,27 | -2,27 | 123,66 | 7,665 | 16,005 | -16,005 | 125,19 | -31,395 |
| | L5 | 16,725 | -16,725 | 149,43 | 141,72 | 32,765 | -32,765 | 120,15 | -18,935 |
| IC | L1 | 15,97 | -15,97 | 139,46 | 110,24 | 34,955 | -34,955 | 114,24 | -3,185 |
| | L2 | 20,365 | -20,365 | 122,44 | 77,935 | 36,695 | -36,695 | 113,86 | -0,495 |
| | L3 | 26,12 | -26,12 | 116,29 | 47,915 | 38,955 | -38,955 | 110,51 | 7,1 |
| | L4 | 14,985 | -14,985 | 162,95 | 146,58 | 49,015 | -49,015 | 99,565 | -7,975 |
| QL | L1 | 16,875 | -16,875 | 151,1 | 115,17 | 52,06 | -52,06 | 97,655 | -3,96 |
| | L2 | 18,655 | -18,655 | 134,27 | 80,005 | 52,7 | -52,7 | 95,96 | -7,005 |
| | L3 | 21,985 | -21,985 | 125,03 | 51,315 | -53,085 | 53,085 | 95,18 | -2,92 |
| | L4 | 26,56 | -26,56 | 114,66 | 24,015 | 45,7 | -45,7 | 106,24 | 14,33 |

*Table A.7: Muscles coordinates as we implemented in the model, after the scaling process and anatomical reconstructions*

# Appendix B

# Appendix B

A collection of the numerical values for IVA and IVR obtained from maximum and minimum *k* values is reported in table B.1.

| k | L1-2 | | L2-3 | | L3-4 | | L4-5 | | L5-S1 | |
|---|---|---|---|---|---|---|---|---|---|---|
| | IVR [°] | IVA [°] | IVR [°] | IVA [°] | IVR [°] | IVA [°] | IVR [°] | IVA [°] | IVR [°] | IVA [°] |
| 1.31 | 1,28 | 0,56 | -0,33 | -1,09 | -1,45 | -9,98 | -2,50 | -11,56 | -3,49 | -23,88 |
| 1.45 | 1,16 | 0,44 | -0,75 | -1,51 | -1,76 | -10,30 | -2,99 | -12,05 | -4,45 | -24,84 |

*Table B.1: Numerical values of IVR and IVA*

In table B.2 are presented the average, median, standard deviation and approximate average pressure values for all the intervertebral discs.

| | | *k* value | | | | | | | |
|---|---|---|---|---|---|---|---|---|---|
| | | 1.31 | 1.33 | 1.35 | 1.37 | 1.39 | 1.41 | 1.43 | 1.45 |
| L1-2 | average | 0,1661 | 0,1672 | 0,1673 | 0,1678 | 0,1681 | 0,1686 | 0,1690 | 0,1694 |
| | median | 0,1631 | 0,1642 | 0,1645 | 0,1650 | 0,1654 | 0,1659 | 0,1664 | 0,1669 |
| | SD | 0,0542 | 0,0536 | 0,0526 | 0,0518 | 0,0510 | 0,0501 | 0,0492 | 0,0484 |
| | (max+min)/2 | 0,1587 | 0,1599 | 0,1593 | 0,1592 | 0,1591 | 0,1590 | 0,1590 | 0,1589 |
| L2-3 | average | 0,1973 | 0,1992 | 0,2000 | 0,2012 | 0,2022 | 0,2033 | 0,2044 | 0,2055 |
| | median | 0,2027 | 0,2039 | 0,2041 | 0,2045 | 0,2051 | 0,2058 | 0,2067 | 0,2075 |
| | SD | 0,0208 | 0,0220 | 0,0238 | 0,0256 | 0,0276 | 0,0296 | 0,0321 | 0,0345 |
| | (max+min)/2 | 0,1834 | 0,1877 | 0,1910 | 0,1941 | 0,1968 | 0,1993 | 0,2020 | 0,2042 |
| L3-4 | average | 0,2453 | 0,2496 | 0,2539 | 0,2580 | 0,2620 | 0,2660 | 0,2706 | 0,2747 |
| | median | 0,2324 | 0,2360 | 0,2397 | 0,2434 | 0,2469 | 0,2502 | 0,2541 | 0,2579 |
| | SD | 0,1004 | 0,1030 | 0,1057 | 0,1083 | 0,1108 | 0,1134 | 0,1163 | 0,1190 |
| | (max+min)/2 | 0,3559 | 0,3654 | 0,3734 | 0,3817 | 0,3897 | 0,3976 | 0,4070 | 0,4154 |
| L4-5 | average | 0,3415 | 0,3480 | 0,3551 | 0,3619 | 0,3687 | 0,3744 | 0,3827 | 0,3896 |
| | median | 0,3313 | 0,3368 | 0,3434 | 0,3499 | 0,3562 | 0,3613 | 0,3688 | 0,3753 |
| | SD | 0,1118 | 0,1147 | 0,1176 | 0,1204 | 0,1232 | 0,1258 | 0,1293 | 0,1324 |
| | (max+min)/2 | 0,4299 | 0,4443 | 0,4537 | 0,4648 | 0,4751 | 0,4842 | 0,4979 | 0,5093 |
| L5-S1 | average | 0,3823 | 0,3931 | 0,4061 | 0,4184 | 0,4305 | 0,4414 | 0,4556 | 0,4680 |
| | median | 0,3680 | 0,3787 | 0,3915 | 0,4034 | 0,4165 | 0,4278 | 0,4422 | 0,4544 |
| | SD | 0,1476 | 0,1522 | 0,1560 | 0,1600 | 0,1639 | 0,1676 | 0,1726 | 0,1769 |
| | (max+min)/2 | 0,4244 | 0,4391 | 0,4514 | 0,4642 | 0,4763 | 0,4879 | 0,5032 | 0,5166 |

*Table B.2: Statistical data for pressures registered on the intervertebral discs; values are expressed in MPa*

Below (fig. B.1, B.2, B.3, B.4 and B.5) the complete statistical information in the form of boxplots on the pressure distribution within the discs are reported.

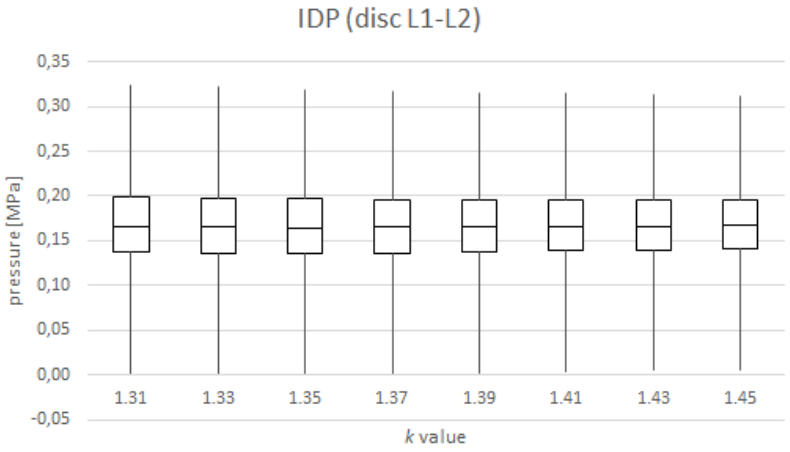


*Figure B.1: Boxplot for pressure values on the L1-L2 disc, for different k values*

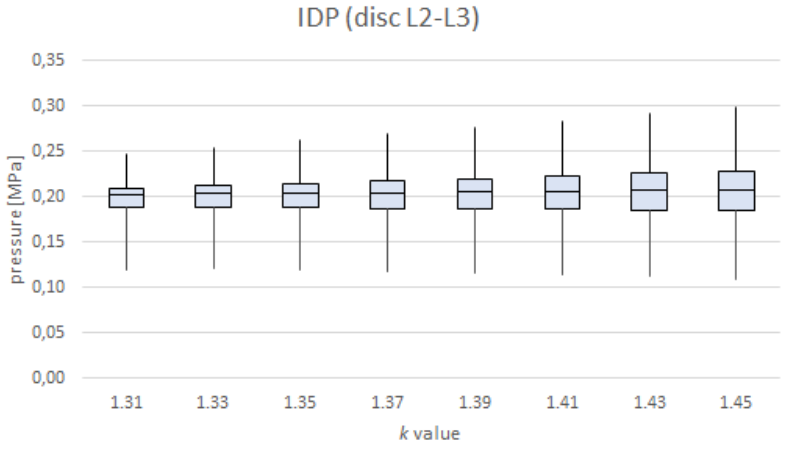


*Figure B.2: Boxplot for pressure values on the L2-L3 disc, for different k values*

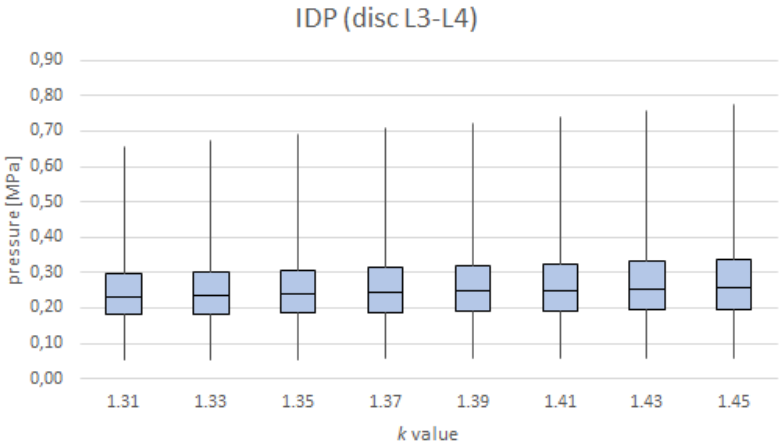


*Figure B.3: Boxplot for pressure values on the L3-L4 disc, for different $k$ values*

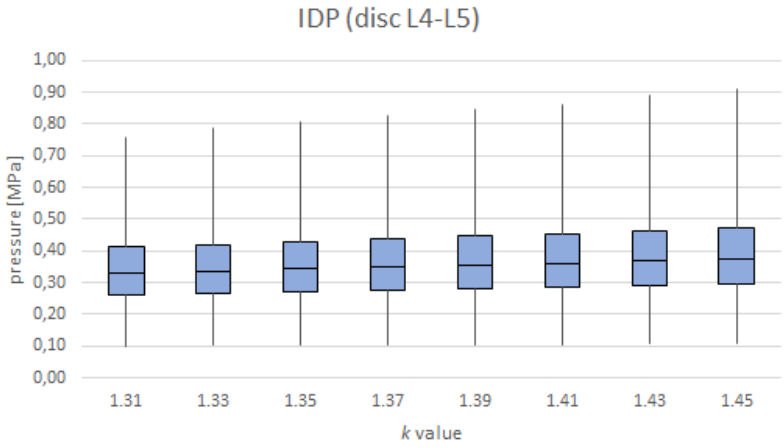


*Figure B.4: Boxplot for pressure values on the L4-L5 disc, for different $k$ values*

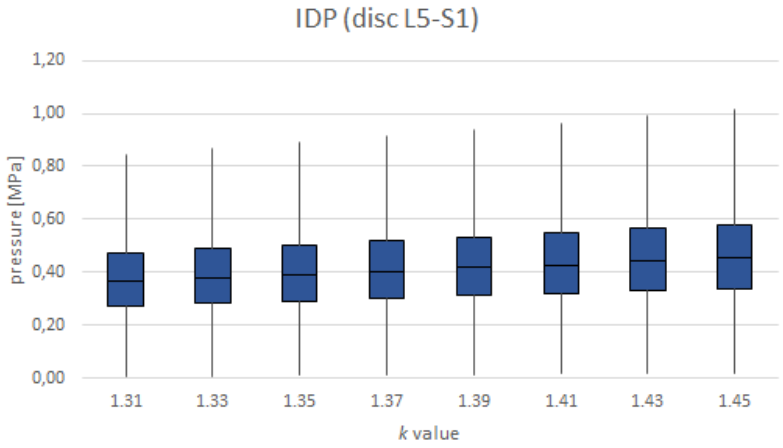


*Figure B.5: Boxplot for pressure values on the L5-S1 disc, for different k values*

In figures B.6, B.7, B.8, B.9 and B.10 we report the normal distribution for k 1.31, k 1.45 and follower load (FL), divided for each disc.

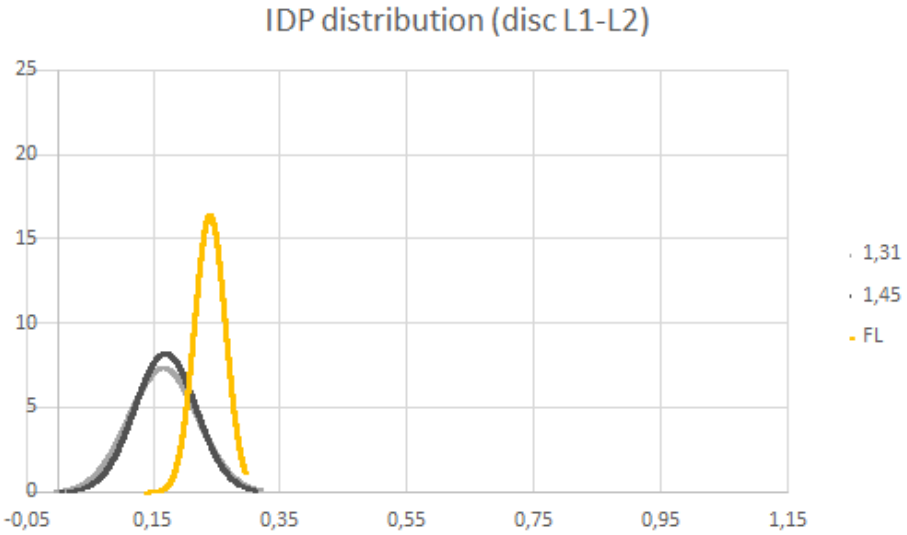


*Figure B.6: Normal pressure distribution in the disc L1-L2*

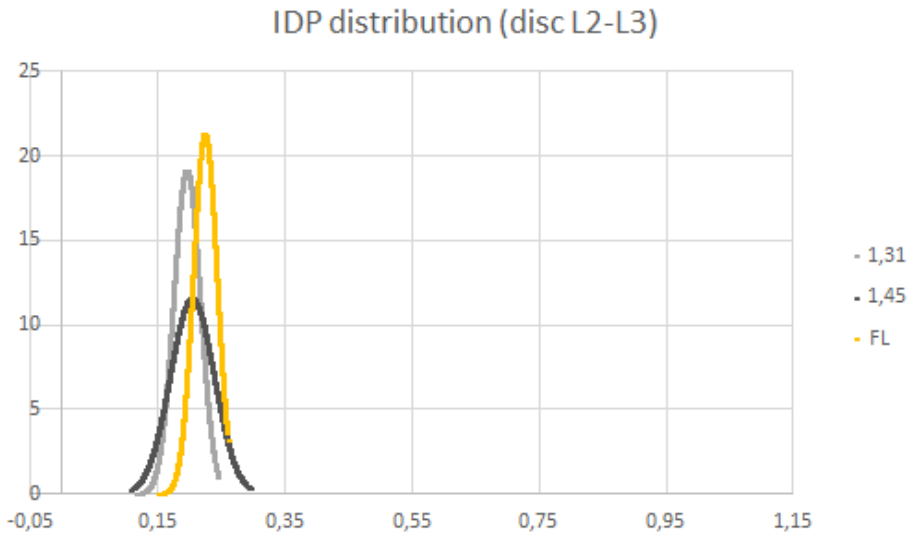


*Figure B.7: Normal pressure distribution in the disc L2-3*

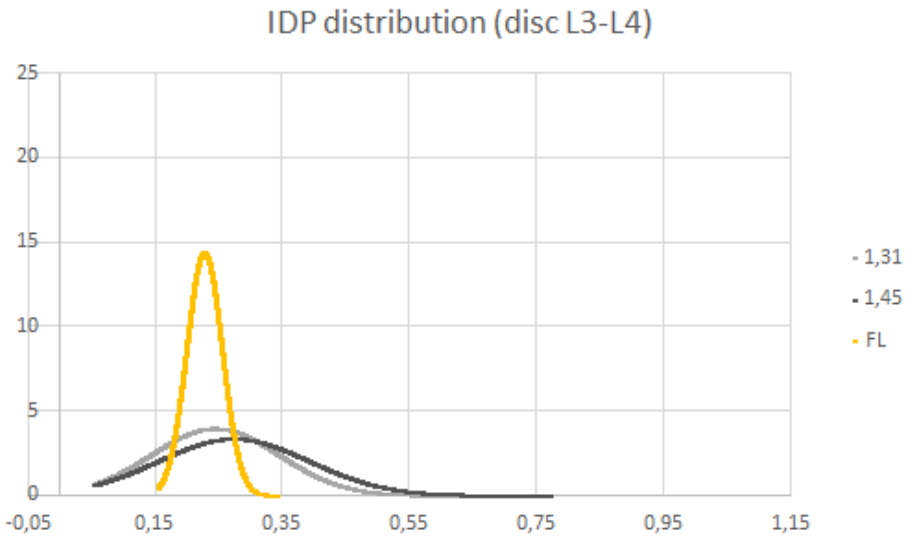


*Figure B.8: Normal pressure distribution in the disc L3-L4*

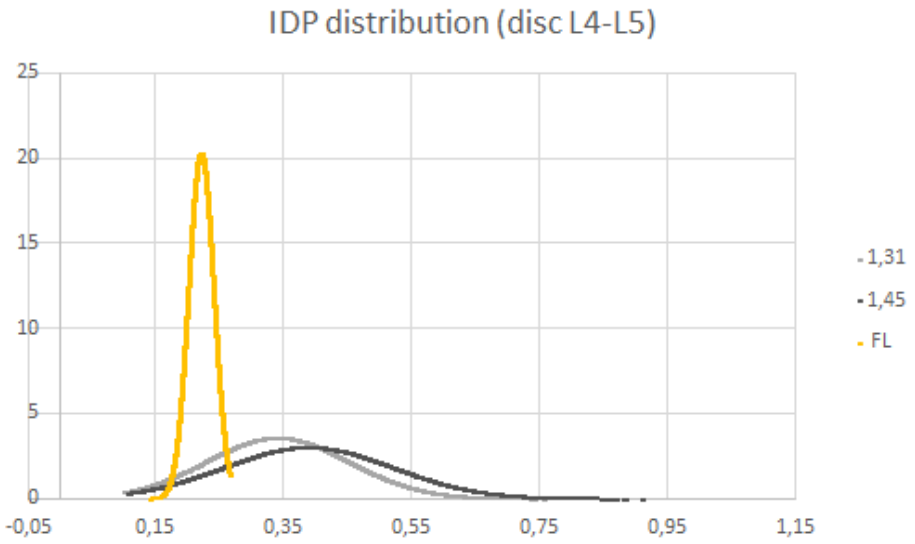


*Figure B.9: Normal pressure distribution in the disc L4-L5*

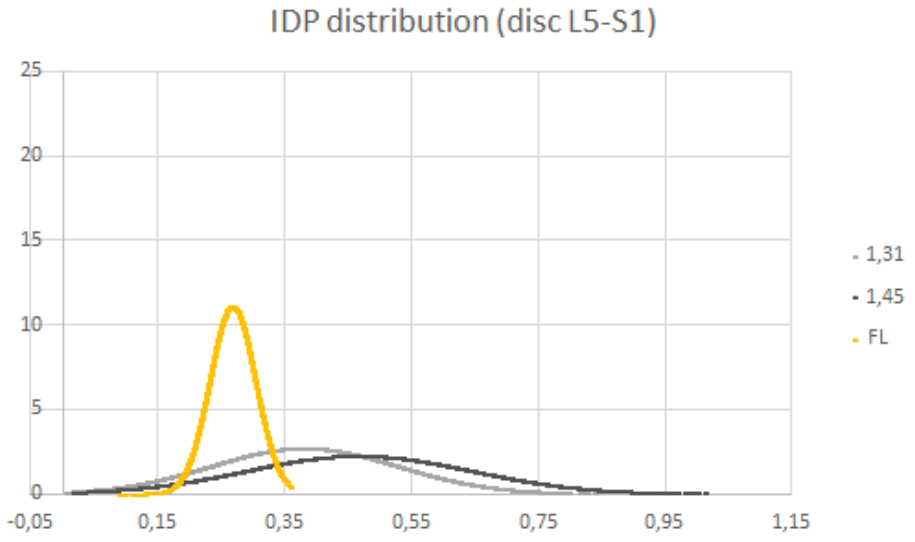


*Figure B.10: Normal pressure distribution in the disc L5-S1*